SYNTHESIS AND CHARACTERIZATION OF Ga/F CO-DOPED ZnO NANOSTRUCTURES PREPARED BY HYDROTHERMAL PROCESS

KRISANA CHONGSRI

A THESIS SUBMITTED IN PARTIAL FULFILLMENT

OF THE REQUIREMENT FOR THE DEGREE OF

DOCTOR OF PHILOSOPHY IN NANOSCIENCE AND NANOTECHNOLOGY

COLLEGE OF NANOTECHNOLOGY

KING MONGKUT'S INSTITUTE OF TECHNOLOGY LADKRABANG

2018

KMITL-2018-NT-D-001-003

หัวข้อวิทยานิพนธ์	การสังเคราะห์และการตรวจเอกลักษณ์เฉพาะของซิงค์ออกไซด์โครงสร้างนาโนที่เจือด้วยแกลเลียมและฟลูออรีนเตรียมด้วยกระบวนการไฮโดรเทอร์มอล
นักศึกษา	นาย กฤษณะ ช่องศรี
รหัสประจำตัว	57607001
ปริญญา	ปรัชญาดุษฎีบัณฑิต
สาขาวิชา	นาโนวิทยาและนาโนเทคโนโลยี
พ.ศ.	2561
อาจารย์ที่ปรึกษาวิทยานิพนธ์	รศ.ดร.วิษณุ เพชรภา
อาจารย์ที่ปรึกษาวิทยานิพนธ์ร่วม	ดร.กนกทิพย์ บุณยรัตกลิน

บทคัดย่อ

วิทยานิพนธ์นี้ได้เตรียมซิงค์ออกไซด์โครงสร้างนาโนที่เจือด้วยแกลเลียมและฟลูออรีนด้วยวิธีการโฮโดรเทอร์มอล ชั้นก่อผลึกซิงค์ออกไซด์สำหรับซิงค์ออกไซด์โครงสร้างนาโนปลูกบนฐานรองรับที่เป็นกระจกด้วยวิธีการจุ่มเคลือบ การสังเคราะห์วัสดุโครงสร้างนาโนนี้เตรียมภายใต้เงื่อนไขที่แตกต่างกัน ทำการศึกษาผลกระทบของตัวแปรในการสังเคราะห์ที่สำคัญ ได้แก่ ความหนาของชั้นก่อผลึกโดยการเพิ่มจำนวนเคลือบของชั้นก่อผลึก อุณหภูมิในการเผาชั้นก่อผลึกและการปรับปรุงคุณภาพชั้นก่อผลึกด้วยการอบภายใต้บรรยากาศยูวีโอโซน ที่มีผลต่อสมบัติทางกายภาพ ทางแสงและทางสัณฐานวิทยาของโครงสร้างนาโนซิงค์ออกไซด์โครงสร้างนาโนที่เจือด้วยแกลเลียมและฟลูออรีน ทำการวิเคราะห์โครงสร้างและพื้นผิวของซิงค์ออกไซด์โครงสร้างนาโนที่เจือด้วยแกลเลียมและฟลูออรีนด้วยเทคนิคการเลี้ยวเบนของรังสีเอกซ์ (XRD) กล้องจุลทรรศน์อิเล็กตรอนแบบส่องกราด (FE-SEM) และกล้องจุลทรรศน์อิเล็กตรอนแบบส่องผ่าน (TEM) ผลการวิเคราะห์ของ XRD และ FE-SEM แสดงให้เห็นว่าเงื่อนไขของชั้นก่อผลึกซิงค์ออกไซด์เป็นตัวแปรสำคัญที่มีผลต่อ รูปร่าง ความหนาแน่น การเรียงตัว ความเป็นผลึกและความเป็นระเบียบ ของซิงค์ออกไซด์โครงสร้างนาโนที่เจือด้วยแกลเลียมและฟลูออรีน นอกจากนี้ยังพบว่า รูปร่าง ความหนาแน่น ขนาด ความเป็นผลึก และสมบัติทางแสงของวัสดุดังกล่าวขึ้นอยู่กับชนิดและความเข้มข้นของสารเจือด้วย พบว่าความเข้มข้นในการเจือแกลเลียมและฟลูออรีนมีผลต่อขนาดเกรนอย่างชัดเจน การเพิ่มความเข้มข้นในการเจือแกลเลียมทำให้ขนาดของแท่งนาโนลดลง และการเจือด้วยฟลูออรีนส่งผลต่อความเป็นระเบียบ ขนาดและความยาวของแท่งนาโนซิงค์ออกไซด์ ซึ่งขนาดแท่งนาโนจะลดลงอย่างมีนัยสำคัญเมื่อเพิ่มความเข้มข้นของการเจือฟลูออรีน นอกจากนี้ซิงค์ออกไซด์ที่เจือด้วยแกลเลียมร้อยละ 1 จะมีลักษณะสัณฐานวิทยาเป็นลักษณะผสมระหว่างแผ่นนาโนและแท่งนาโน ทำการศึกษาการแทนที่ของสารเจือแกลเลียมและฟลูออรีนในโครงสร้างซิงค์ออกไซด์ด้วยเทคนิคโฟโตลูมิเนสเซนส์สเปกโตรสโกปี (Photoluminescence

Spectroscopy) จากผลการศึกษาพบว่ามีการเปล่งแสงย่านแสงสีม่วงและย่านแสงสีเหลือง-ส้ม การเปล่งแสงของสารตัวอย่างที่แตกต่างกันขึ้นอยู่กับจุดบกพร่องที่เกิดขึ้นและการเพิ่มขึ้นของที่ว่างออกซิเจนหรือการลดลงของที่ว่างซิงค์ซึ่งเกิดจากการเจือแกลเลียมหรือฟลูออรีน โดยการสารเจือแกลเลียมจะเข้าไปแทนที่ตำแหน่งของอะตอมซิงค์ขณะที่ฟลูออรีนจะเข้าไปแทนที่ตำแหน่งอะตอมออกซิเจน

คำสำคัญ: ซิงค์ออกไซด์ที่เจือด้วยแกลเลียมและฟลูออรีน กระบวนการไฮโดรเทอร์มอล โครงสร้างนาโน

Thesis Title	Synthesis and characterization of Ga/F co-doped ZnO nanostructures prepared by hydrothermal process
Student	Mr. Krisana Chongsri
Student ID	57607001
Degree	Doctor of Philosophy
Program	Nanoscience and Nanotechnology
Year	2018
Thesis Advisor	Assoc. Prof. Dr. Wisanu Pecharapa
Thesis Co-advisor	Dr. Kanokthip Boonyarattanakalin

ABSTRACT

In this thesis, Ga/F co-doped ZnO (GFZO) nanostructures were synthesized by hydrothermal technique. The ZnO seeding layers for ZnO nanostructure growth were firstly deposited on borosilicate substrates by dip-coating method. The nanostructures were synthesized under various growth conditions. The effects of crucial growth parameters including seeding layer thickness by mean of number of coating layer, seeding layer annealing temperature and UV-Ozone baking treatment process of seeding layer on relevant physical, optical and morphological properties of the obtained GFZO nanostructures were extensively investigated. The microstructures and surface morphology of the synthesized GFZO nanostructures were observed by X-ray diffraction (XRD), Field emission scanning electron microscope (FE-SEM) and Transmission electron microscopy (TEM). Corresponding XRD and SEM results suggest that growth conditions of ZnO seeding layers are important parameters that affect the shape, density, alignment, crystallinity and orientation of GFZO nanostructures. The different morphologies and exceptional shapes of GFZO nanostructures could be controlled and obtained by controlling seeding layer condition. In addition, the results indicated that the shape, density, size, crystallinity and optical properties of the synthesized structures were strongly dependent on types and concentration of dopants. The effects of Ga and F doping concentration on grain size of the nanorod structure can be clearly observed. Increasing Ga doping concentration can induce the reduction in rod size. The F dopant strongly affects the size, length, and orientation of ZnO nanorods while the nanorod size

shows significant decrease with increasing F doping concentration. Moreover, nanodisk/nanorod morphology could be obtained in the samples doped with 1%Ga doped ZnO. The role of Ga and F substituting into ZnO structures were investigated by photoluminescence (PL) spectroscopy. The PL spectra of GFZO nanorods showed strong UV emission band and yellow-orange emission band. The luminescence could be described the increase in the oxygen vacancy (V_O) emission or the decrease of the Zinc vacancy (V_{zn}) induced by either Ga or F dopants. Ga dopants would substitute Zn atoms while F dopants prefer to substitute O atoms in the as-grown GFZO.

Keywords: Ga/F co-doped ZnO, hydrothermal process, nanostructures

ACKNOWLEDGEMENT

First, I would like to give my deep thanks to my academic advisor and my academic co-advisor, Assoc. Prof. Dr. Wisanu Pecharapa and Dr. Kanokthip Boonyarattanakalin, who accepted me as his Ph. D. student without any hesitation. During my study, they gave kind contribution to my Ph. D life of study and experience by supporting me intellectual and academic freedom in my work, guiding me in new ideas, and leading me a quality of work in all my study.

I would like to give a special thanks to Professor Hidenori Mimura, Director Research Institute of Electronics, Shizuoka University, for his help on photoluminescence measurement.

I would like to give my thanks to all member in Nano Materials Research Laboratory (NMRL) for providing not only willing help, but also friendly social atmosphere.

I would like to acknowledge College of nanotechnology, KMITL, for allowing me to study for Doctoral degree.

I would like to express my deep appreciation to my institute, Rajabhat Rajanagarindra University for financial support Ph. D scholarship.

Finally, I would like to deliver my honourable thank to my parent and my family for their constant support and love. They are the greatest people in my life and I dedicate this thesis to all of them.

Krisana Chongsri

CONTENTS

CONTENTS(CONT.)

Page

LIST OF TABLES

Page

LIST OF FIGURE

Page

LIST OF FIGURE(CONT.)

Page

LIST OF FIGURE(CONT.)

Page

LIST OF FIGURE(CONT.)

Page

LIST OF FIGURE(CONT.)

Page

CHAPTER 1

INTRODUCTION

1.1. Introduction

It has been known that nanotechnology recently requires specific synthesis to obtain designated shape, size and morphology of synthesized nanomaterials for their suitable applications. Surfactants have been employed as directing agents for effective shape control in various nanomaterial synthesis processes due to the correlation of the surface adsorption of surfaces active species on different crystal planes which can effectively control their structures and shapes. Various types of surfactant agents have been effectively utilized for synthesis of nanomaterials with desired shapes [1]. Recently, zinc oxide-based nanostructures have achieved considerable attention regarding to their unique and exceptional characteristic properties that lead them to practical applications including transparent conducting oxide (TCO) in optoelectronic devices. ZnO-based thin films have many advantages such as rather economical material cost, less toxicity, and good chemical stability when comparing to conventional tin-doped indium oxide (ITO). ZnO is normally an n-type semi-conductoring compound with rather wide band gap of 3.2-3.4 eV at room temperature together with a large exciton binding energy of about 60 meV [2]. It has been reported in several literatures that electrical and optical properties of ZnO can be further heightened by proper doping with either metal or non-metal elements. Much more interest has been focused on ZnO-based TCOs including undoped ZnO nanowire [3], Al-doped ZnO (AZO) nanostructures [4] F-doped ZnO (FZO) thin films [5], and Ga-doped ZnO (GZO) nanorods [6]. When metallic group III dopants are incorporated into ZnO, they would preferably replace the Zn host atoms and could provide extra free electrons to the host resulting an enhancement in conductivity and greater carrier mobility. When comparing the ionic and covalent radius of Ga to those of Zn, Ga is an appropriate dopant that can replace at Zn site due to the close values [7]. The similar ionic radius would result in lower lattice distortion, when doping, compared with other group III metals. Moreover, fluorine with the ionic radius of 0.117 nm that is close to that value of oxygen (0.122 nm) may be determined as a suitable anion doping

candidate at oxygen site in ZnO matrix. Although, several methods have been employed to prepare ZnO nanostructures, hydrothermal growth technique is still one of dominating processes due to its considerable advantages including low temperature processing, low cost, ease of apparatus set-up, and environmental friendliness. With exceptional shapes and structures obtained by specific hydrothermal growth conditions, one-dimensional ZnO nanostructures in form of nanorod or nanowire structures can be utilized in wide variety of applications, including ultraviolet light-emitting devices [8], chemical sensors [9], solar cells [10], water splitting [11], and ultraviolet detector devices [12]. During growth, both kinetic energy transfer from the incident ions to the host atoms at the surface and the physical momentum affect the density distribution of the nanorods at specific position on the substrate in the hydrothermal chamber. Therefore, at different incident angles, the morphology, shape, aspect ratio and orientation planes of as-synthesized nanorods could be highly involved by the atoms impinging onto the substrate.

In this thesis, we have experimentally examined the influence of crucial process parameters including ZnO seeding layer thickness, annealing temperature and UV-Ozone treatment, angle-dependent substrate placement for hydrothermal growth on structural, optical properties and morphologies of Ga/F co-doped ZnO nanostructures. All conditions were found to be the significant factors that can modify or alter the shape, density, length, alignment, crystallinity and preferential orientation of the Ga/F co-doped ZnO nanostructures during hydrothermal process.

1.2. Objectives of this work

1. To study the process for synthesizing ZnO seeding layer by dip coating.
2. To study the process for synthesizing Ga/F co-doped ZnO nanostructures by hydrothermal process.
3. To study the effect of seeding layers prepared at various deposition conditions on structural properties and morphologies of Ga/F co-doped ZnO nanostructures grown by hydrothermal process.
4. To study the effect of Ga and F doping species on relevant physical properties of ZnO-based nanostructures by hydrothermal process.

1.3. Scope of this work

1. To study on the theory of ZnO structures.
2. To study on the theory of dopant for ZnO-based nanostructures.
3. To synthesize ZnO seeding layer by dip coating with various deposition conditions.
4. To synthesize Ga/F co-doped ZnO nanostructures by conventional hydrothermal process with various Ga and F doping concentrations.
5. To study the effect of seeding layers on structural, morphological and optical properties of Ga/F co-doped ZnO nanostructures prepared by hydrothermal process.
6. To study the effect of dopants including Ga and F on structural, morphological and optical properties of ZnO-based nanostructures prepared by hydrothermal process.

1.4. Expected results of this work

1.Understand the important theories of ZnO structures, dopant and their functionalities.
2. Obtain the optimized preparation conditions of ZnO seeding layer for the growth of Ga/F co-doped ZnO nanostructures.
3. Understand the effect of annealing temperature and seed layer thickness on structural, morphological and optical properties of ZnO seeding layer.
4. Understand the effect of seeding layers on structural, optical and morphological properties of Ga/F co-doped ZnO nanostructures synthesized by hydrothermal process.

5. Understand the effect of Ga and F dopants on structural, optical and morphological properties of hydrothermally grown ZnO-based nanostructures.

CHAPTER 2

THEORY AND LITERATURE REVIEWS

2.1. Background

Zinc oxide (ZnO) is an n-type semiconductor compound with a wide band gap (Eg∼3.2–3.4 eV) at 300 K and a large exciton binding energy (60 meV). ZnO nanostructures have been extensively studied as optoelectronic materials due to the combination of their electrical and optical properties. The applications of ZnO-based materials for transparent and flexible devices such as ultraviolet light-emitting devices, chemical sensors, solar cells, and ultraviolet detector devices have been widely developed. However, the electrical conductivity of ZnO materials are rather low. Many studies have reported methodologies to increase their conductivity [13]. Doping small amount of some elements into ZnO is an interesting method.

Gallium (Ga) and Fluorine (F) are the good candidates as the dopants to improve ZnO properties. Gallium has atomic number of 31 and mostly in +3 oxidation state. Gallium is usually used in electronic applications. It has electronic configuration as $1s^2 2s^2 2p^6 3s^2 3p^6 4s^2 3d^{10} 4p^1$. Fluorine has atomic number of 9 with the highest electronegativity. When comparing the ionic radius of gallium and fluorine to zinc (Zn) and Oxygen (O) (table 2.1), it is found that the ionic radius of Ga and F are similar to Zn and O, respectively. In addition to the similarities in the ionic radius, the higher charge of Ga^{3+} than Zn^{2+} make gallium the preferably dopants to replace the Zn host atoms that could offer extra free electrons to the system, resulting in enhancement in electrical conductivity and carrier mobility. The higher electronegativity of F than O affects the distribution of electrons in the system. It is implied that F may be a suitable anion doping candidate at O site, while Ga may be a suitable cation doping candidate at Zn site in ZnO matrix [14].

ZnO nanostructures normally have been used in nanoelectronic and optoelectronic devices. Various techniques have been employed and developed for synthesizing 1D nanostructures such as thermal chemical vapor deposition, metal-organic chemical vapor deposition (MOCVD), electrodeposition, and hydrothermal

method. The hydrothermal method has become one of promising routes for synthesizing nanomaterials because of its simplicity, ease of equipped system, fastness, economical and using low temperature.

Table 2.1 Electronic configuration of Zn, Ga, O, and F

Element	Electronic configuration	Ionic radius (nm)
Zn	[Ar] $4s^2 3d^{10}$	7.400
Ga	[Ar] $4s^2 3d^{10} 4p^1$	6.200
O	[He] $2s^2 2p^4$	0.122
F	[He] $2s^2 2p^5$	0.117

2.2. Synthesis of nanomaterials

The preparation of nanomaterials can be separated into two techniques; top down and bottom up processes. The first technique is slicing of bulk material to obtain nano sized particles. Second, the bottom up technique is the process to form nano sized materials from atoms such as sol-gel process, chemical vapor deposition (CVD), hydrothermal process, and laser pyrolysis. The scheme of the synthesis of nanomaterials is shown in figure 2.1.

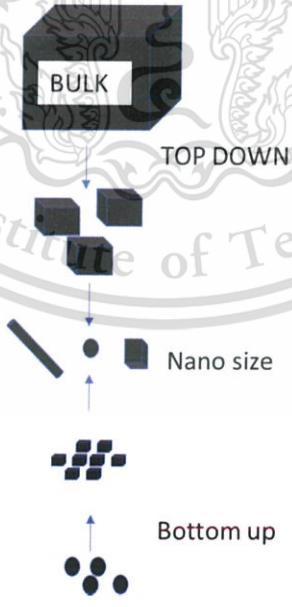

Figure 2.1 Schematic of the preparation of nanomaterials.

2.3. Hydrothermal process

The definition of hydrothermal is 'hydro' which means water and ' thermos ' which means heat (from the Greek). The hydrothermal process gives high product purity and homogeneity of nanomaterials (metastable compounds with extraordinary properties, symmetry of crystal, and narrow particle size distributions). Hydrothermal processing is heterogeneous response within fluid solvents under high pressure and low temperature conditions. This technique is important for preparation of nanomaterials for many applications such as optoelectronics, electronics, ceramics and catalysis as shown in figure 2.2. Clearly, it is technique of materials with a high coveted application potential.

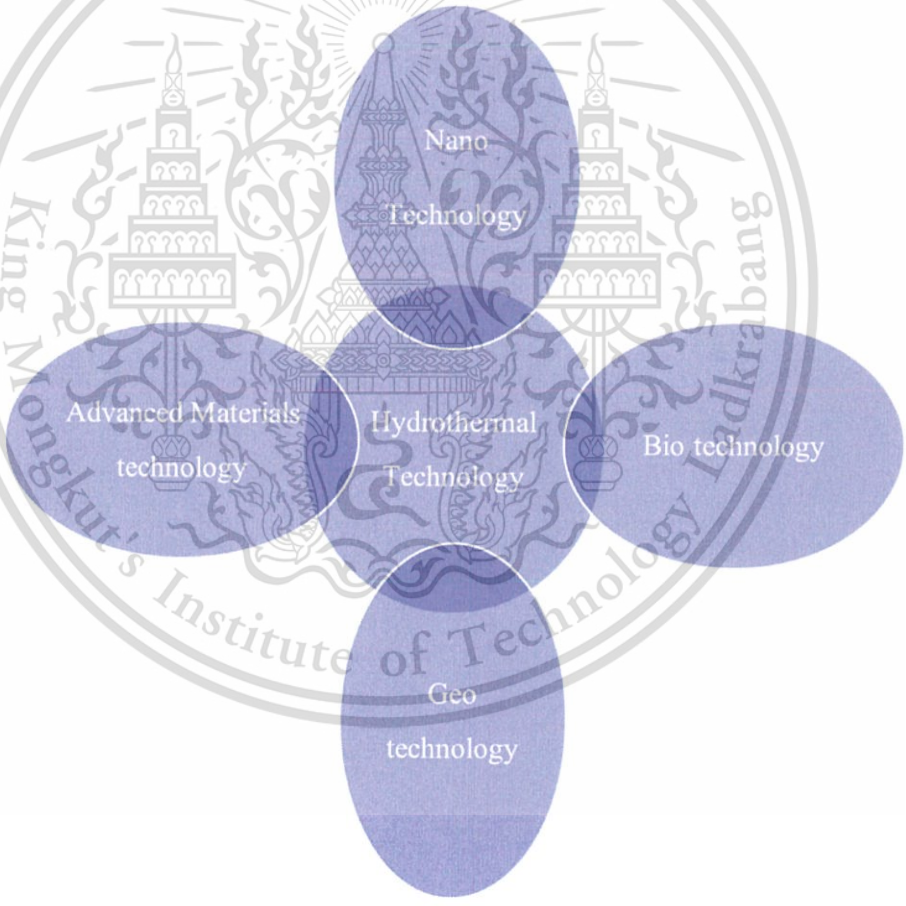

Figure 2.2 Hydrothermal technology

2.4. Characterization techniques

2.4.1. X-Ray Diffractometer (XRD)

The periodic structures are observed through the diffraction with electromagnetic radiation encroaching on geometrical minor departure and the radiation wavelength. The increasing of distances about 0.15– 0.4 nm from the interaction in crystals results in an increasing of x-ray photon energies up to 3 and 8 keV, comparing in the electromagnetic spectrum. The results might be checked with an alternate translation of the hkl integer triple. The periodicity and high level of order in a crystal of crystallographic lattice planes are involved by the atoms in crystal. The integer triple hkl indicates the crossing point of the lattice planes with the unit cell edges. The crystallographic planes of atoms are shown by the Miller lists hkl. For example, figure 2.3 shows the lattice planes of the basic cubic lattice with Miller indices (110) and (111). The distance between two planes can be calculated by interplanar spacing d_{hkl} with the Miller indices of the fitting lattice planes. The other of lattices are found the interplanar spacing depending upon the Miller indices and the unit cell parameter a as follows

$$d_{hkl} = \frac{a}{\sqrt{h^2+k^2+l^2}} \tag{2.1}$$

For

$$2\frac{a}{\sqrt{h^2+k^2+l^2}} sin\theta = \lambda \tag{2.2}$$

So

$$2d_{hkl} sin\theta_B = \lambda \tag{2.3}$$

Figure 2.4 shows the geometry of the Bragg equation (Eq. 2.3) and the Laue conditions. They show the connection between the scattering vector for a x- ray reflection and the lattice vectors. The well-known Bragg's equation is regularly is in the form of $2dsin\theta_B = \lambda$.

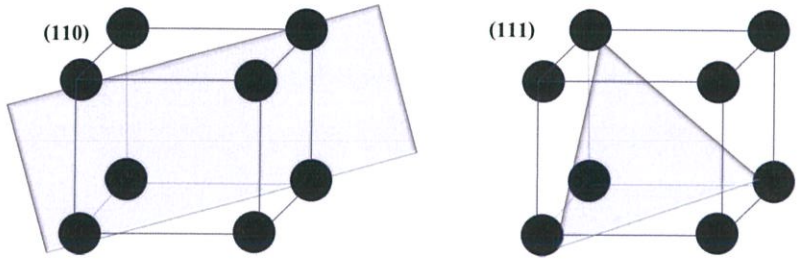

Figure 2.3 Lattice planes and Miller indices of (110) and (111).

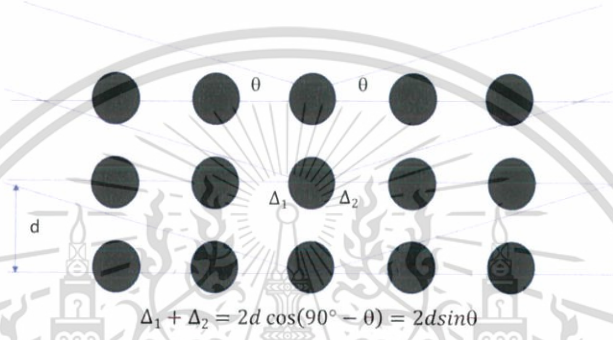

Figure 2.4 The scattered intensity and Bragg equation.

2.4.2. Field Emission Scanning Electron Microscopy (FE-SEM)

The difference between the the Scanning Electron Microscope (SEM) and the Field Emission Scanning Electron Microscope (FE-SEM) is the emitter type. Tungsten (W) or Lanthanum hexaboride (LaB6) is a filament for electrical current of Thermionic Emitters in Scanning Electron Microscope. The FE-SEM was frequently used for nanotechnology applications. The Field Emission Scanning Electron Microscope images use high-energy beam of electrons for sample surface. The electrons and atoms in the sample deliver signals that contain information on the surface with different properties. The electron gun provides a stable current and a small beam. FE-SEM is a method for creating electrons that maintains a strategic distance from these problems. The electric field can be concentrated to an unusual level due to the small tip radius (~ 100 nm), resulting in the brought down of work function of the material. Then, electrons can leave from the cathode. The voltage between cathode and anode is an extent of 0.5 to 30 kV and using vacuum system in the segment of the microscope. The high qualities image will be enhanced such as determination is on the request of ~2 nm at 1 keV and ~1 nm at 15 keV by FE-SEM. The specification of FE-SEM resolution was shown in table 2.2. Moreover, the Energy Dispersive X-beam Spectroscopy (EDX or EDS) is used to determine the elemental composition of materials. EDX is connected to the SEM to take into elemental information to be accumulated about the example under investigated. EDX works by identifying X-rays that are created by an example put in an electron pillar. As the electron beam can be definitely controlled, EDX spectra can be gathered from a particular point/molecule on the example, giving an investigation of a couple of cubic microns of material. On the other hand, the bar can clear finished a chose territory of the example to distinguish the components in that district. Also, line profiles and X-ray maps can be gained which portray the natural conveyance over the example.

Table 2.2 Specification of FE-SEM resolution.

Electron source	Cross over diameter	Final spot diameter	Demagnification
Therminonic	10-50 μm	1 nm - 1μm	10,000-50,000
Field Emission Source	10 nm	1 nm	10

2.4.3. Basic Mechanisms of Photoluminescence

Luminescence is absorption phenomena of energy and subsequent emission of light. The fluorescence and phosphorescence are important in luminescent technique. The fluorescence is "fast" (in ns), while the phosphorescence is "slow". The analyzing spectrometer scanner observes spectrum of the fluorescent emission. The broad band of sun light is from 320-2,500 nm. It can divide color spectra by wavelength of light as follows: visible spectrum (violet (400–450 nm), blue (450–500 nm), green (500–570 nm), yellow and orange (570–610 nm) and red (610 - 750 nm)), short-wavelength (near-ultraviolet 320-400 nm) and long-wavelength (near-infrared 750-2,500 nm). Photoluminescence process in ZnO structures are possibly proceeded via the following mechanisms as shown in figure 2.5. First, the ZnO nanostructures are excited by intense light at approximately 375 nm or < 375 nm. UV light create a non-thermal distribution of electrons and holes in ZnO structures. These electrons and holes are created due to the electron transfer to the conduction band (from the valence band). Then, the non-equilibrium electron distributions tend to relax back to the ground state or valence band. Non-radiative processes will rapidly move the carriers to a similarly equilibrium explained by the similarity of fermi levels. After that, the electron and hole recombine under emission of UV light which is the luminescence process. Figure 2.6 shows the schematic of photoluminescence process.

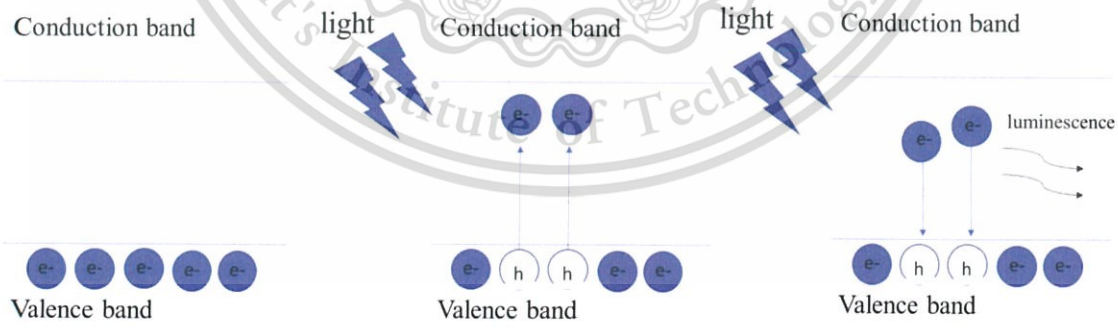

Figure 2.5 Photoluminescence process of ZnO structures.

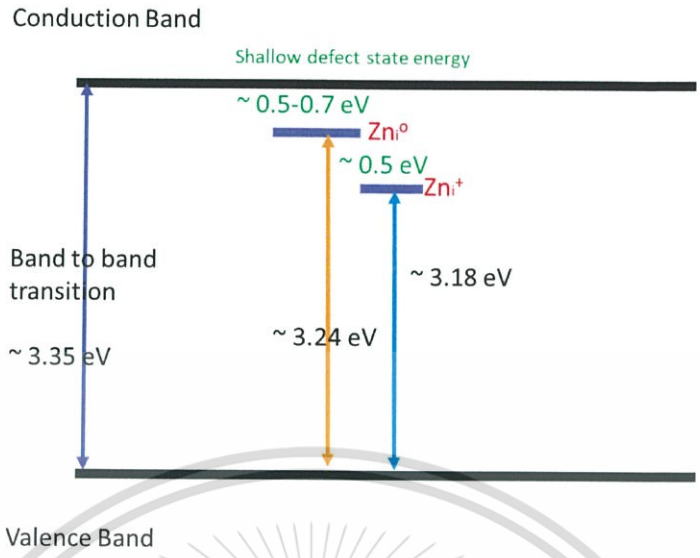

Figure 2.6 Schematic electronic level of ZnO structures [62].

2.5. Literature Reviews

In 2013, Thirunavukkarasu and Jothiramlingam [6] synthesized Ga-ZnO nanodisk/nanorods by hydrothermal process. They found that the growth of Ga-ZnO nanodisk/nanorods on AlN substrate were success when adding polymer assisted into Ga doped ZnO solution as shown in Figure 2.7. Moreover, they reported that 1% Ga doped ZnO thin films, 1% Ga doped ZnO nanorods and 1% Ga doped ZnO nanodisk/nanorods have a good sensing activity on UV light (Figure 2.8).

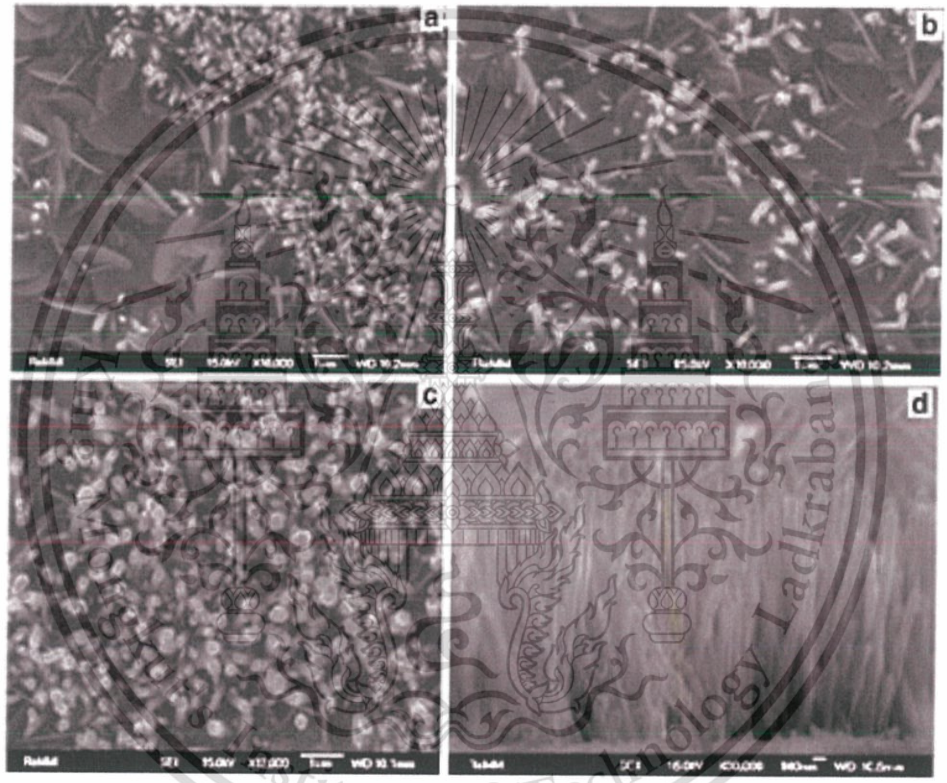

Figure 2.7 FE-SEM images of (a) 1% Ga-ZnO (0.2) nanodisk/rods, (b) 1% Ga-ZnO (0.2) at 3% polymer, (c) surface view of 1%Ga-ZnO (0.2) nanodisk/rods (0.2), and (d) cross sectional view of 1% Ga-ZnO (0.2) at 3% polymer concentration [6].

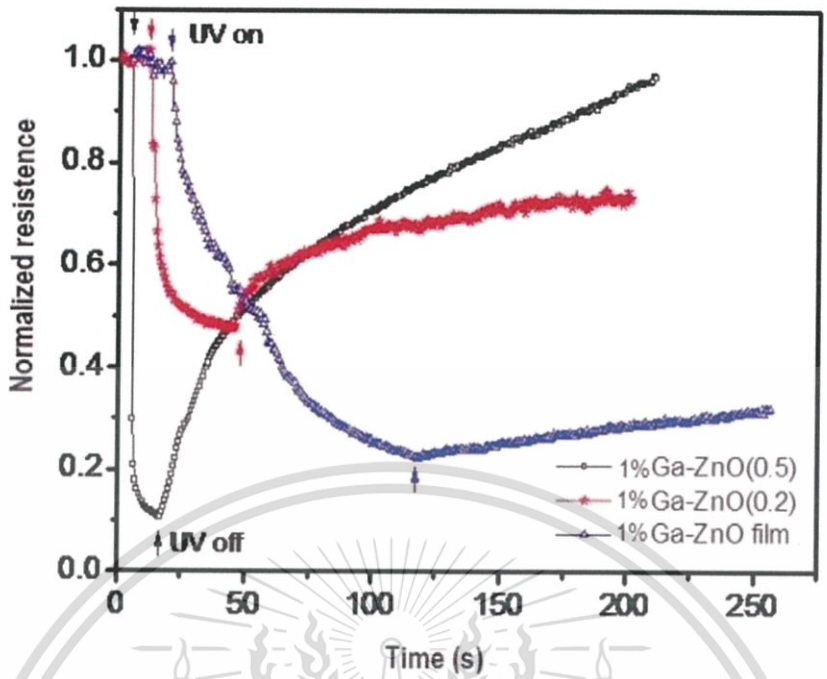

Figure 2.8 Efficiency of UV light sensor of (Black line) 1% Ga-ZnO (0.5) nanodisks, (Red line) 1% Ga-ZnO (0.2) nanodisk/rods and (Blue line) 1% Ga-ZnO film [6].

Moholkar et. al. [13] reported the effect of fluorine doping on highly transparent conductive tin oxide thin films. They found that the decreasing of sheet resistance about from 67.1 Ω to 3.42 Ω occurs when fluorine doping concentrations are increase. The high intensity of XRD patterns at (200) plane of the FTO thin films deposited with different fluorine doping concentrations were reported (as shown in figure 2.9 and figure 2.10).

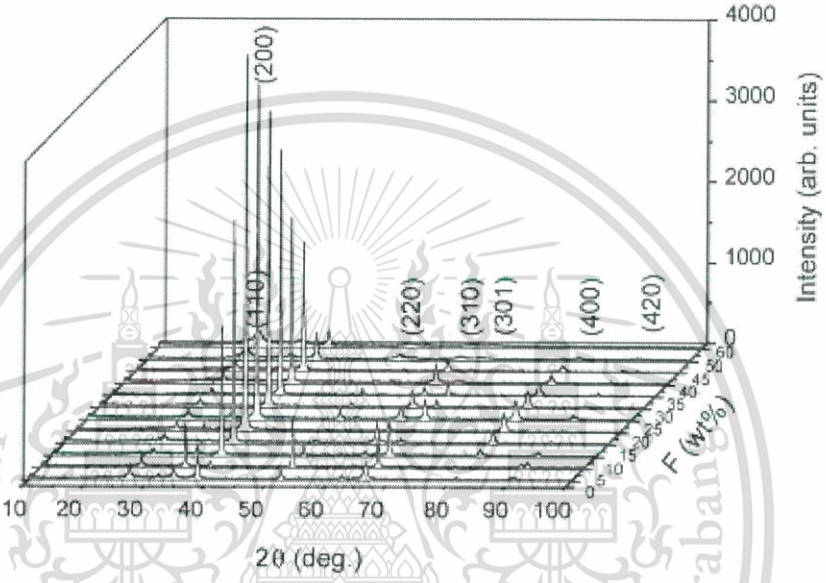

Figure 2.9 XRD patterns of FTO thin films growth with varies F concentrations [13].

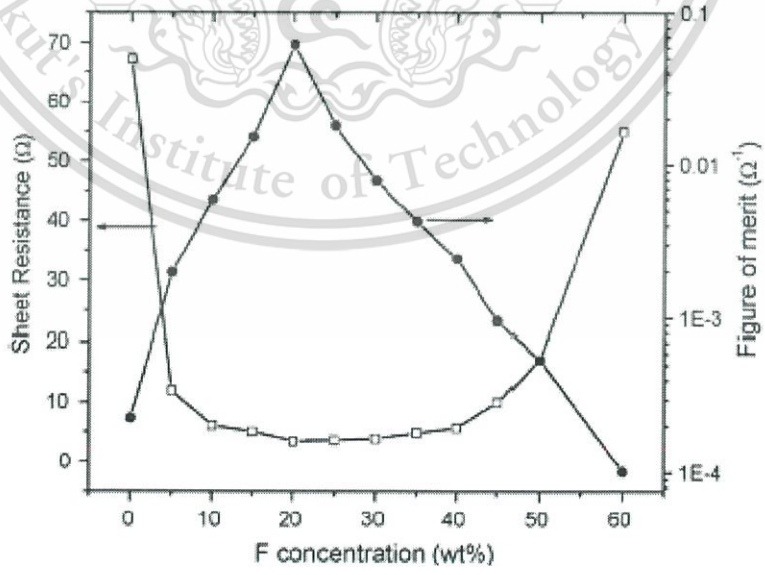

Figure 2.10 The sheet resistance and merit of F concentration [13].

In 2014, Pan et. al. [14] reported that the annealing temperature directly affects the structures and properties of AFZO (Al and F co-doped ZnO) nanostructures. The higher annealing temperature increases electrical resistivity, decreases in carrier concentration and decreases Hall mobility with associated of the larger crystal and low crystallinity of AFZO thin films. They found that AFZO thin films annealing temperature at 500 °C exhibited the best crystal quality that preferred the growth direction in (002) plane (highest intensity of the (002) peak (figure 2.11). At this condition, AFZO showed the better electrical resistivity at 1×10^{-3} Ω cm and the higher carrier concentration as shown in figure 2.12.

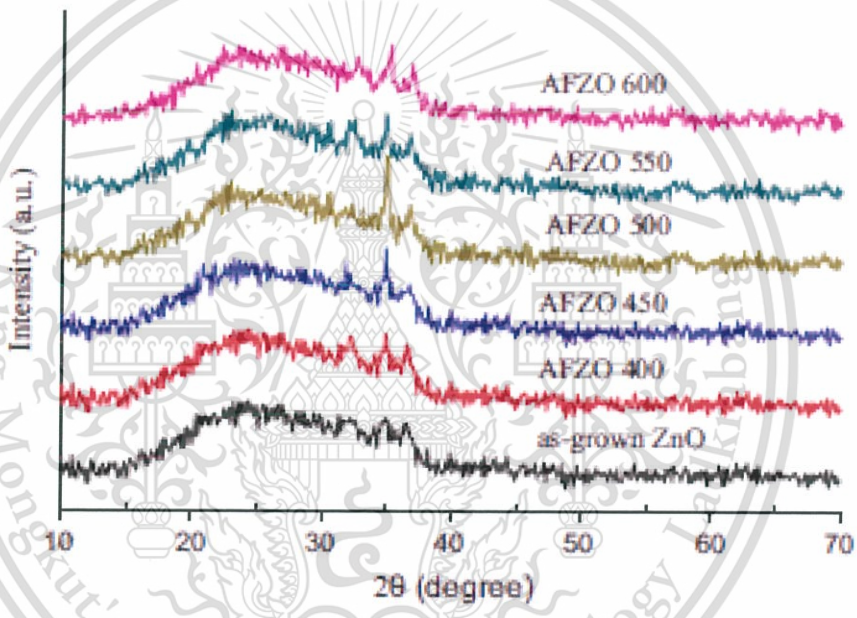

Figure 2.11 XRD patterns of ZnO and AFZO thin films [14].

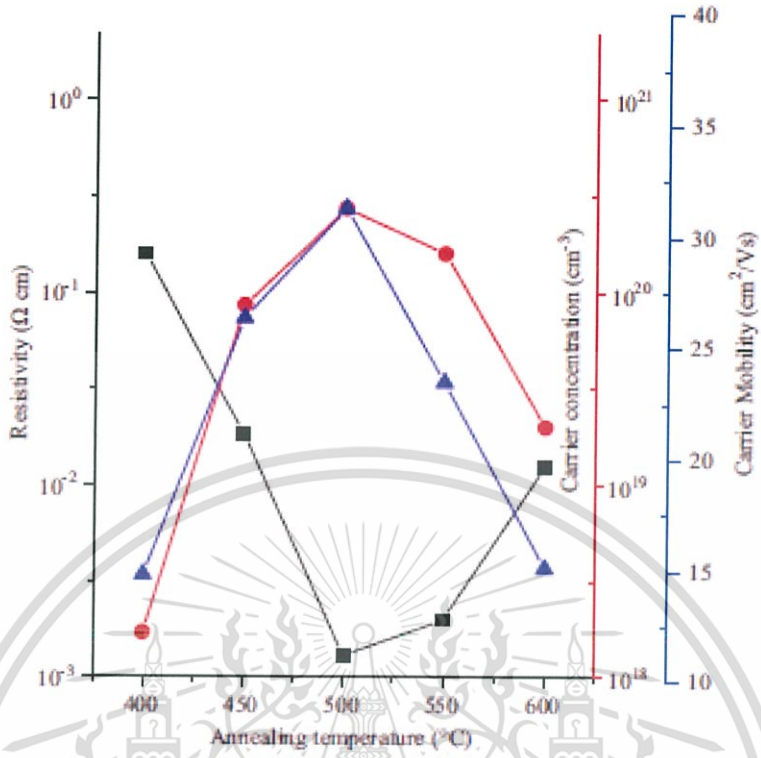

Figure 2.12 The resistivity(ρ), carrier concentration (n) and mobility (μ) of AFZO thin films [14].

Shin et. al. [15] report the characteristics of gallium and aluminum co-doped ZnO (GAZO) transparent thin films deposited by using the PLD process. The results as shown in figure 2.13 indicated the strong preferred orientation along the c-axis of the ZnO crystal (strong (002) and (004) peaks of X-ray patterns) Moreover, they reported that at deposition temperature of 400 °C, X-ray patterns showed high-quality hexagonal ZnO films because the full width half maximum (FWHM) value is about 0.20° (Figure 2.14 and 2.15).

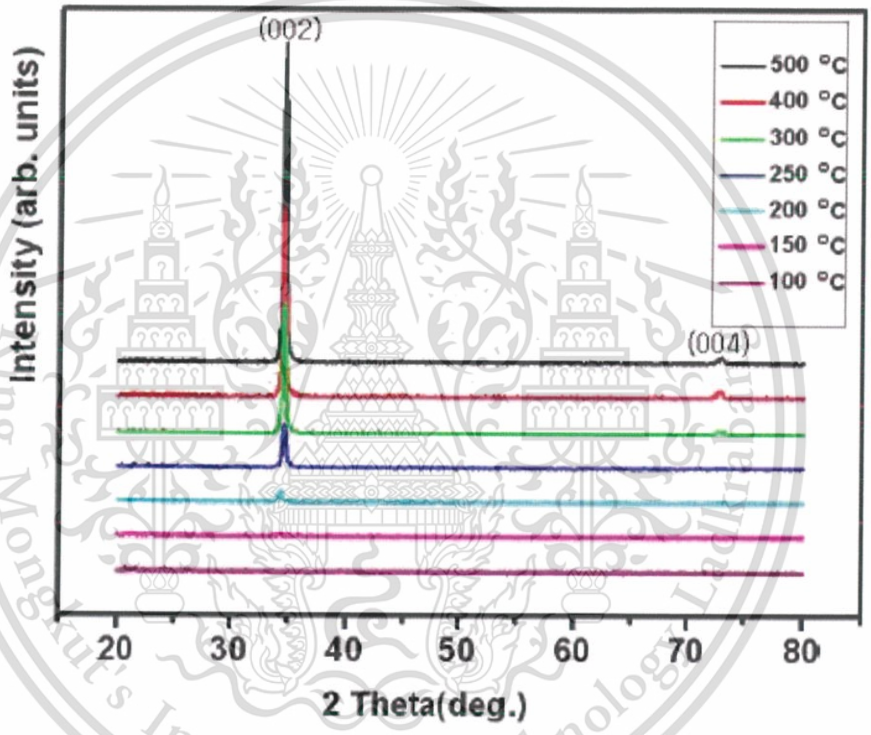

Figure 2.13 XRD patterns of the 1.5 at% Ga/Al doped ZnO (GAZO) thin films deposited [15].

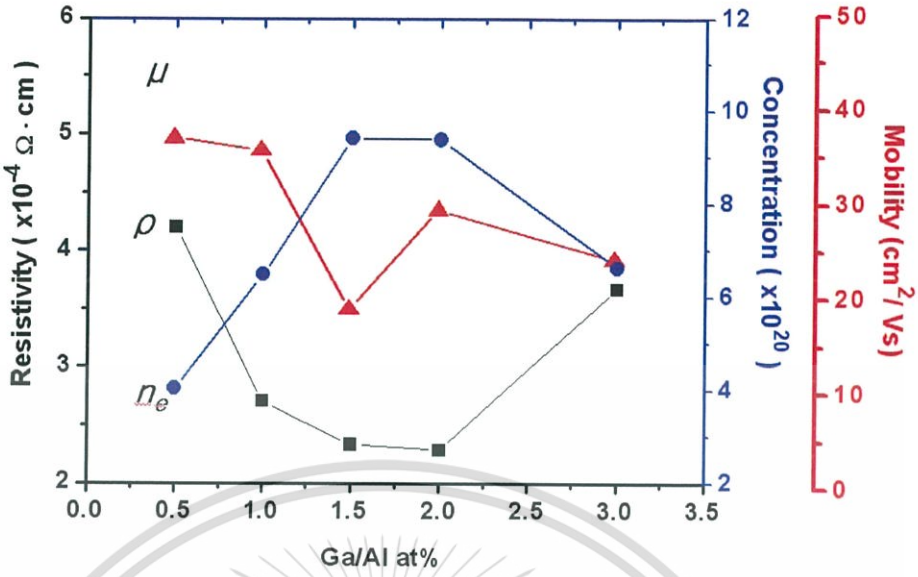

Figure 2.14 The resistivity, carrier concentration, and mobility of the GAZO thin films. The substrate temperatures of the samples were 400 °C [15].

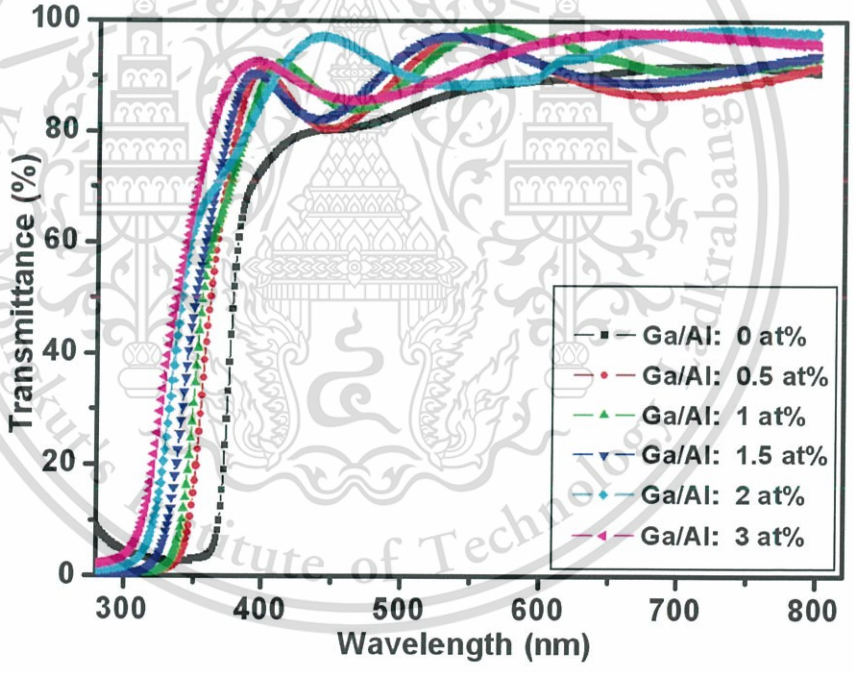

Figure 2.15 Optical transmittances of GAZO thin films [15].

In 2015, Pugalenthi et. al. [16] reported the effect of thickness on the properties of RF magnetron sputtered GZO thin films (structural, optical and electrical properties). The obtained XRD pattern indicates hexagonal wurtzite structure of the films and strong peak along (002) orientation as shown in figure 2.16. The growth along (002) orientation is generally influenced by the surface energy and the surface energy density of surface structure. In addition, the decreasing in resistivity of GZO film with difference thickness was mainly attributed to the better crystallization of the sample.

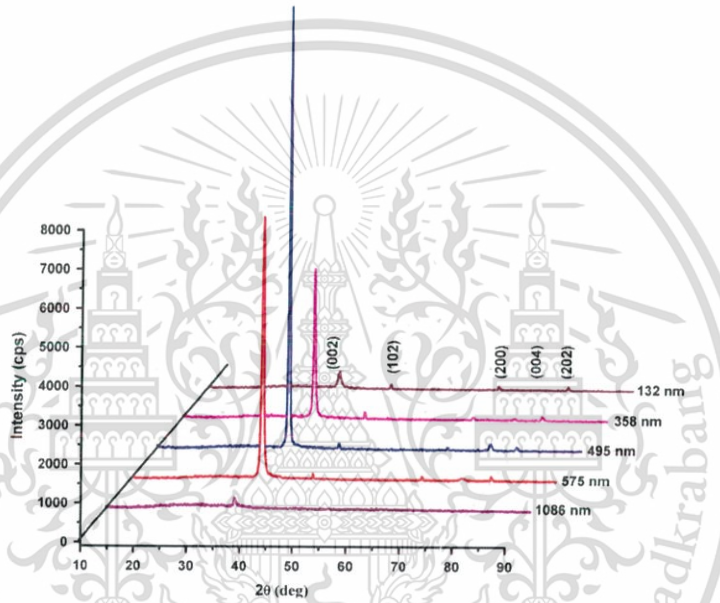

Figure 2.16 XRD pattern of GZO thin films [16].

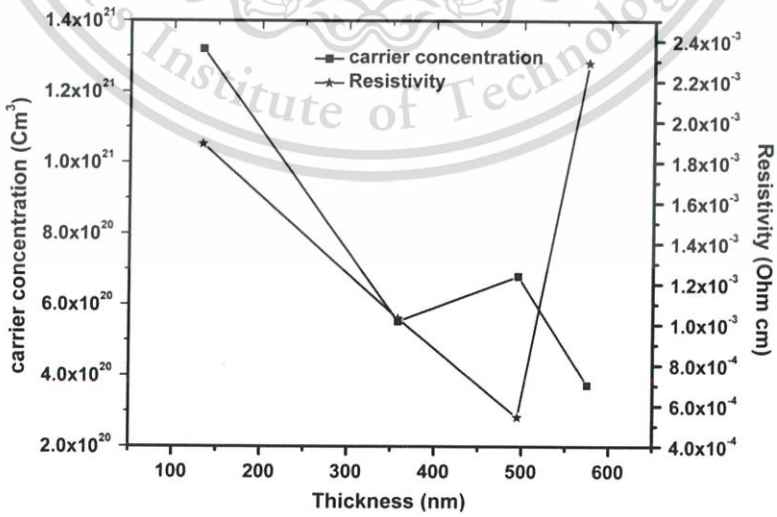

Figure 2.17 The carrier concentration and resistivity of GZO thin films [16].

Moreover, in 2016 Park et. al. [17] studied the effect of surface energy, annealing temperature on both ZnO seed layer formation and ZnO nanowire growth. They found that the UVO treatment and different $T_{annealing}$ conditions affected the growth density and aspect ratio of ZnO NWs on ZnO seed layer formation. The UVO treatment, moderately distributed higher density growth of ZnO NWs. Furthermore, the higher aspect ratio was observed in the case of different $T_{annealing}$ conditions for growth of ZnO NWs as shown in figure 2.18. Other research works are summarized in table 2.3.

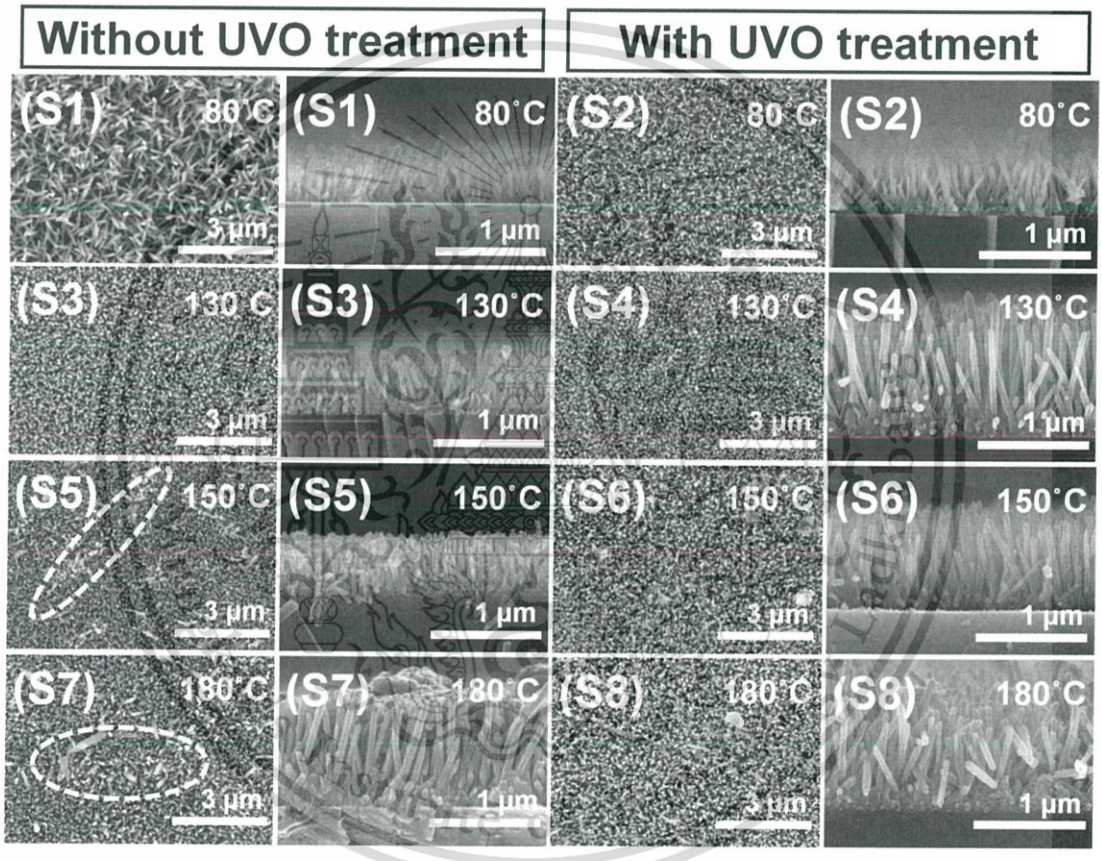

Figure 2.18 FE-SEM images of hydrothermally grown ZnO NWs on different seed layers prepared with different T annealing and UVO treatment conditions. The marked areas in samples S5 and S7 show the agglomerated regions in ZnO NW growth [17].

Table 2.3 Preparations of ZnO nanomaterials

System	Method	Remark	Author(s)
Al doped ZnO hexagonal nanoplastes on a zinc substrate	Hydrothermal process	- The charge compensation of anionic AlO_2^- at the Zn^{2+} surface of ZnO affects the formation of hexagonal nanoplates. - The blue shifts of PL spectra indicate the Al^{3+} doping into ZnO nanoplates.	Jia Liu, Lingling Xu, et. al. (2011) [18]
Y-doped ZnO nanorods	Hydrothermal process	- Yttrium-doped ZnO nanorods can be used as sensors for acetone, ammonia, benzene, formaldehyde, toluene and methanol with high selectivity.	Peng yu, Jing Wang, et. al. (2013) [19]
P-doped ZnO nanorods	Hydrothermal process	- P-doped ZnO nanorods can beused for LED applications.	Sanjit Sarkar and Durga Basak (2014) [20]

Cu-doped ZnO films	Radio frequency reactive magnetron sputtering	- Cu-doped ZnO films were deposited on p-Si substrates. - The blue-green emission had confirmed that the Cu^{+} and Cu^{2+} substitutions and interstitial into ZnO structures. - Cu-doped ZnO films show high UV photosensitivity.	F.M. Li, C.T. Zhu, et. al. (2013) [21]
Ga-doped ZnO nanosheets structure	Aqueous solution method.	- Ga-doped ZnO nanosheets were fabricated on a glass substrate. - Ga-doped ZnO nanosheets can be apply for UV photodetector.	Sheng-Joue Young and Yi-Hsing Liu. (2015) [22]
Fluorine doped ZnO thin films	Magnetron sputtering	- Fluorine doped ZnO films were prepared on corning glass. - FZO films shows the relatively low level of the carrier concentrations.	H.S. Yoon, K.S. Lee, et. al. (2008) [23]
Al and Ga co-doped ZnO thin films	Sol-gel method	- The single doped ZnO thin films (AZO and GZO) show the decrease of crystallinity, reduction of particle size and increase of the band gap values. - The co-doped AGZO thin films show lower electrical resistivity.	Reza Ebrahimifard, Mohammad Reza, et. al. (2014) [2]

ZnO nanowire arrays	Solvothermal method	- The self-seeded growth of ZnO nanowire on glass substrates were prepared by simple solvothermal method. - The sample shows hexagonal shaped and trapezoidal shaped of ZnO nanowire. - A model was proposed to analyze the photocurrent of ZnO nanowire in air and vacuum.	R. Ghosh, M. Dutta and D. Basak (2007) [24]
ZnO Nanostructures	Electrodeposition	- Electrodeposition method can be used to control the morphology of ZnO nanostructures from hexagonal rods to nanoneedles and rhombohedral rods.	Lifen Xu, Yi Guo, et. al. (2005) [25]
ZnO nanodisk, nanospindles and nanoflowers	Facile aqueous chemical method	- ZnO nanodisk, nanospindles and nanoflowers are synthesized by facile aqueous chemical method varied pH from 5 to 10 of HCl and ammonia. - The pH of the solution is the key factor to use to control the morphology of the obtained ZnO.	R.C. Pawar, J.S. Shaikh, et. al. (2012) [26]
ZnO Nanorods	Hydrothermal process	- Effects of the seed layer (ZnO, AZO and GZO seed layer) for growth of ZnO nanorods by hydrothermal process was reported. - Different seed layer affects the changes in	Jaejin Song and Sangwoo Lim (2007) [27]

		diameter, density and surface area of highly oriented ZnO nanorods.	
ZnO nanostructures	Hydrothermal process	- The growth of ZnO NWs on silicon substrates when vary seed layer thickness, seed layer annealing and different substrates were investigated. - Diameter, density and orientation of ZnO NWs can be controlled by vary seeding layer preparation conditions.	Eleni akarona, Barbara Athanassiou, et. al. (2015) [28]
ZnO:Ga Thin films	Radio frequency reactive magnetron sputtering	- The tilted columnar crystalline structure and inclined c-axis are related to substrate plane for growth ZnO:Ga thin films by Oblique Angle sputtering.	V. Tvarozek, I. Novotny, et. al. (2012) [29]

CHAPTER 3

RESEARCH METHODOLOGY

Chapter 3 explains the preparation of ZnO seeding layer and Ga/F co-doped ZnO nanostructures. For the preparation process, it can be divided into 3 steps, first step (topic3.1) is the film preparation by sol-gel method with dip coating step for seed layer formation. The second step (topic3.2) is preparation of solution for the growth of Ga/F co-doped ZnO nanostructures. The final step (topic3.3) is Ga/F co-doped ZnO nanostructures growth preparation by hydrothermal process.

3.1. Preparation of ZnO seeding layers

First, deionized water (DI) were used to clean glass substrates, then continue cleaning substrates by using 95% ethanol and acetone in an ultrasonic cleaner for 10 min, respectively. After that, dissolved zinc acetate dihydrate ($Zn(Ac)_2 \cdot 2H_2O$) and diethanolamine (DEA) in 100 mL absolute ethanol and stirred at 80 °C for 6 hr to use as the precursor solution for dip coating process. Finally, the cleaned glass substrates were dip-coated into the solution followed by a 15 min-annealing step on a hot-plate at 100 °C after each coating. Finally, annealing process in a furnace for 2 h. Moreover, we found that the ZnO seeding layers is an important parameter that affects the shape, density, alignment, crystallinity and preferred c-axis orientation of GFZO nanostructures formed during hydrothermal process. Thus, the ZnO seeding layers were prepared with various deposition conditions such as varied annealing temperature (200-500 °C), number of coating (5-15 times) and various UV-Ozone treatment durations (0-20 min) for the growth of GFZO nanostructures. The experiment procedure flow chart for the fabrication of ZnO seeding layers is illustrated in figure 3.1

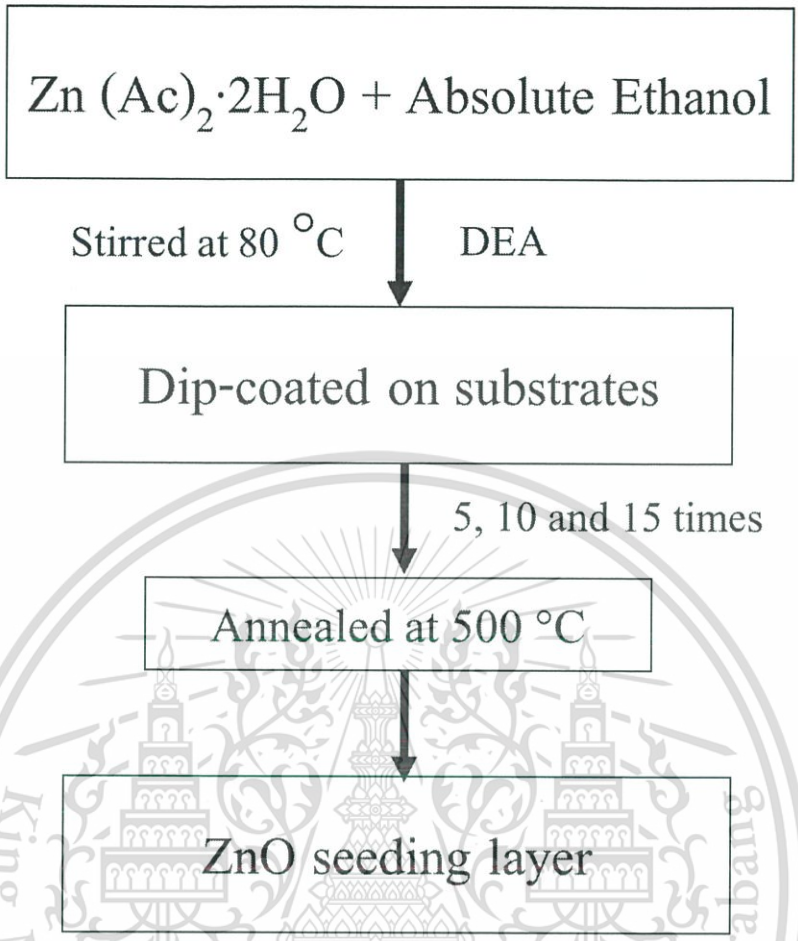

Figure 3.1 Flow chart for the preparation of ZnO seeding layers.

3.2. Preparation of Ga/F co-doped ZnO solution

For the growth of Ga/F co-doped ZnO nanostructures, figure 3.2 shows the experiment procedure flow chart for preparing Ga/F co-doped ZnO solution. It started with the preparation of 100 mL of 0.05 M zinc nitrate hexahydrate ($Zn(NO_3)_2 \cdot 6H_2O$), ammonium fluoride (NH_4F) as a F doping source, gallium (III) nitrate hydrate (GaN_3O_9) as a Ga doping source, and hexamethylenetetramine (HMTA). The concentration of gallium (III) nitrate hydrate and ammonium fluoride was varied at 1-5% and 1-5%, respectively.

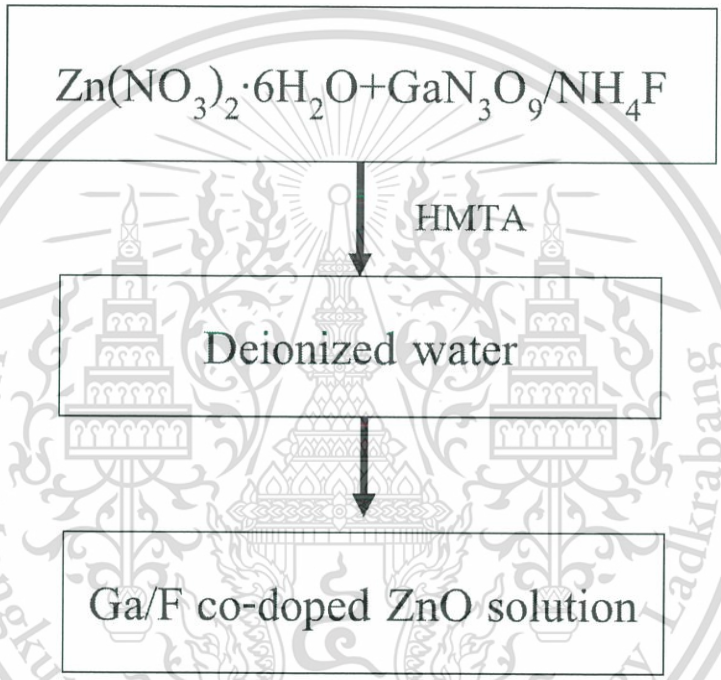

Figure 3.2 Flow chart for the preparation of Ga/F co-doped ZnO solution.

3.3. Preparation of Ga/F co-doped ZnO nanostructures

Figure 3.3 illustrates the experiment procedure diagram for the growth of Ga/F co-doped ZnO nanostructures grown on ZnO seeding layer. First, ZnO seeding layer was dipped into Ga/F co-doped ZnO solution and then loaded into a Teflon autoclave for the hydrothermal synthesis operating at 90°C for 2 hr. After the operation time was reached, the obtained white solid product was separated from the solution by ultrasonic and was washed with distilled water then dried in an oven at 100°C for 24 hr.

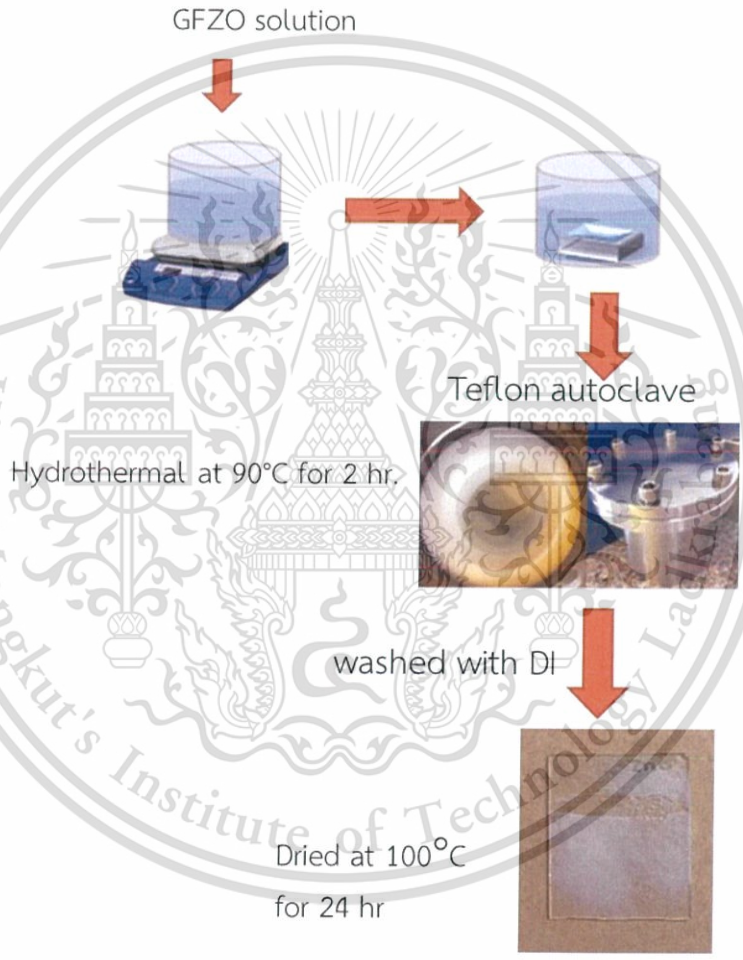

Figure 3.3 Diagram of Ga/F co-doped ZnO nanostructures.

3.4. Characterization

1. FE-SEM (JEOL JSM-7500F) was used to investigate morphologies of all samples. EDS (Bruker AXS Quanta 4010) was employed for confirming the existence of fluorine and gallium contents in the samples as shown in figure 3.4.

2. XRD (X'Pert PRO) was used to characterize the crystal structures of all samples as shown in figure 3.5.

3. Optical transmittance (T) measurement was carried out using a spectrophotometer (Thermo electron corporation) as shown in figure 3.6.

4. Photoluminescence spectroscopy (set up at Shizuoka university) was used to detect the luminescence of all samples in order to investigate the effect of Ga and F dopants (shown in figure 3.7).

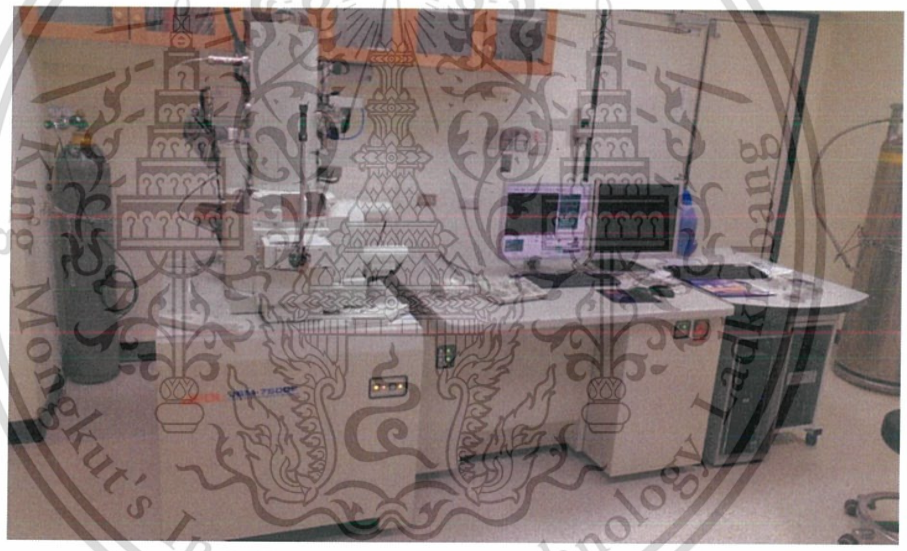

Figure 3.4 Field Emission Scanning Electron Microscope (JEOL JSM-7500F).

Figure 3.5 X-ray diffractometer (X'Pert PRO).

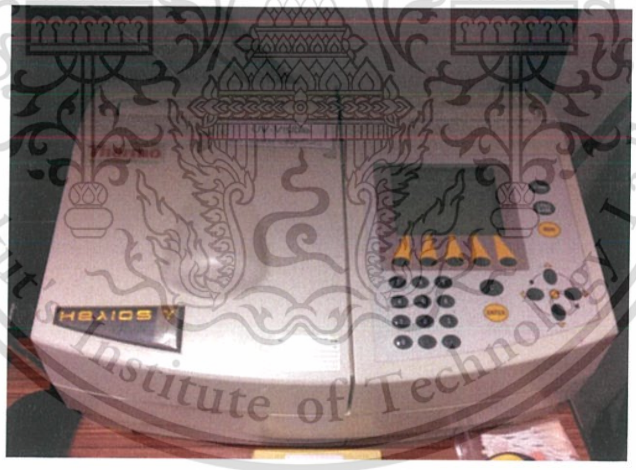

Figure 3.6 UV-vis spectrometer (Thermo electron corporation).

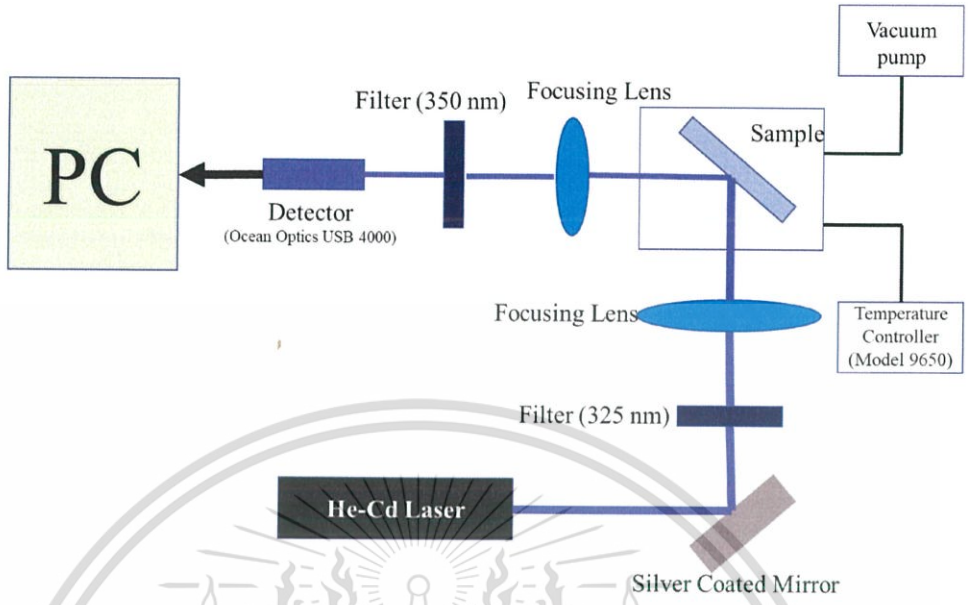

Figure 3.7 Photoluminescence spectroscopy set up at Shizuoka university.

CHAPTER 4

RESULTS AND DISCUSSION

The influence of crucial process parameters including Ga and F dopants, seeding layer thickness, seed layer annealing temperature and tilted-angle of seeding layer on relevant physical properties of the grown materials were experimentally conducted and investigated. The results evidently disclosed that Ga and F dopants have strong influence not only in an alternation of its morphological properties including shape, size and density but also in the structural defect-related optical properties of grown structures. Meanwhile, growth direction and morphology of the hydrothermally grown structures were significantly affected by number of coating layers, seed layer annealing temperature and tilted-angle of seeding layer. We found that the ZnO seeding layers is an important parameter that affects the shape, density, alignment, crystallinity and preferred c-axis orientation of GFZO nanostructures formed during hydrothermal process. FE-SEM was used to investigate the morphologies of all samples. EDS was employed for confirming the existence and content of relevant elements in the samples. XRD was used to characterize the crystal structures of all samples. The photoluminescence spectroscopy was conducted to investigate the defect induced by dopant in the sample. Helium-cadmium laser (λ = 325 nm) was used as optical excitation source in photoluminescence (PL) experiment. Each sample was cooled down from room temperature (RT) to 25 K in a typical cryostat. Fiber optic spectrophotometer (Ocean Optics Inc. USB 4000) was used to collect the luminescence signal.

4.1 Preparation of ZnO seeding layer

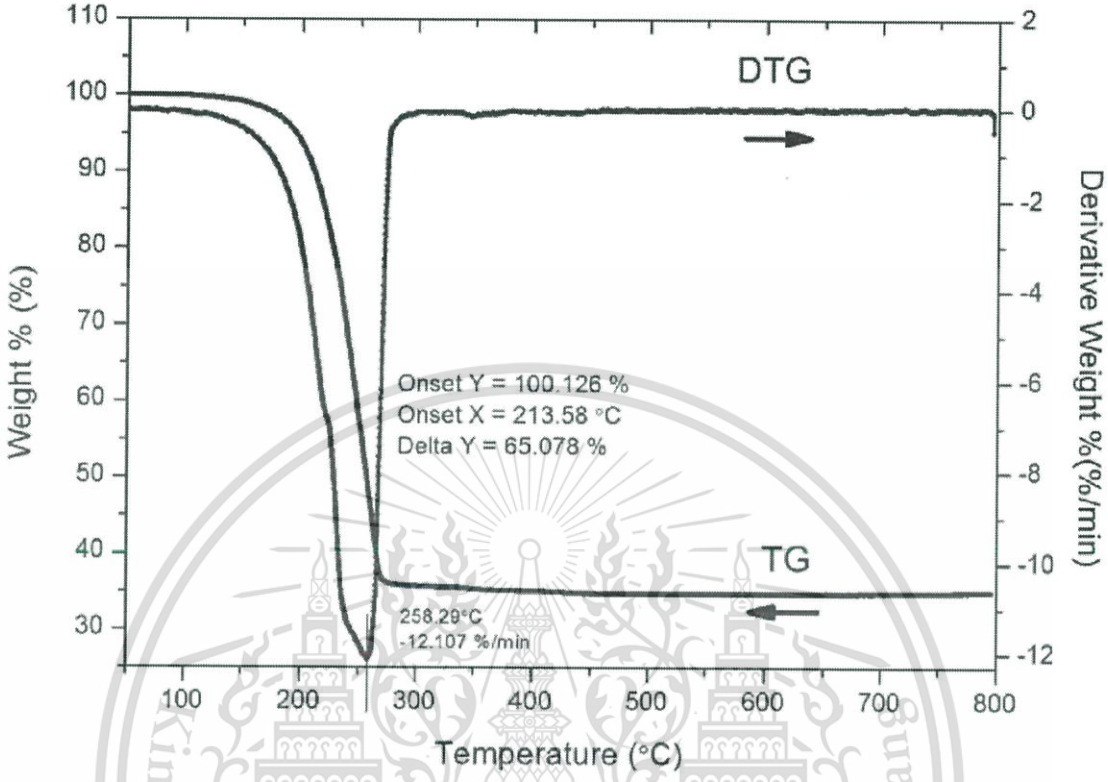

Figure 4.1 TG-DTA data of zinc acetate precursor.

The differential temperature analysis (DTA) and thermogravimetric analysis (TG) are shown in figure 4.1. The differential temperature analyses were measured to investigate thermal behavior of zinc acetate dehydrate $(CH_3COO)_2Zn{\cdot}2H_2O$ solution. As observed in figure 4.1, the weight loss (~ 60%) of differential temperature analysis range 200 °C–250 °C was accredited to the loss of acetate groups. In addition, thermal decomposition curve at 258.29 °C in TG curve shows the decomposition of organic residuals [30-33]. Moreover, insignificant change of TG result beyond this temperature is noticed, indicating the good thermal stability of the last product of this starting precursor. This feature suggests that zinc acetate precursor can be chosen as sol-gel based precursor for ZnO seed layer with high stability beyond certain decomposition temperature.

4.1.1 The effects of annealing temperature on physical properties of ZnO seed layers

Partial results of the presented work have been published in:
Journal of Nanoscience and Nanotechnology Vol. 18, 7296–7301, 2018

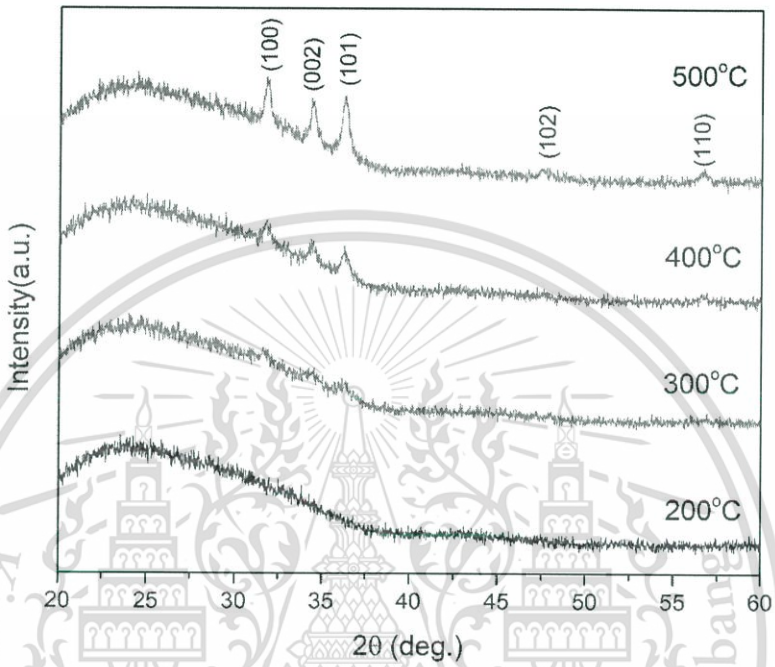

Figure 4.2 XRD patterns of ZnO seed layers annealed at different temperatures of 200-500°C.

Figure 4.2 shows XRD graphs of deposited ZnO seed layers by the dip coating process (at 200°C, 300°C, 400°C and 500°C annealing temperature). The results show that at 200°C, the amorphous phase of the seed layer is indicated because no noticeable diffracted peak is observed. At 300°C and 400°C, the diffraction patterns of ZnO began to appear. This feature specifies the change of the seed structure from amorphous phase to polycrystalline phase ZnO. The diffraction peaks became pronounced and distinct as annealing temperature was further increased at 500°C due to the better ZnO crystallization. The (100), (002) and (101) peaks are positioned at 2θ = 31.8°, 34.5° and 36.2°, respectively. The orientation informed by XRD data of samples annealed at this temperature range indicates the polycrystalline nature of these seed layers that are well agreeable to JCPDS Card No. 36-1451[34]. The crystal size can

be calculated from the XRD spectra following the Scherrer's relation expressed in equation (4.1).

$$D = \frac{K\lambda}{\beta \cos\theta}. \quad (4.1)$$

Where λ is the wavelength of Cu $K\alpha$ (0.154 nm), D is the sample crystallite size, shape factor constant K is 0.9, β is the full-width at half maximum (FWHM), and θ is the Bragg angle. It is obviously noticed the significant increasing of the seeding layer crystal size from 12.36 nm to 26.23 nm when increasing annealing temperature from 400°C to 500°C.

Moreover, the effect of annealing temperature on the structural and morphological of ZnO seed layers for growth of GFZO nanostructures was studied and corresponding results are shown in figure 4.3 and figure 4.4. The X-ray diffraction patterns of 5G3FZO nanostructures grown on ZnO seed layers with different temperatures are displayed in figure 4.3. With different annealing temperatures, the characteristic peaks indicate that wurtzite structure of 5G3FZO nanostructures are successfully fabricated on ZnO seed layers. Regarding to the difference in XRD patterns, it is suggested that seed layer with different annealing temperature has strong influence on crystallinity and preferred orientation direction of the grown structure. At annealing temperature of 200-300°C, no any characteristic peak of ZnO was observed, reflecting to imperfection of crystal growth or amorphous phase of the product. As the annealing temperature was raised to 400°C, corresponding XRD pattern indicated the crystal growth of hexagonal wurtzite ZnO structure without preferable growth direction onto the seeding layer. After the annealing temperature of seed layer elevated to 500°C, the hydrothermally grown structure had wurtzite structure with (002) preferable growth direction, implying the vertically-aligned rod structures of the product.

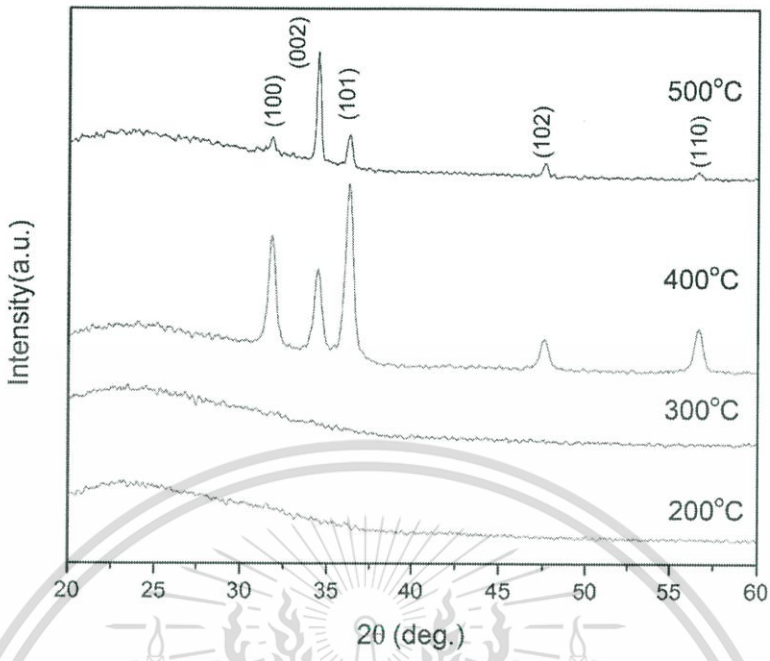

Figure 4.3 XRD patterns of 5G3FZO nanostructures annealed with different temperatures of 200-500°C.

Moreover, no second phase of impurity was detected in XRD pattern, suggesting good incorporation of the dopants in ZnO structure. In addition, the lattice constant, *c*, of the (0 0 2) plane was evaluated by following equation:

$$c = \frac{\lambda}{\sin\theta} \tag{4.2}$$

Another important parameter is the strain ε_{zz} along the c-axis that can be calculated using the following formula.

$$\varepsilon_{zz} = \frac{C - C_o}{C_o} \times 100 \tag{4.3}$$

where standard lattice constant C_o is 0.5206 nm.

Table 4.1 shows the c-axis lengths for 5G3FZO nanostructures grown on ZnO seed layers at annealing temperature at 400-500°C that calculated using the standard equation for the wurtzite crystal structure. These results show the effect of seed

annealing temperatures. The nanostructures could grow with different values of c-axis lattice parameter. The strain values along the c-axis (ε_{zz}) of the seed layer has been calculated. In typical, strain ε_{zz} of the seed layer is considered to be one crucial factor that has momentous influence on the grown structural properties on the layer due to the lattice mismatch of two materials. However, it has been also proved that at early stages of the deposition when the crystallite sizes are small enough, a tensile stress of the film can be developed due to the attraction forces between grain boundary atoms. The morphologies of 5G3FZO nanostructures grown on ZnO seed layers annealed at 200 °C, 300 °C, 400 °C and 500 °C, measured by FE-SEM are shown in figure 4.4. Increase annealing temperature of seed layer shows the structure of 5G3FZO nanodisks has been changed to nanorods hexagonal-like structure [36]. The diameters and length of 5G3FZO nanorods evaluated from SEM image are found to be in the range of 50-200 nm and approximately 1 μm, respectively. During GFZO nanostructures growth, the increase in annealing temperature gives the positive effect of enhancing strain of the ZnO seed layers performing as the active nucleation sites. ZnO seed layers annealed at 500 °C is the best conditions for growth of 5G3FZO nanorods. In this research used this condition anyway.

Table 4.1 Structural properties of 5G3FZO nanostructures deposited on ZnO seeding layer at different annealing temperatures.

Seed layers annealing Temp. (°C)	$2\theta_{(002)}$ (°)	FWHM (°)	C (Å)	D(nm)	Strain ε_{zz} (%)
400	34.40	0.488	5.210	15.54	0.0901
500	34.46	0.281	5.443	26.98	0.0945

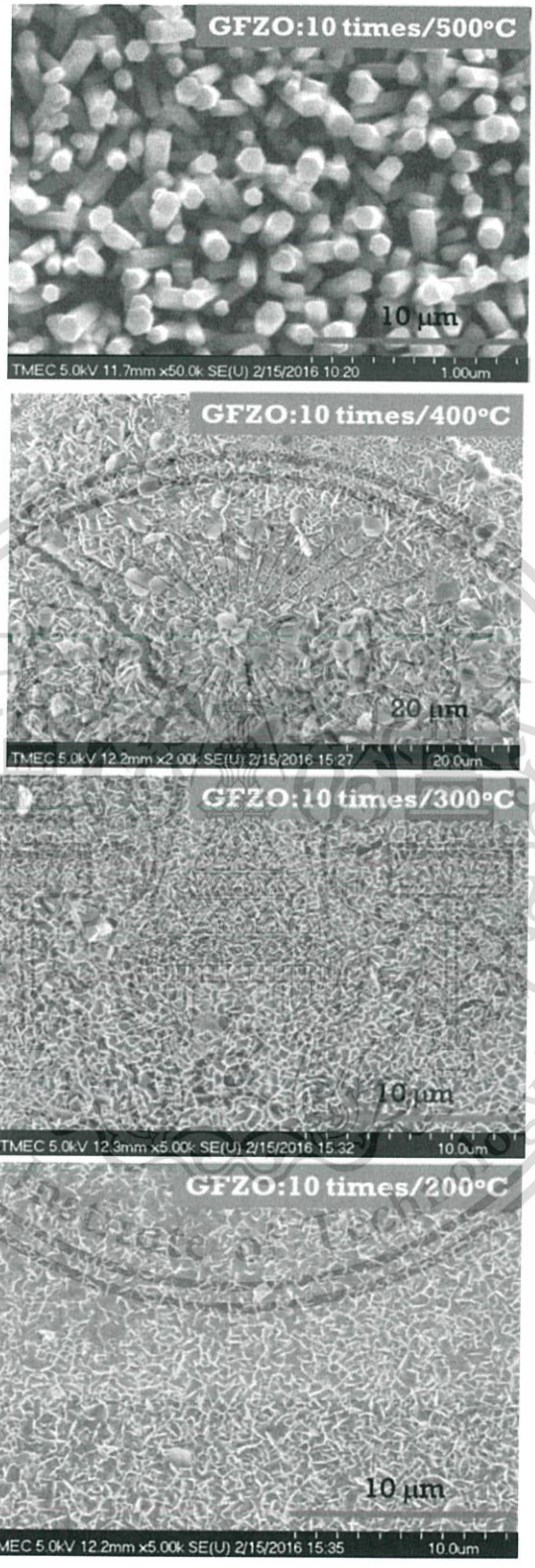

Figure 4.4 FE-SEM images of 5G3FZO nanostructures with the different annealing temperature of seed layer as 200-500°C.

4.1.2 The effect of number of coating layer on physical properties of ZnO seed layers

Partial results of the presented work have been published in:
Materials Today: Proceedings 4 (2017) 6129–6133

The morphological and structural properties of seed layers with different number of coating layers were determined using XRD and FE-SEM measurements as shown in figure 4.5 and figure 4.6, respectively. Figure 4.5 shows the X-ray diffraction patterns of ZnO seed layers with 5, 10 and 15 coating times and annealed at 500°C. A broad XRD pattern appeared in all samples in the low 2θ region ranging from 20° to 40° attributes to a typical diffraction pattern of a glass substrate. XRD results indicate the characteristic phase of wurzite-ZnO (100), (002) and (101) positioned at 2θ = 31.8°, 34.5° and 36.2°, respectively [35]. It was observed that the peak intensities of characteristic XRD peaks and crystallinity of ZnO thin films are stronger as the films are assembled with more thicknesses. The wurtzite structure of ZnO formed by the tetrahedral sp^3 –hybridization shows the parallel direction of each apex to the c axis. ZnO thin films are subject to grow toward the (002) direction [37-40]. The crystallite size of ZnO seed layers prepared at different coating times was calculated using the Scherrer's formula as shown in the equation (4.1). Figure 4.6 shows the change in crystallite size depending on the number of coating time. The size of the crystal increases as the coating time or thickness of the ZnO seed layers increases. The cross-section images of the seed layers with various coating times revealed from FE-SEM images in Figure 4.7 exhibit quite uniform crystal grains, which is in good agreement with the results calculated by XRD pattern. It is also noticed from both FE-SEM and calculated results that its crystallite size significantly increases as the number of dip coating increases. From cross-sectional FE-SEM images, the average number of coating layers of the ZnO seed layers was increased from 165 nm, 186 nm and 228 nm with increasing number of coating from five, ten and fifteen times, respectively. The number of the coating has a significant influence on the geometrical characteristic of the ZnO-based nanorods as well as the alignment, which becomes more directional and vertical with increasing number of coating layers of seed layers. Thus, the study of effect number of coating layers on structure and morphology

of ZnO seed layers for growth of GFZO nanostructures are shows in figure 4.8 to figure 4.9.

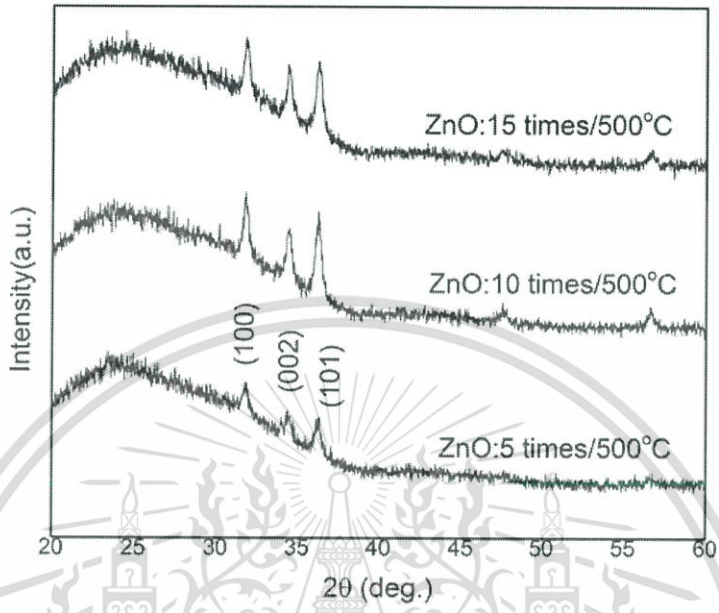

Figure 4.5 XRD patterns of ZnO seed layers when the seed layers were dip-coated for 5 to 15 times and annealed at 500°C.

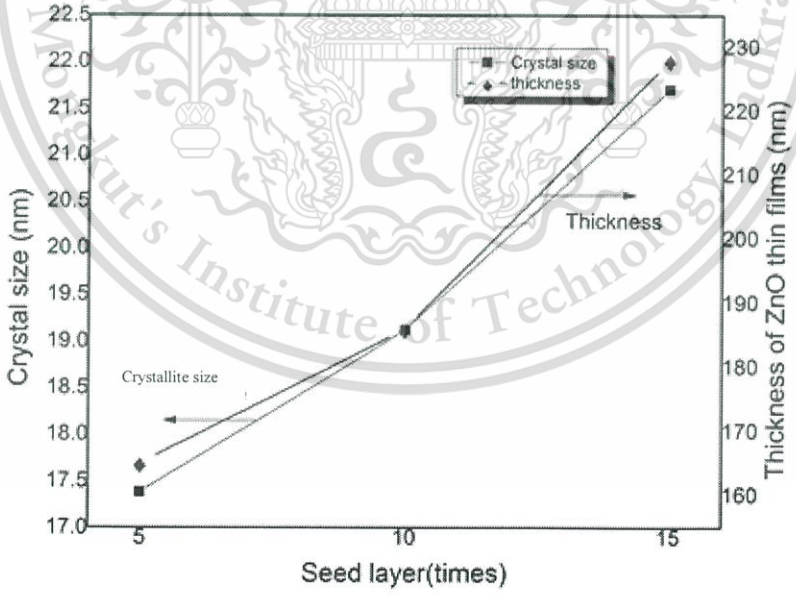

Figure 4.6 Crystal sizes and thickness of ZnO seed layers of solution was dip-coated 5 to 15 times and annealed at 500°C.

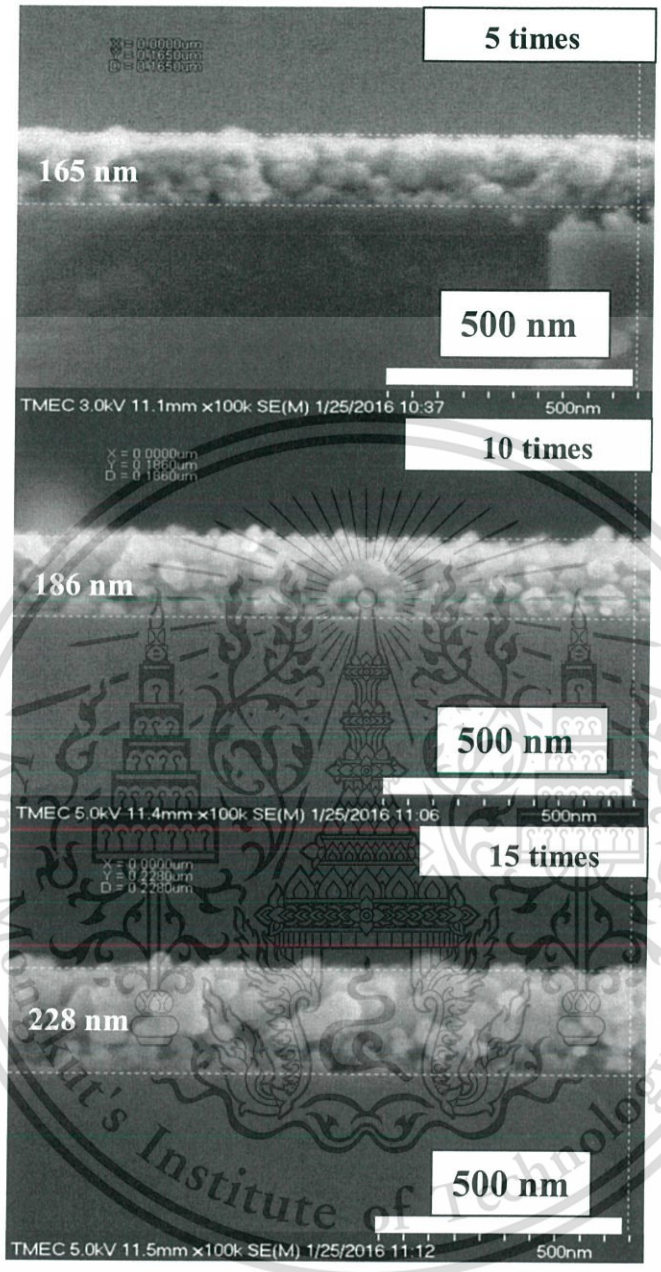

Figure 4.7 FE-SEM images of ZnO seed layers when the seeding layer solution was dip-coated for 5 to 15 times.

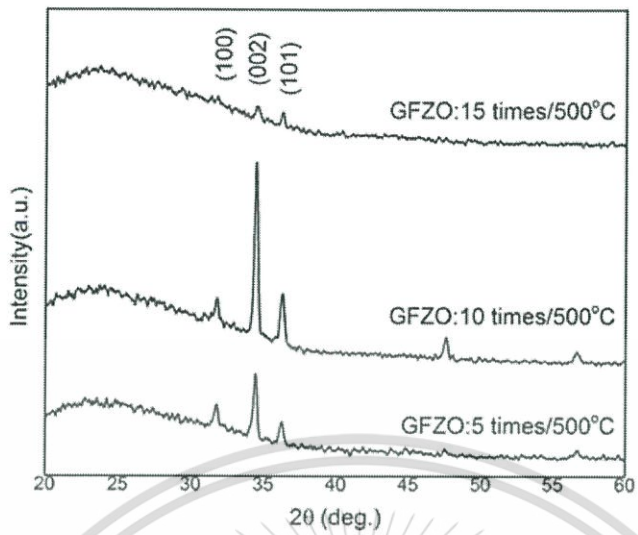

Figure 4.8 XRD patterns of GFZO nanostructures when the seed layers were dip-coated for 5 to 15 times.

The XRD patterns of GFZO nanorods grown on seed layers with different number of coating layers are shown in figure 4.8. XRD analysis reveals that the growth of GFZO nanorods occurs mainly along the (002) direction, which may lead to the highest growth of GFZO nanorods. The broader (002) orientation peaks of the ZnO seed layers at five and fifteen times are the results of the smaller and bigger crystal sizes compared to the ZnO seed layers deposited at ten times of coating, which is the main reason for the higher density of nanorods. Top view and cross-sectional FE-SEM images of GFZO nanorods grown on glass substrates when the seeding layer solution was dip-coated for 5, 10, and 15 times, and annealed at 500°C are shown in figure 4.9. The hexagonal pillars with a flat facet surface of GFZO nanorods were grown in vertical direction. It is also clear that ZnO seed layers with various number of coating affect the size and orientation of the nanorods. The GFZO nanorods active nucleation sites possess higher density with an increase in the ZnO seed layers number of coating at ten times. The cross-sectional analyses illustrate that the hydrothermally grown GFZO forms the large area of uniform rods with an average length of ~613 nm (for five times of coating) and ~343 nm (for ten times of coating). ZnO seed layers at ten times is the best conditions for growth of 5G3FZO nanorods. In this research used this condition anyway.

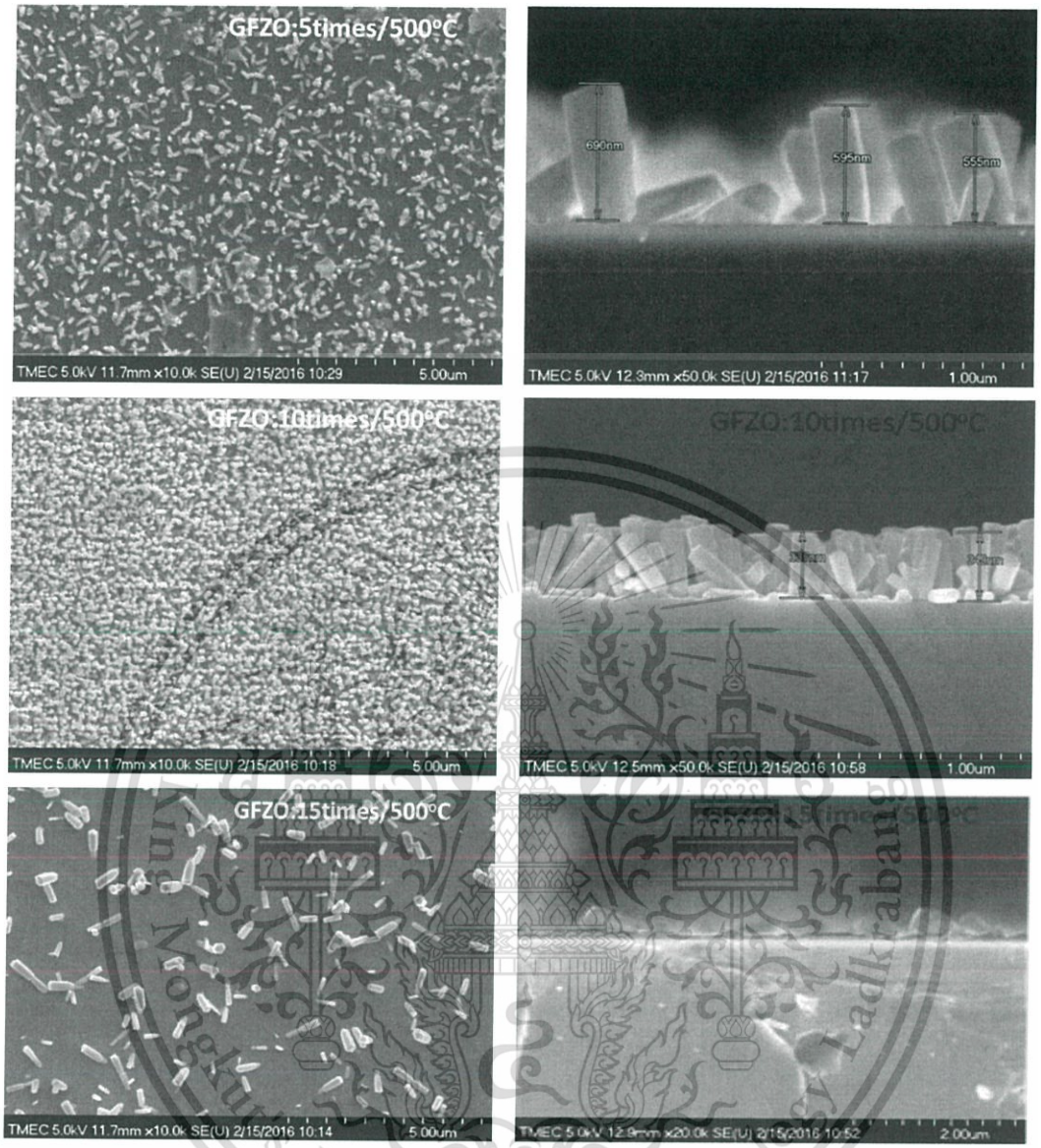

Figure 4.9 FE-SEM images of GFZO nanostructures when the seeding layer solution was dip-coated for 5 to 15 times.

4.1.3 Physical, optical and morphological properties of ZnO seed layers

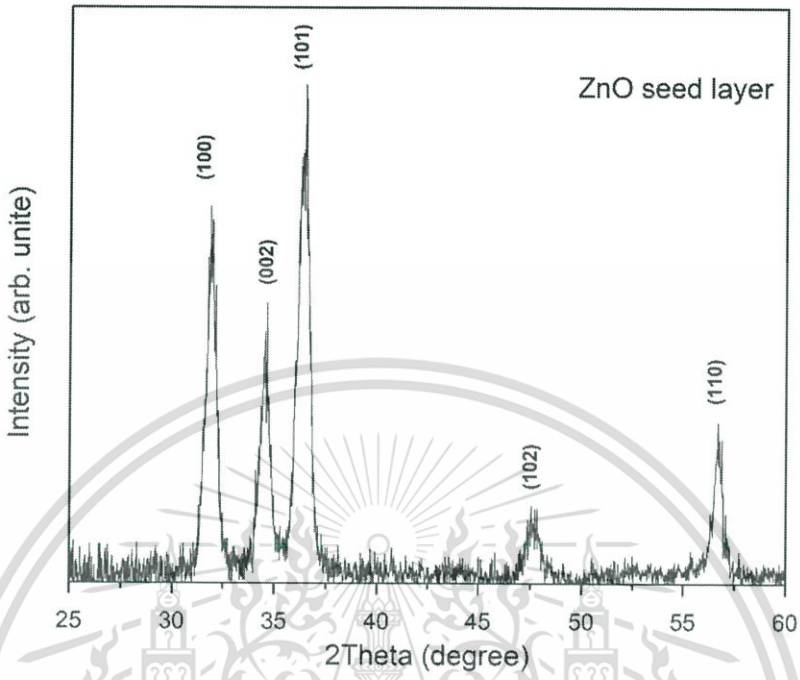

Figure 4.10 XRD patterns of ZnO seed layer.

Figure 4.10 shows the X-ray diffraction patterns of ZnO seed layer when the seeding layer solution was dip-coated at 10 times and annealed at 500°C. XRD results indicate the characteristic phase of wurtzite ZnO (100), (002), (101), (102) and (110) centered at 2θ =31.8°, 34.5°, 36.2°, 47.1° and 56.2°, respectively (JCPDS card No. 36-1451) [35]. In addition, the XRD result confirms the formation of ZnO structure of the seed layer without any preferential grown direction. The crystal sizes of ZnO seed layers was calculated using the Scherrer's formula as shown in the equation (4.1). The crystal size of the particles can be calculated from the full width at half maximum (FWHM) and angular position of the (100), (002), and (101) diffraction peak. The average crystal size of ZnO seeding film layer is found to be altered from 20 to 30 nm. The optical transmission spectra of ZnO seed layer at room temperature is shown in figure 4.11 The transmission spectra indicate sharp absorption edge in the vicinity of 370 nm. To calculate the energy ga (E_g) of the ZnO seed layer, the absorption coefficient was estimated using the following relation:

$$\alpha = \frac{1}{D} In(\frac{1}{T}) \quad (4.4)$$

Where α is absorption coefficient, T is transmittance, and D is thickness of the film.

The E_g for a direct transition is given by:

$$h\nu = A(h\nu - Eg)^{1/2} \quad (4.5)$$

where A is a constant, and $h\nu$ is the incident photon energy.

A semiconductor absorbs the light below a threshold wavelength (λc), i.e., [$h\nu \geq E_g$] or

$$h\nu = \frac{1240}{\lambda} \quad (4.6)$$

The E_g of the samples was derived by plotting the Tauc's formula and taking the extrapolation of the linear portion from the plot of $(\alpha h\nu)^2$ versus the photon energy ($h\nu$), as shown in figure 4.12 The E_g is 3.28 eV of ZnO seed layer confirming the good formation of ZnO.

The FE-SEM image of ZnO seed layer is shown in figure 4.13. The FE-SEM image shows that the smooth surface and uniform grain size that is in good agreement with the results revealed by XRD pattern. The incorporation of Zn and O is confirmed by the EDS result as shown in figure 4.14. The table inserted in the figure (inset of figure 4.14) shows the content of the elements presented in the ZnO seed layer. The elemental content of the marked area is as follows: Zn = 13.063 wt.% and O = 28.608 wt.%. In the EDS spectrum, numerous well-defined peaks for Zn and O clearly indicate that the ZnO seed layer is made of Zn and O. No other peaks related to impurities were detected in the spectrum, confirming that the synthesized seed layers are ZnO.

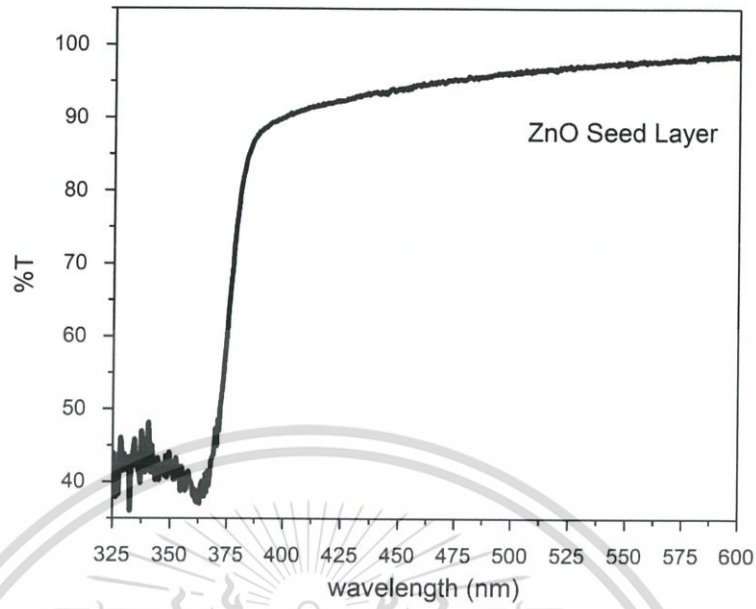

Figure 4.11 Transmission spectra of ZnO seed layer when the thin film solution was dip-coated at 10 times and annealed at 500°C.

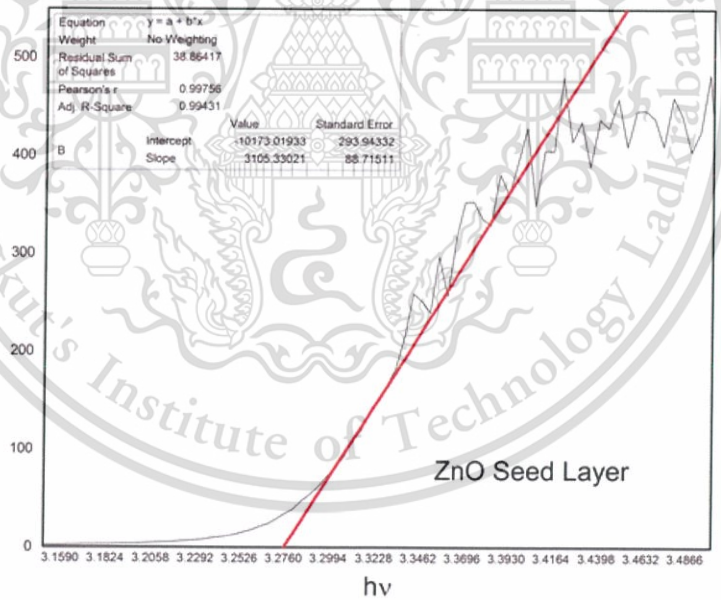

Figure 4.12 The energy gap (E_g) of ZnO seed layer when the thin film solution was dip-coated at 10 times and annealed at 500°C.

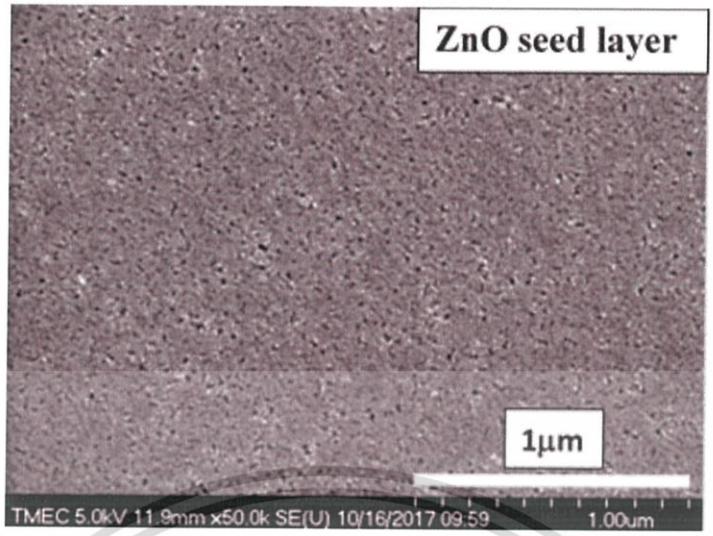

Figure 4.13 FE-SEM images of ZnO seed layer when the thin film solution was dip-coated at 10 times and annealed at 500°C.

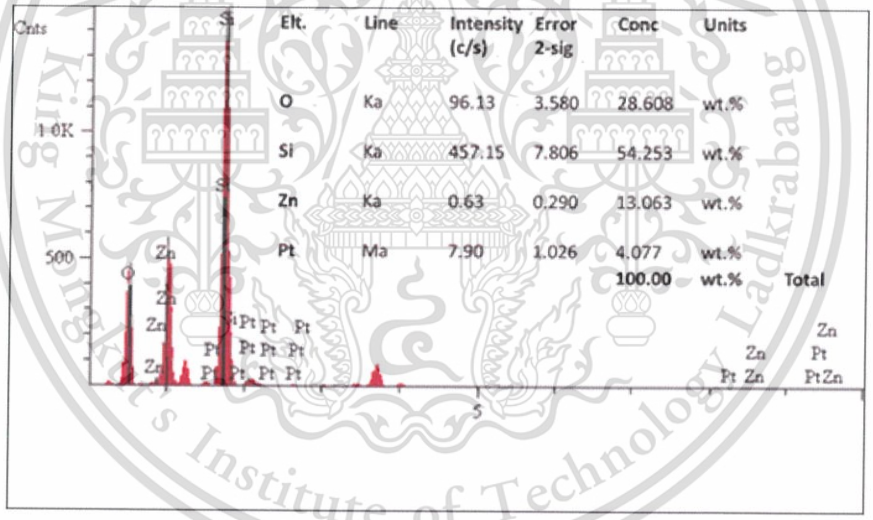

Figure 4.14 EDS spectrum of ZnO seed layer.

4.1.4 The effect of UV-Ozone treatment on ZnO seed layers

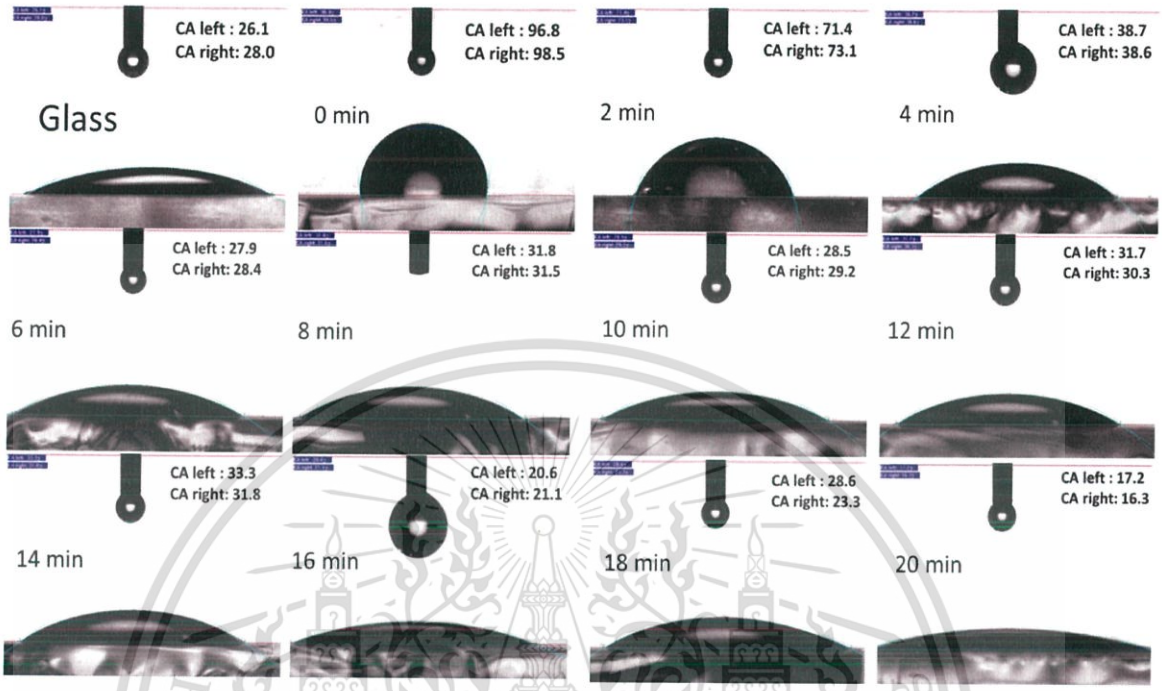

Figure 4.15 Contact angles between water droplets on glass and ZnO seed layers with various UV-Ozone exposure times.

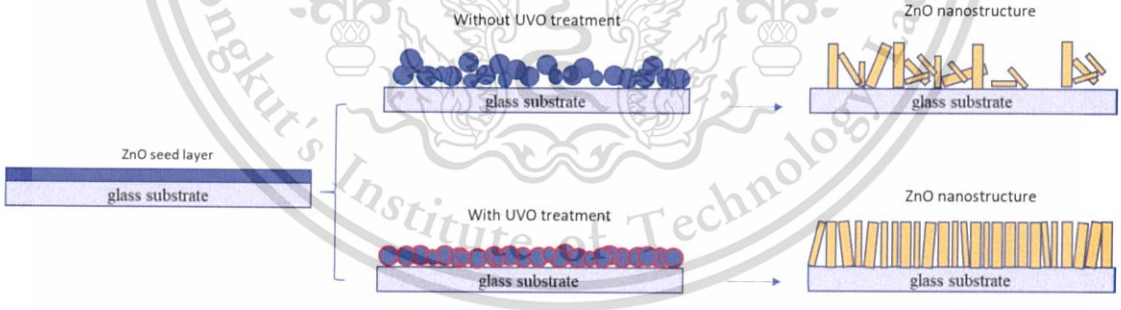

Figure 4.16 Schematic of the best condition for grown of ZnO nanostructures.

In this work, we found the low surface wettability of GFZO nanostructures on ZnO seed layers when the thin film solution was dip-coated at 10 times and annealed at 500°C. Therefore, the effect of surface wettability for high density of GFZO nanostructures on ZnO seed layers that can be modified by UV-Ozone treatment was

investigated. The surface wettability is measured by water contact angle. Figure 4.15 shows contact angle between water droplets on glass and ZnO seed layers with various UV-Ozone times of 0 to 20 min. The sample treated with UV-Ozone exposure for 0 and 2 min shows hydrophobicity on ZnO seed layer with corresponding water contact angle of about 97° and 72°, respectively. After treatment for 4 to 20 min, hydrophilic surface was obtained accompanying water contact angle of 38° to 17°, respectively. The results show that the smaller contact angle can be obtained with longer treatment times. It is confirmed that the surface cleanliness and surface wettability can be improved by using this technique. Generally, the irradiated wavelengths of UV-Ozone system are about 185 nm to 254 nm. At the wavelength of 200 nm [41-43], oxygen free radicals are formed from the oxygen molecule (O_2) dissociation due to the photon energy. Then O2 on the surface are reduced. These generated oxygen radicals are intended to further create hydroxyl group at the surface, which directly enhances surface wettability. Figure 4.16 shows the schematic drawing of related possible mechanism. In our method, the best condition of high density, high surface wettability and uniform for ZnO nanostructures on ZnO seed layers are dip-coated at 10 times, annealed at 500°C and UV-Ozone treatment at 20 min. Figure 4.17 shows the X-ray diffraction patterns of GFZO nanostructures grown on ZnO seed layers modified by UV-Ozone treatment. XRD results indicate the characteristic phase of wurzite-ZnO (100), (002) and (101) positioned at 2θ = 31.8°, 34.5° and 36.2°, respectively [35]. At certain treatment times, the peak intensities of characteristic XRD peaks and crystallinity of GFZO nanostructures are stronger. The UV-Ozone treatment times at 18 and 20 min show the strong diffraction (002) peak, which indicates highest crystallinity growth of GFZO nanorods and a stable phase in the ZnO seed layers. As shown in figure 4.18, 4.19, 4.20 and 4.21, the FE-SEM images the GFZO nanostructures grown on ZnO seed layers modified by UV-Ozone treatment. In the case of UV-Ozone treatment at 2, 10 and 18 min (as shown in figure 4.18, 4.19 and 4.20), non-uniform and lower density of GFZO nanostructures growth on the ZnO seed layer were observed. The nucleation site density of the wettability on the ZnO seed layers were insufficient to growth of GFZO nanostructures because of a lower bonding energy for the ZnO seed molecules. The sample with UV-Ozone treatment for 20 min in

figure 4.21 shows product with uniformity and the highest density growth of GFZO nanostructures that can increase the wettability number due to OH groups and higher bonding energy of the ZnO active nucleation sites. It is suggested that the UV-Ozone treatment process is considered to be a simple and efficient method to prepare GFZO nanostructures on ZnO seeding layer. The incorporation of Ga, F, Zn and O is confirmed by the EDS results as shown in figure 4.22.

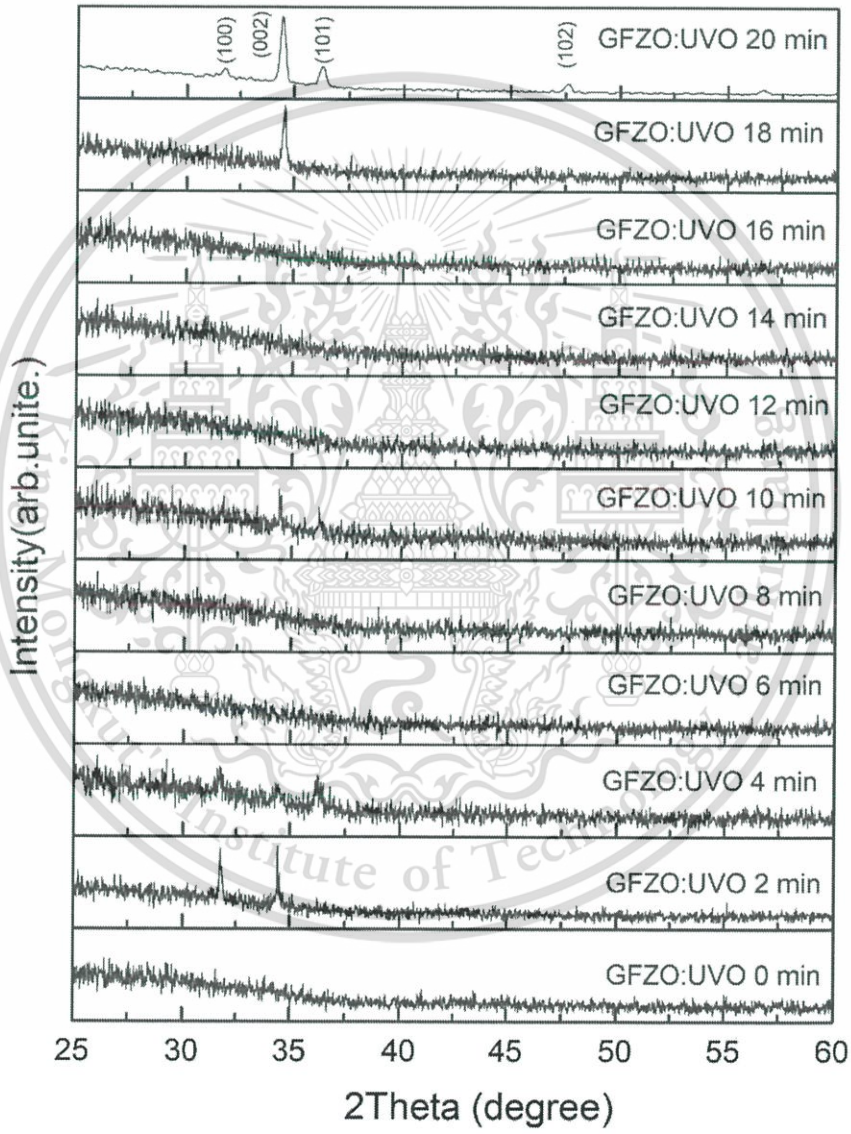

Figure 4.17 XRD patterns of GFZO nanostructures at various UV-Ozone treatments.

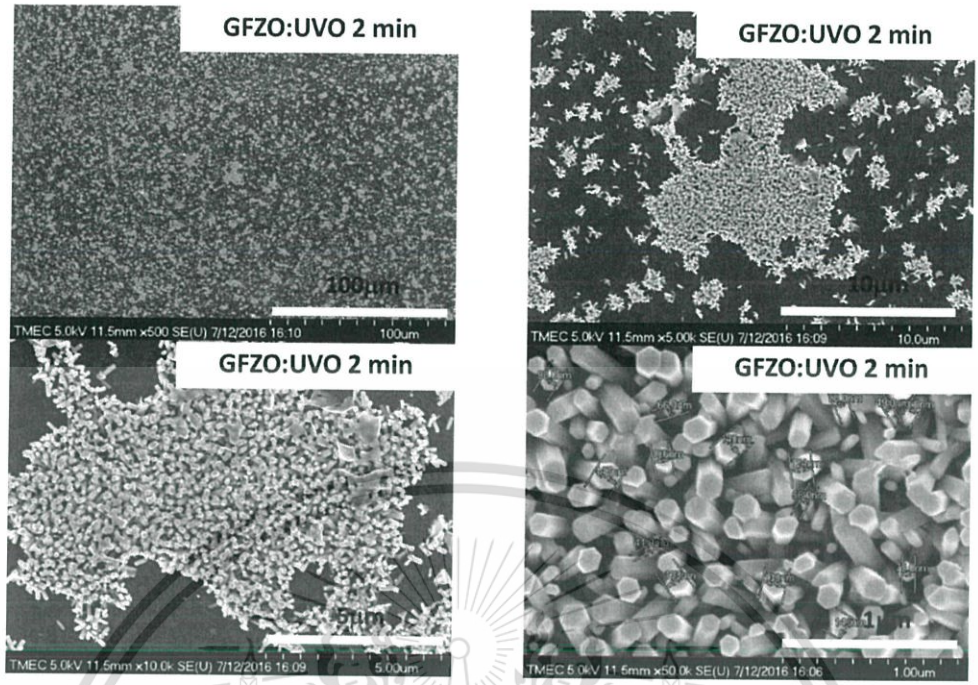

Figure 4.18 FE-SEM micrographs of GFZO nanorods grown on ZnO seed layers after UV-Ozone treatment at 2 min.

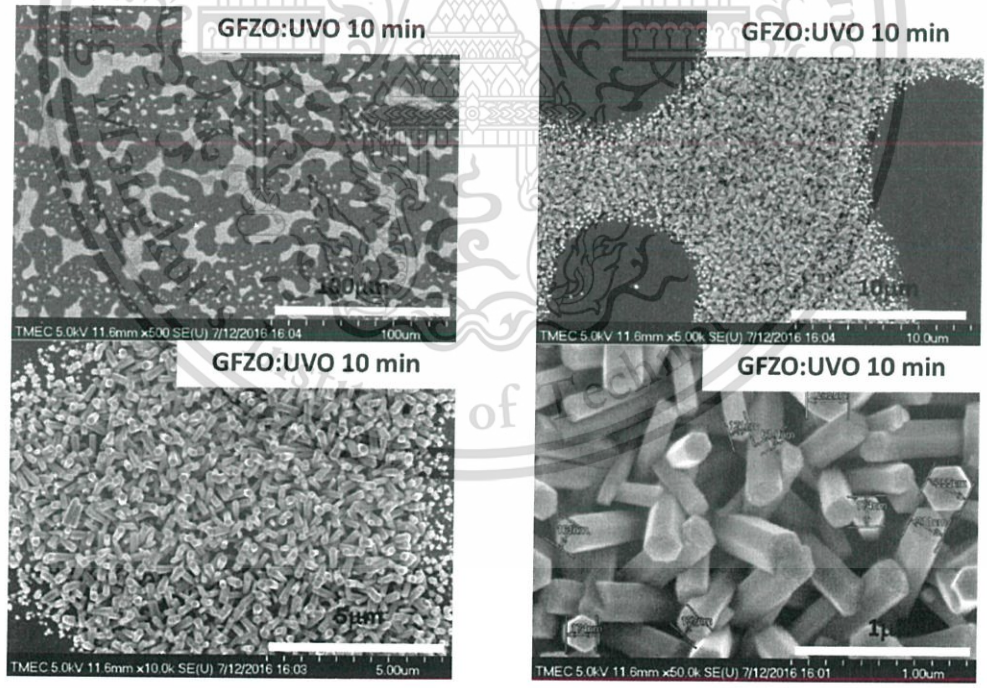

Figure 4.19 FE-SEM micrographs of GFZO nanorods grown on ZnO seed layers after UV-Ozone treatment at 10 min.

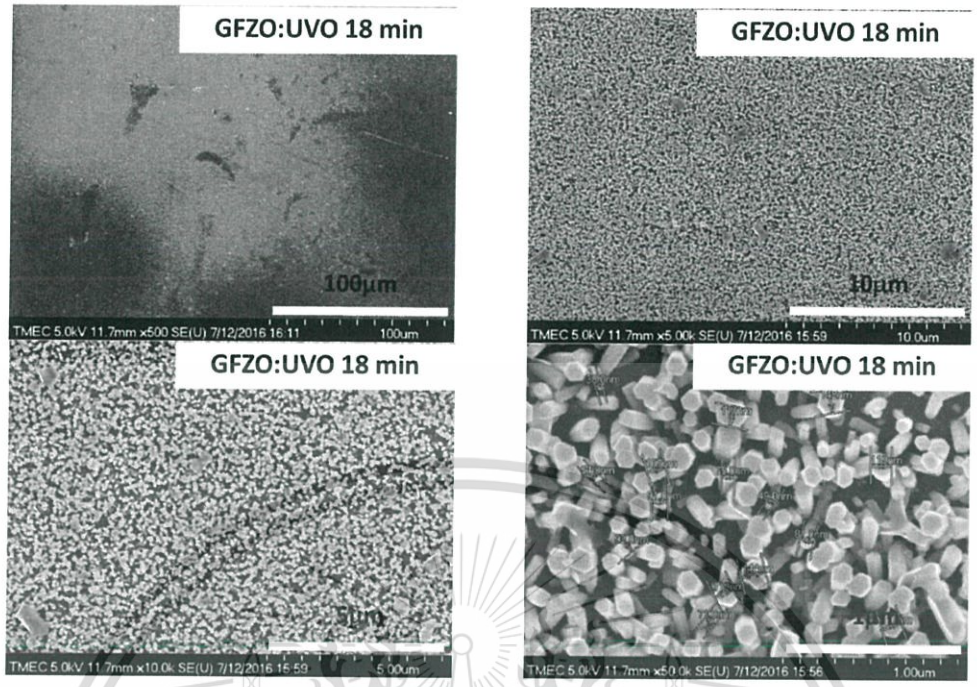

Figure. 4.20 FE-SEM micrographs of GFZO nanorods grown on ZnO seed layers after UV-Ozone treatment at 18 min.

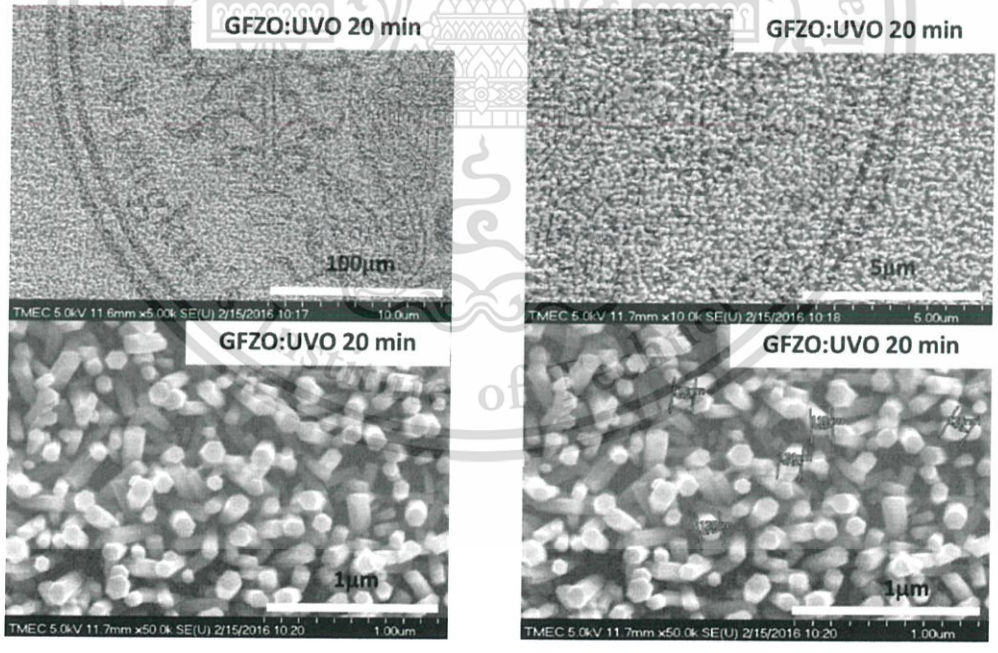

Figure 4.21 FE-SEM micrographs of GFZO nanorods grown on ZnO seed layers after UV-Ozone treatment at 20 min.

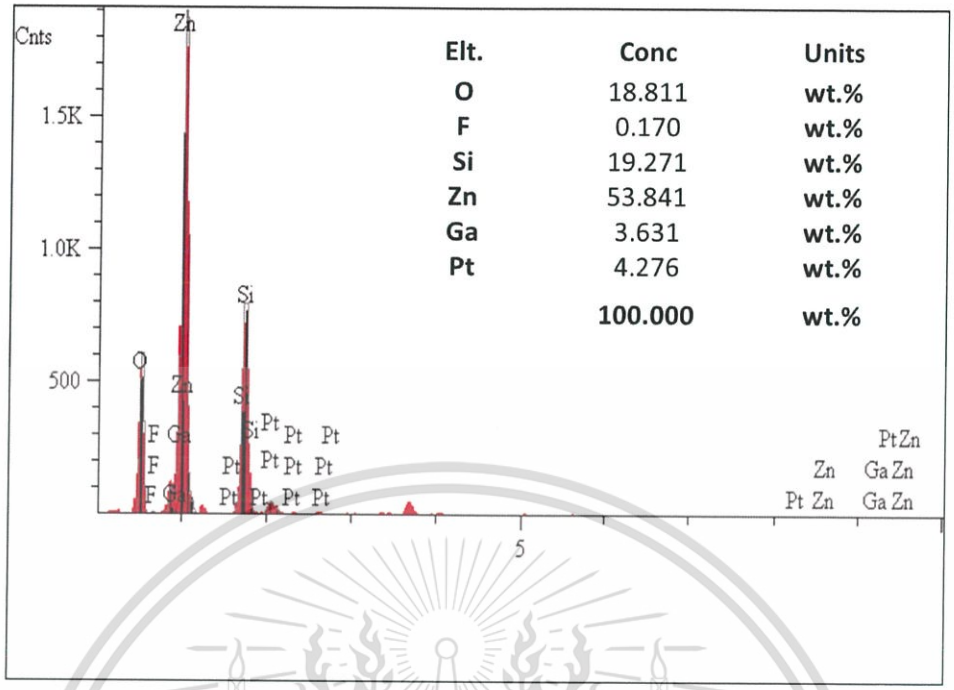

Elt.	Conc	Units
O	18.811	wt.%
F	0.170	wt.%
Si	19.271	wt.%
Zn	53.841	wt.%
Ga	3.631	wt.%
Pt	4.276	wt.%
	100.000	wt.%

Figure 4.22 EDS spectrum of Ga-F co-doped ZnO nanostructures.

It is found that the ZnO seeding layer thickness with ten times of coating, annealed at 500 °C and UV-Ozone treatment for 20 min is considered to be optimized condition to obtained well-defined GFZO nanostructures with high uniformity and density.

4.1.5 The effects of Ga and F doping concentration into ZnO structures

Partial results of the presented work have been published in:
Journal of Nanoscience and Nanotechnology Vol. 16, (2016) 12962–12966.

During hydrothermal process, the formation of ZnO nanostructures are possibly proceeded via the following mechanisms and corresponding equations (4.7) to (4.12): First, $Zn(NO_3)_2$ precursor is dissolved and provides zinc ions as noticed in equation (4.7). Ammonia molecules (NH_3) and hydroxide ions (HO^-), provided by HMTA following equations (4.8) and (4.9). NH_3 and HO^-, abundant in the mixed aqueous solution can react with zinc ions to initially create $Zn(OH)_2$ as expressed in equation (4.10). This intermediate product can be further dissolved by reacting with superfluous HO^- ions and $Zn(OH)_4^{2-}$ solution is consequently achieved following equation (4.11). In the hydrothermal process, the $Zn(OH)_4^{2-}$ would undergo the dehydration process via equation (4.12) to be transformed into ZnO nuclei simultaneously. Under extreme hydrothermal conditions, these ZnO nuclei could be self-assembled to form the rod-like nanostructures along a preferred axis orientation depending upon growth conditions.

$$Zn(NO_3)_2 \rightarrow Zn^{2+} + 2NO_3^- \quad (4.7)$$

$$C_6H_{12}N_4 + 6H_2O \leftrightarrow 6HCHO + 4NH_3 \quad (4.8)$$

$$NH_3 + H_2O \leftrightarrow NH_4 + OH^- \quad (4.9)$$

$$Zn^{2+} + 2OH^- \rightarrow Zn(OH)_2 \downarrow \quad (4.10)$$

$$Zn(OH)_2 + 2OH^- \rightarrow Zn(OH)_4^{2-} \quad (4.11)$$

$$Zn(OH)_4^{2-} \rightarrow ZnO + H_2O + 2OH^- \quad (4.12)$$

Figure 4.23 shows the XRD spectra of ZnO nanostructures growth on ZnO seed layer annealed at 500°C. The clearly seen diffraction peaks positioned at 2θ = 31.77°, 34.42°, 36.25°, 47.54° and 56.60° are assigned to (100), (002), (101), (102) and (110) orientation planes of ZnO with hexagonal wurtzite structure, respectively. The planes of wurtzite ZnO (JCPDS card No. 36-1451) confirm the formation of ZnO structure of the seed layer. Furthermore, the crystal size of the particles can be calculated from the full

width at half maximum (FWHM) and angular position of the (100), (002), and (101) diffraction peak by Scherrer's equation [35].

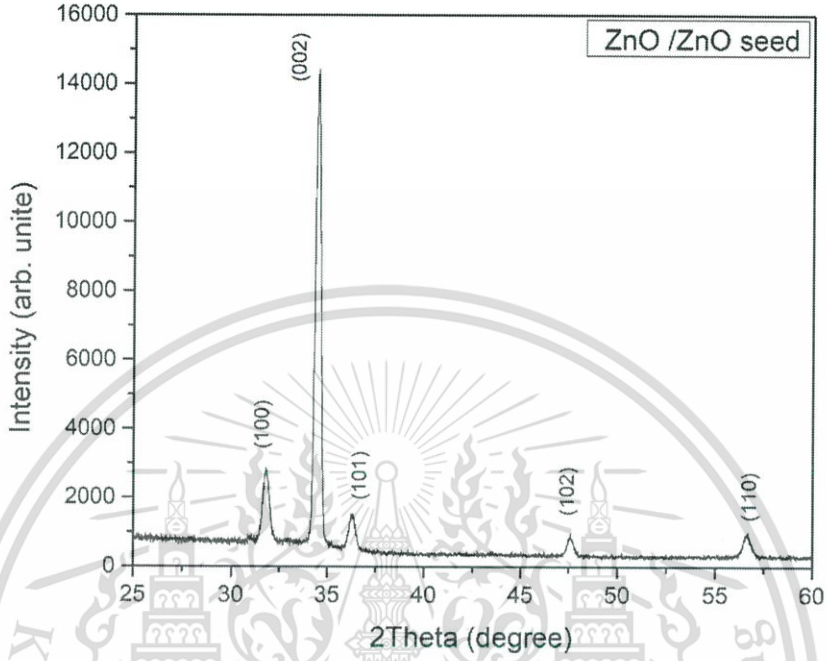

Figure 4.23 XRD patterns of ZnO nanostructures.

The average crystal size of ZnO seed layer is found at about 9.34 nm. The diffraction peaks of crystal plane (100) and (101) in 1%GZO, 5%FZO and 5G3FZO samples are nearly negligible but only the diffraction peak (002) of crystal plane can be observed are shown in figure. 4.24, 4.25 and 4.26. The intensity of (002) peak increases to some extent for the sample incorporated by 1%GZO, 5%FZO and 5G3FZO, but decreases gradually for the samples doped with 3% Ga, 5%Ga, 1%F, 3%F and co-doped with 1%, 3% of Ga and 1%, 5% of F. This variation of ZnO peak intensity might be due to the incorporation of Ga and F in the interstitial sites of ZnO lattice. From figure 4.24, 4.25 and 4.26, it can be seen that all nanostructures have the hexagonal shape, suggesting ZnO nanostructures in all the samples grow along the (002) direction. This may originate from the fact that ZnO crystal growth is inhibited in other directions, while the (002) direction is preferable and has the fastest growth velocity. However, incorparated dopants may also greatly affect the growth rate of ZnO nanostructures along this direction by modifying its surface energies.

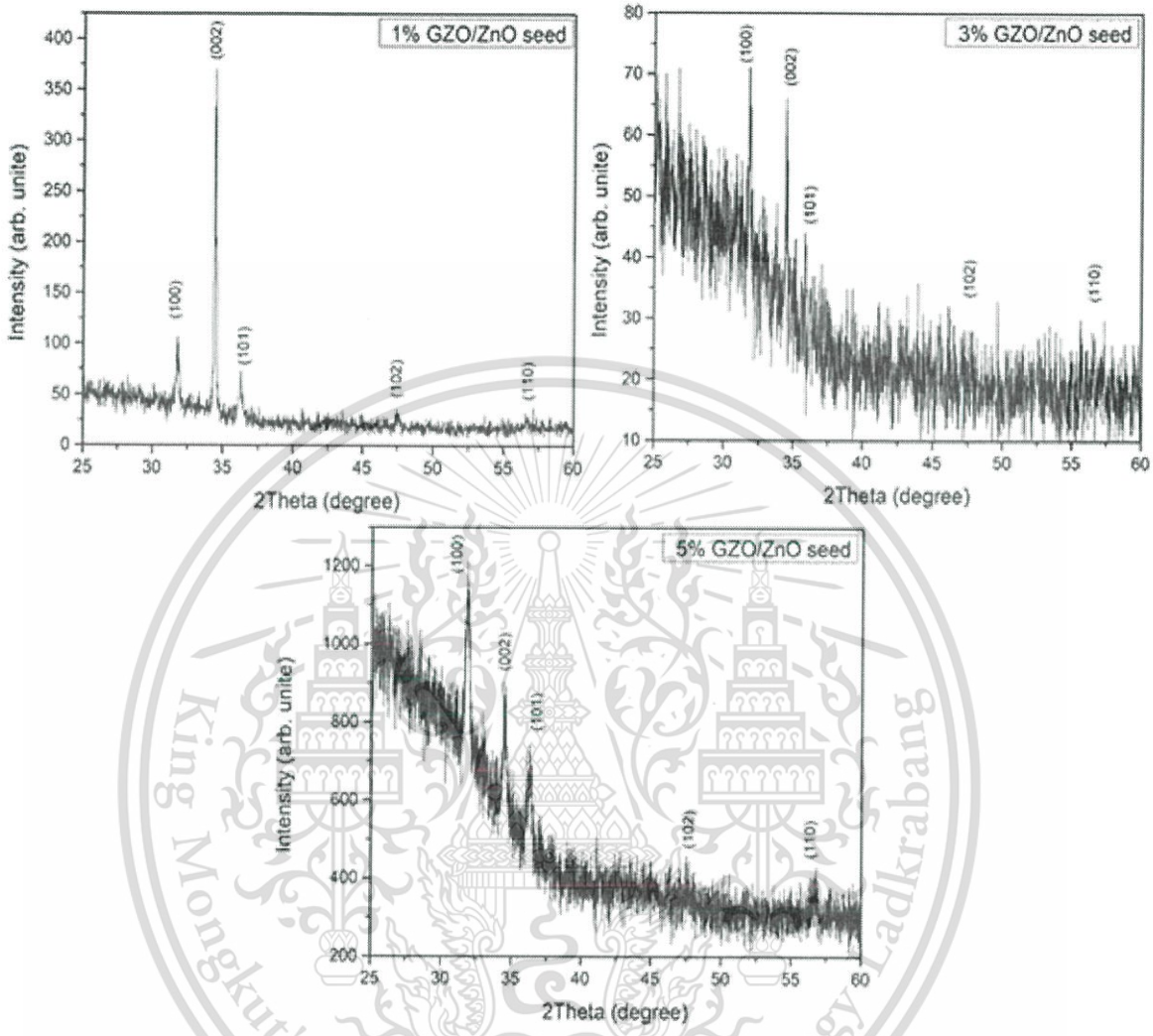

Figure 4.24 XRD patterns of GZO nanostructures with different Ga concentrations.

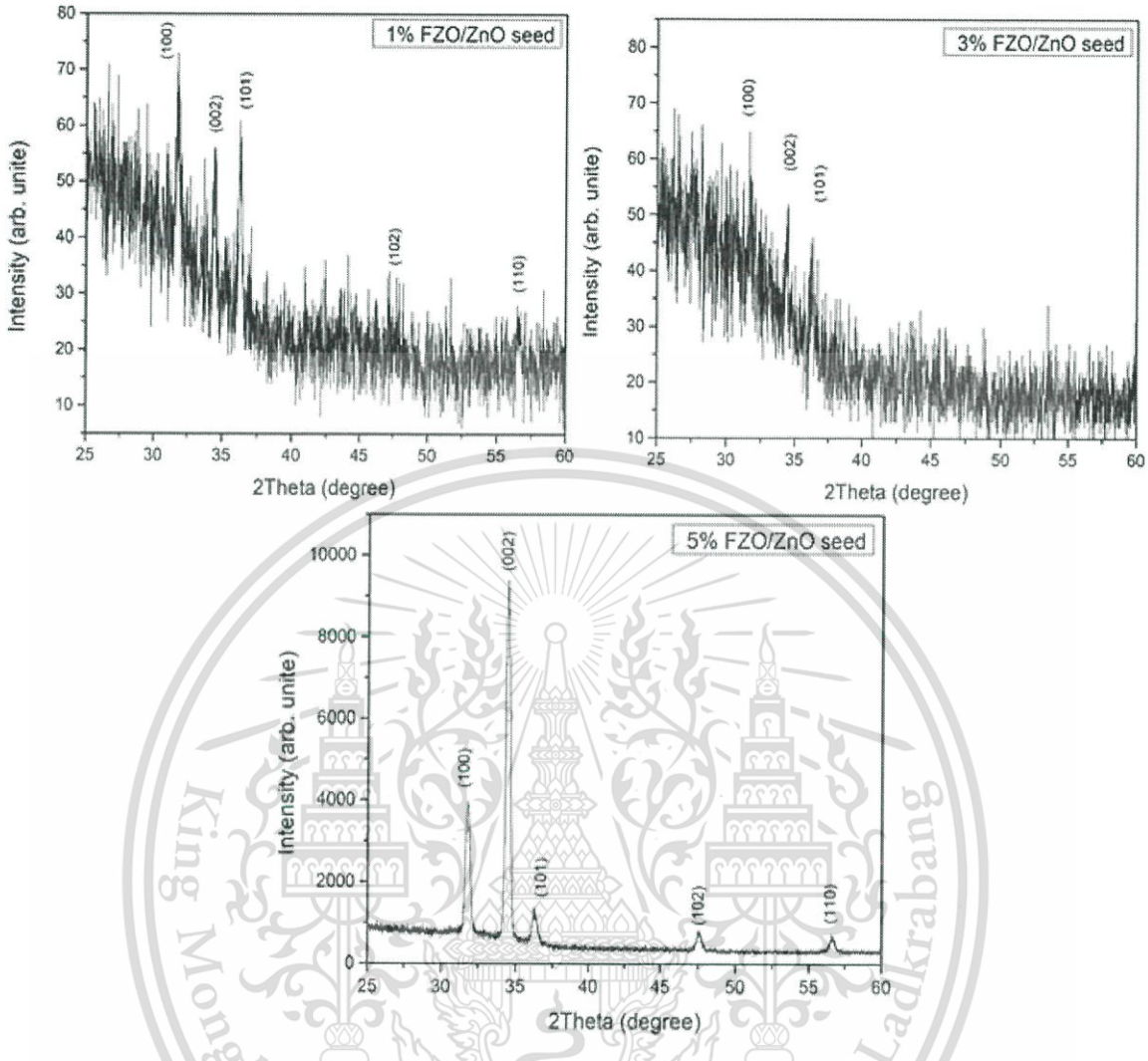

Figure 4.25 XRD patterns of FZO nanostructures with different F concentrations.

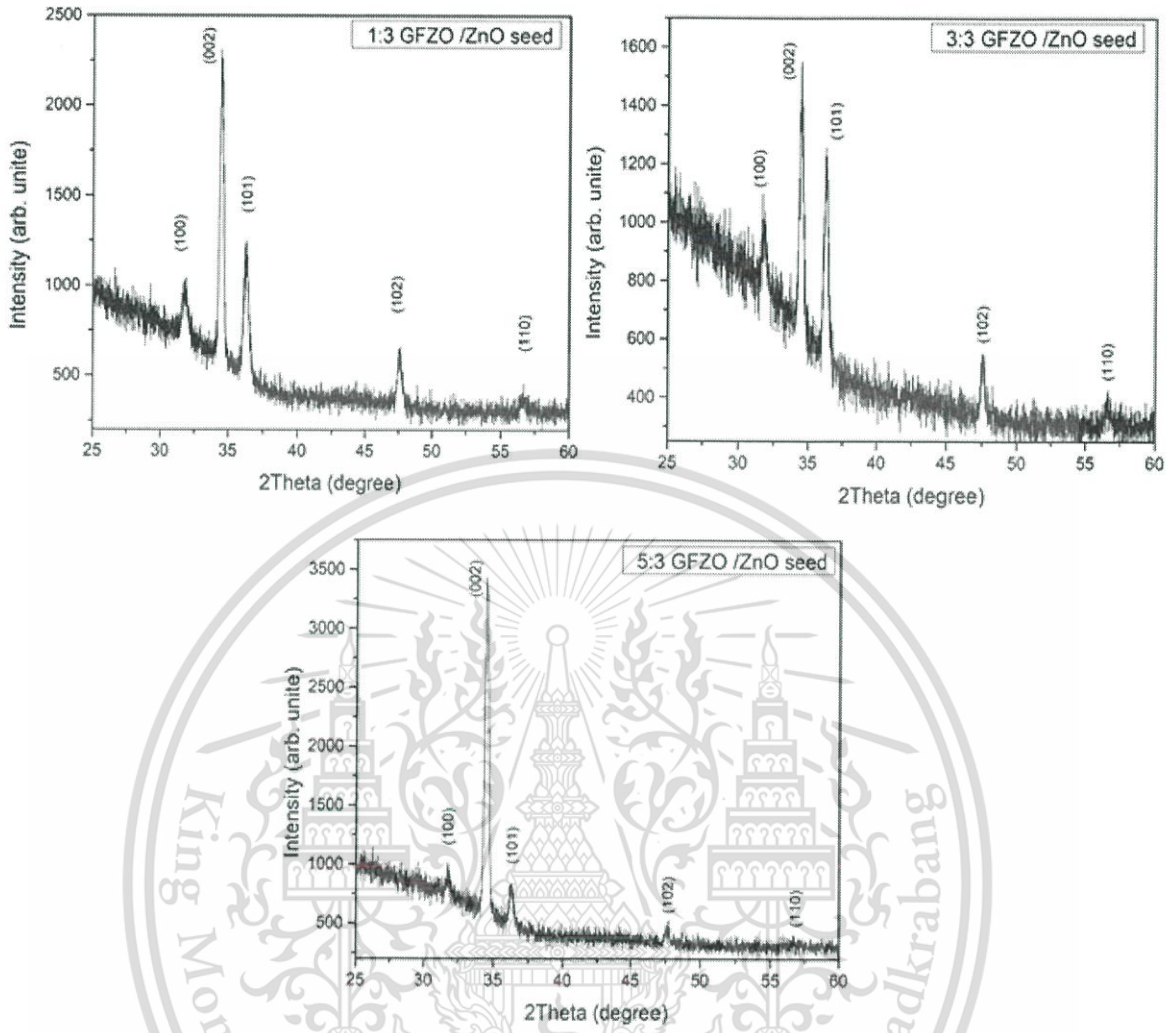

Figure 4.26 XRD patterns of GFZO nanostructures with different Ga and F concentrations.

Figure 4.27 to 4.32 show the FE-SEM images of ZnO, GZO, FZO and GFZO nanorods with different Ga and F contents. The effects of Ga and F doping concentration on grain size can be clearly seen in figure 4.28 to 4.32. ZnO and Ga/F co-doped ZnO exhibit a nanorod structure. The dopant concentration is directly affecting ZnO rod size. Increasing Ga doping concentration can induce the reduction in rod size. The 1%FZO and 3%FZO grown on ZnO seeding layer exhibit slightly poorer vertical alignment as shown in figure 4.28. The hexagonal nanorods are well-grown on seed layers. The orientation, size, and length of hexagonal nanorods can be controlled by F dopant concentration. However, the nanorod size shows significant decrease with increasing doping concentration. The smaller size of FZO nanorods grown on ZnO seeding film

results from the decrease in the F concentration. Moreover, nanodisk/nanorod morphology could be observed in the samples doped with Ga. The nanodisk/nanorod are hexagonal in shape and well-grown on the ZnO seed layers. The 1%Ga dopant strongly affects the orientation and size of ZnO nanodisk/nanorod, especially its size which increases with increasing dopant concentration as observed in figure 4.29. Meanwhile, figure 4.30 to 4.32 show that the GFZO samples have flat hexagonal crystallographic planes indicating that the ZnO nanorods are hexagonal in crystal structure. This feature could be credited to the rapid vertical growth rate of nanodisk/nanorod and its limited growth along the lateral direction. The grain sites of seed layers serve as nucleation sites for nanodisk/nanorod growth, so their roughness is an important factor. The smooth seed layer surface and smaller nucleation size are possibly generated nanodisk/nanorod formation. The growth of smaller grains increases in the density of grains per unit area. At higher nucleation densities, lateral growth is effectively suppressed, which results in rods with smaller sizes. For rod/disk growth, Zn^{2+}ions may diffuse into the growth site and create bonds with O^{2-}ions. A lower nucleation size required a smaller number of Zn^{2+}ion diffusion and less bonding formation to create rods [44-48]. These conditions may result in a higher nanodisk/nanorod growth rate and create mixed morphologies of Ga/F co-doped ZnO nanorod. In addition, we confirm the length and diameter of the nanorod by TEM image. Figure 4.33 shows a typical TEM image of ZnO, GZO, FZO and GFZO nanorods with different Ga and F contents, the all sample have hexagonal shape with the diameter sizes of nanorods are in the range of 50-120 nm and the length about 350-800 nm.

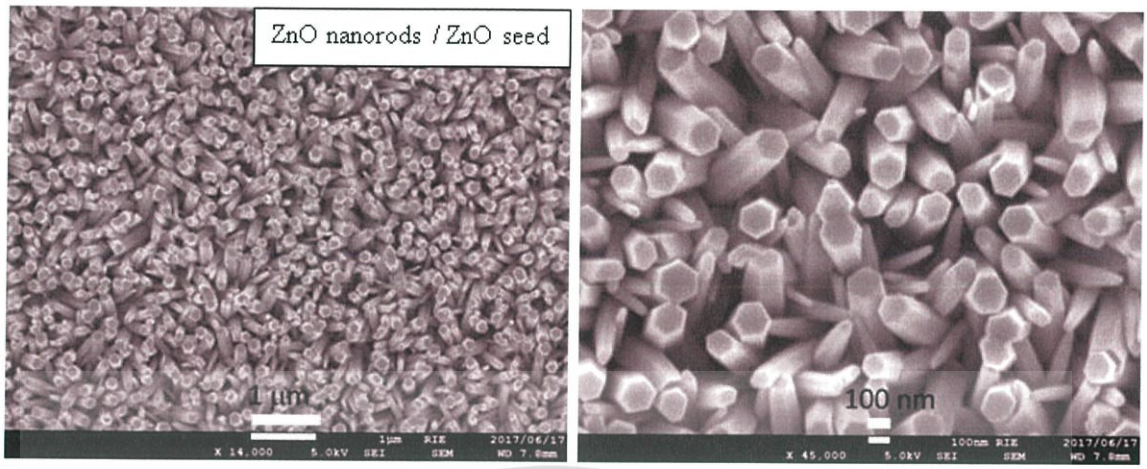

Figure 4.27 FE-SEM images of ZnO nanorods.

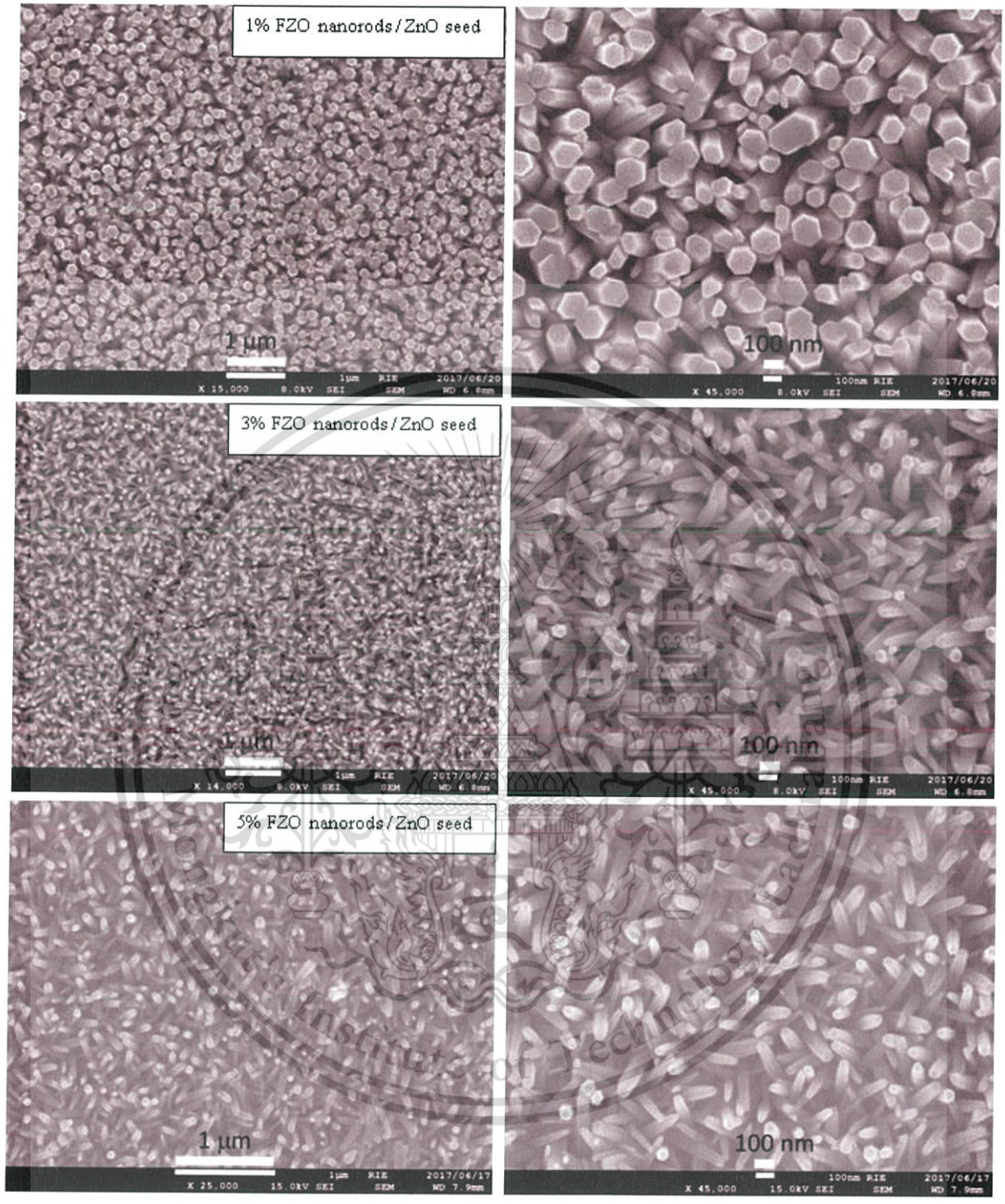

Figure 4.28 FE-SEM micrographs of 1%, 3% and 5% F doped ZnO nanorods.

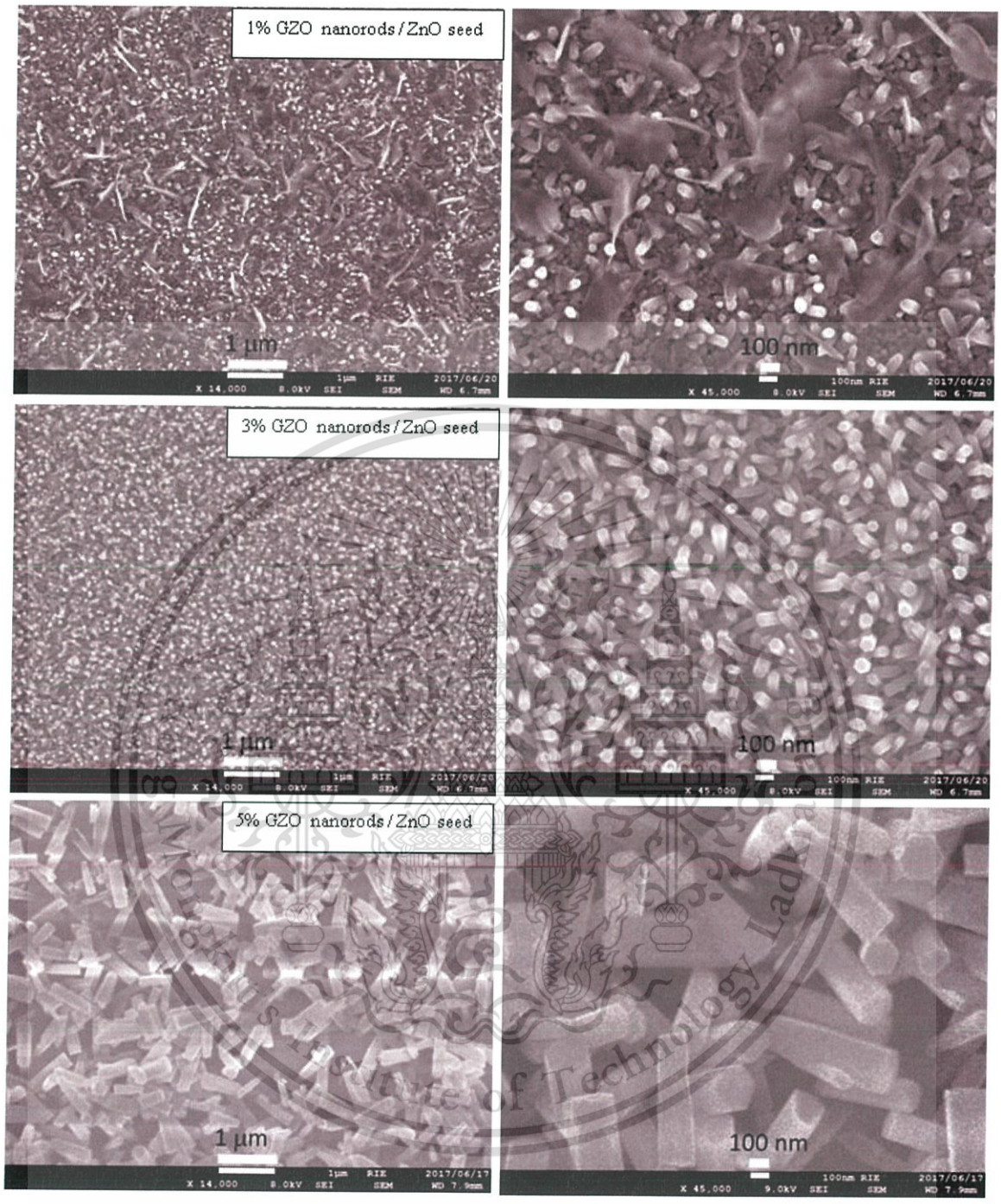

Figure 4.29 FE-SEM micrographs of 1%, 3% and 5% Ga doped ZnO nanorods.

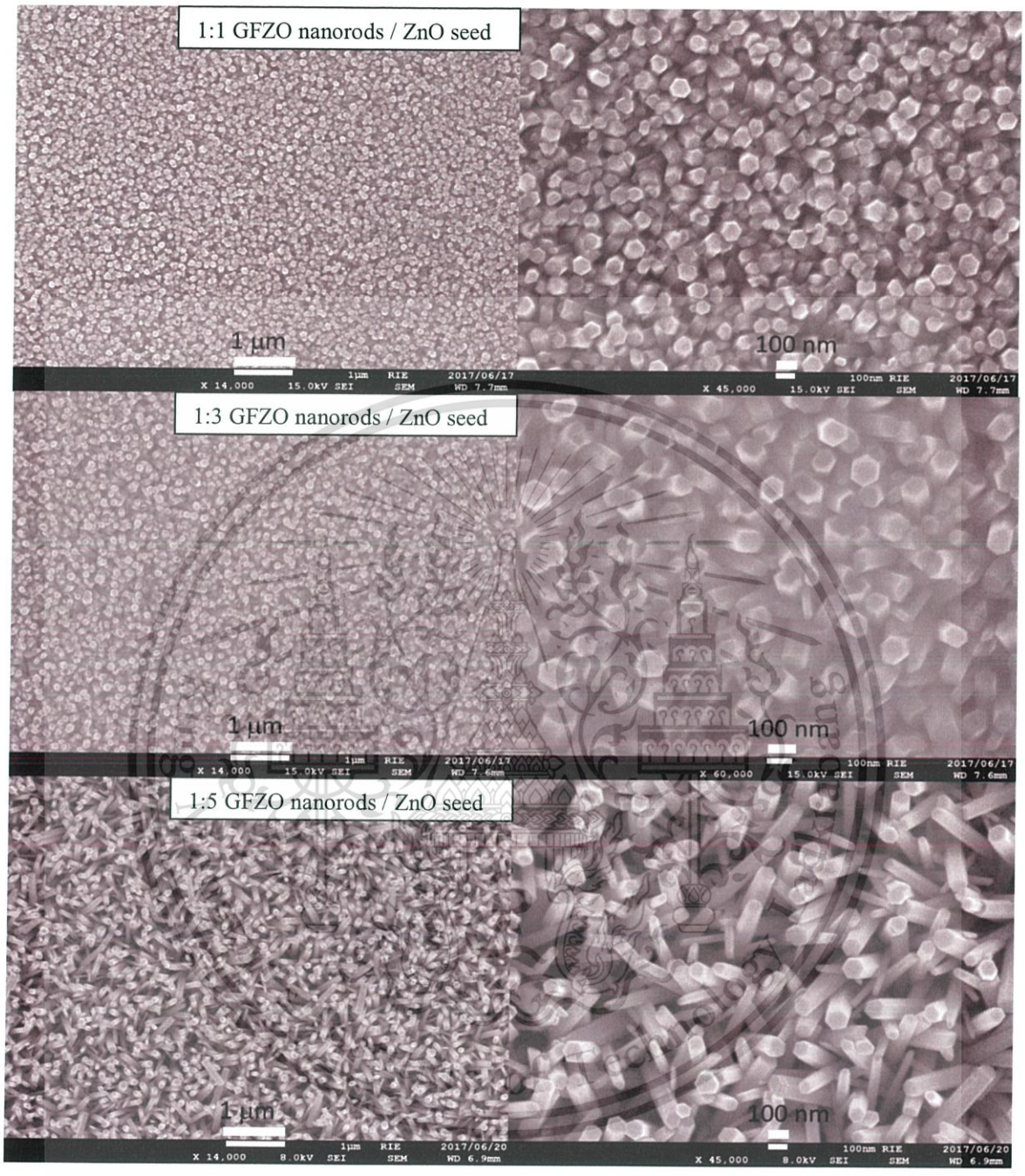

Figure 4.30 FE-SEM micrographs of Ga/F doped ZnO nanorods.

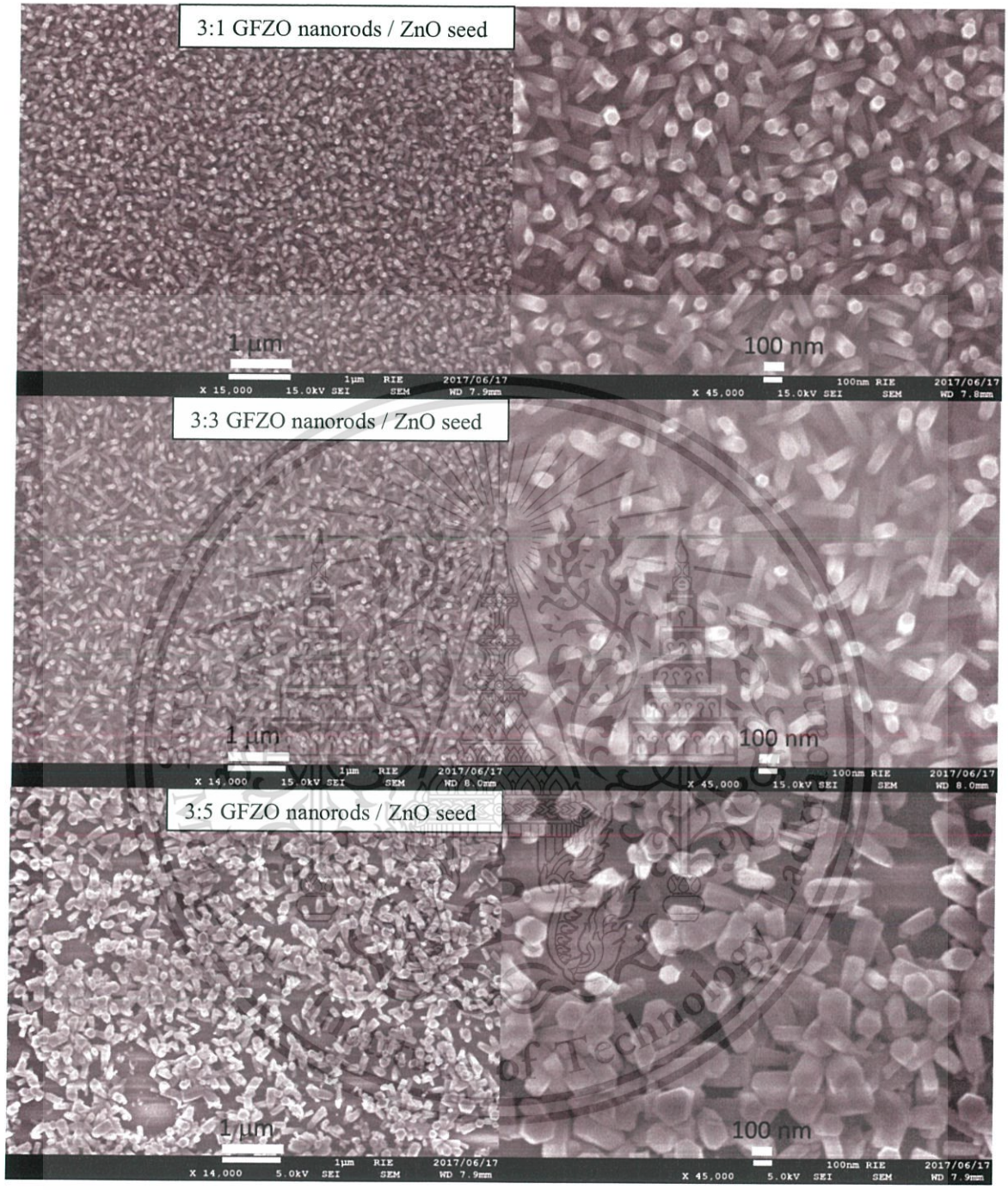

Figure 4.31 FE-SEM micrographs of Ga/F doped ZnO.

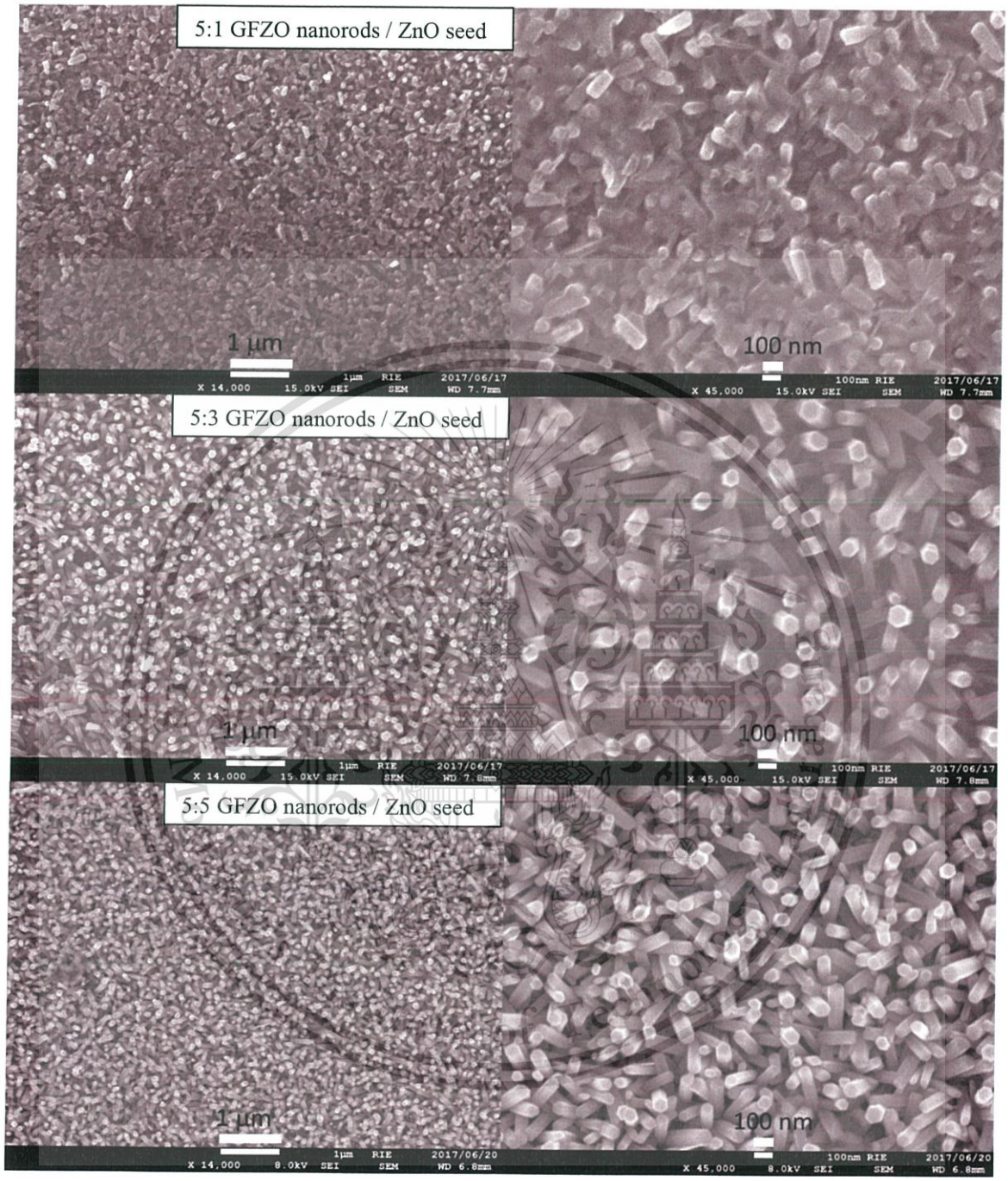

Figure 4.32 FE-SEM micrographs of Ga/F doped ZnO nanorods.

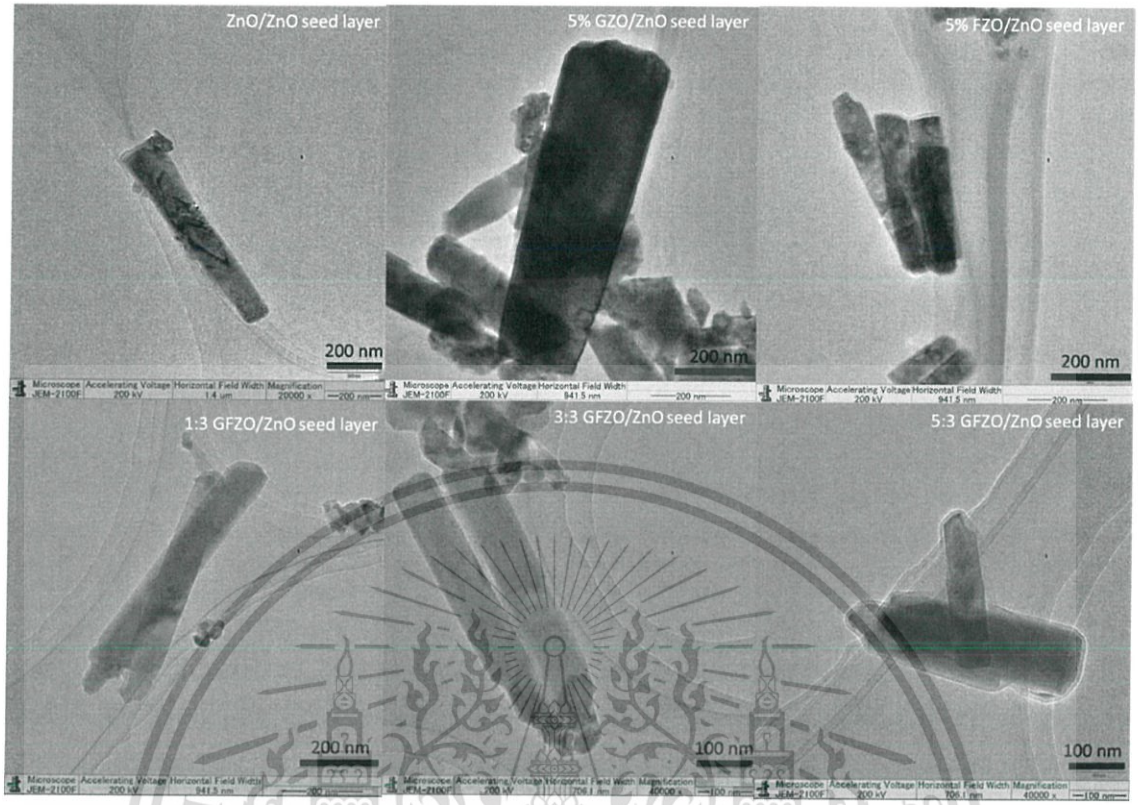

Figure 4.33 TEM micrographs of ZnO, 5% GZO, 5% FZO and GFZO nanorods.

4.1.6 The effect of substrate placement angle-dependent of ZnO seed layers

Partial results of the presented work have been published in:
Ceramics International 43 (2017) S529–S534.

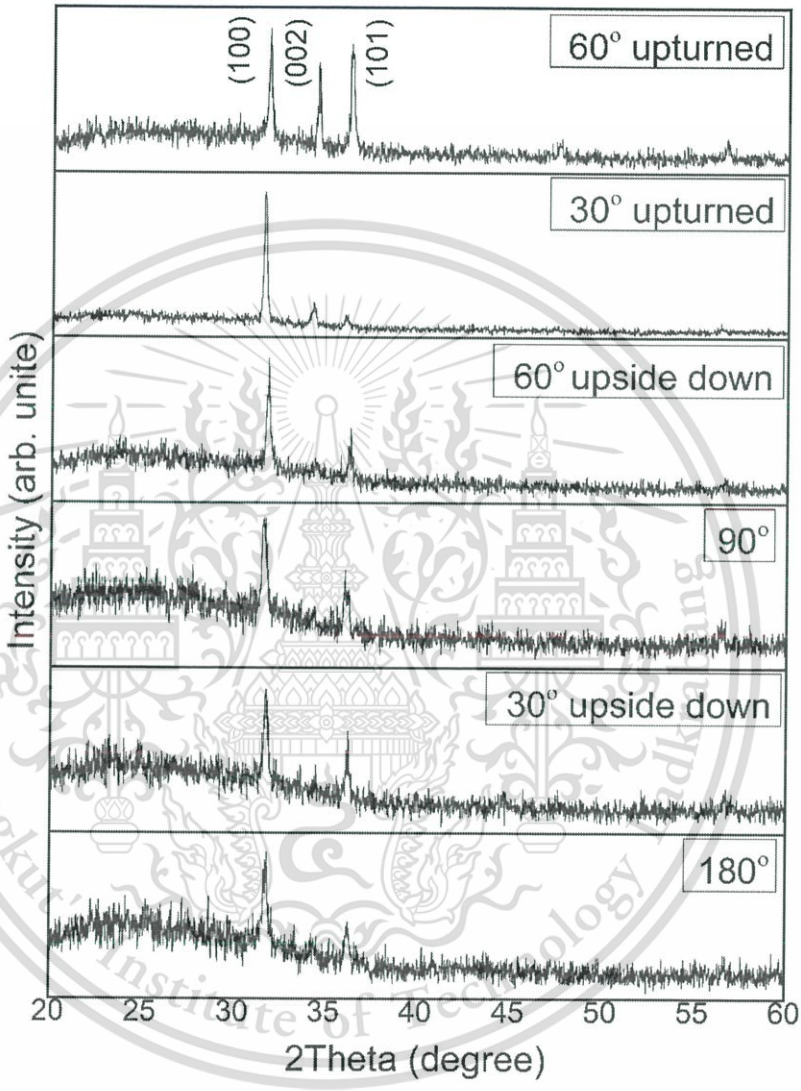

Figure 4.34 XRD patterns of GFZO nanostructures with the ZnO seed layers placed at different tilted-angle.

The systematic way in the influence of angle-dependent substrate placement during hydrothermal growth on structural properties and morphologies of Ga/F co-doped ZnO nanostructures is investigated. The angle-dependent substrate placement has been found to be one of the key factors that can control the density, length and

shape of the hydrothermally grown Ga/F co-doped ZnO nanostructures. The XRD patterns of Ga/F co-doped ZnO nanostructures with the ZnO seed layers placed at different tilted-angle are shown in figure 4.34. A broad XRD pattern appeared in all samples in the low 2θ region ranging from 20° to 40° ascribes to a typical diffraction pattern of a glass substrate. Three strong diffraction peaks are observed at 2θ ranging from 30° to 40°, which can be well indexed as wurtzite ZnO crystal structure (JCPDS card No. 36-1451) [21]. The diffraction peaks of crystal plane (002) and (101) in 180°, 30°upside-down, 90°, 60°upside-down and 60° upturned samples are nearly negligible but only the diffraction peak of crystal plane (100) can only be observed. For the GFZO nanostructures with a substrate-tilt angle of 60° upturned, non-preferential growing direction were observed accompanying three characteristic peaks of wurtzite ZnO crystal structure. The deterioration of the (100) orientation is considered as the result of the energy minimization, which means the sum of the surface energy in the nanorod, the nanorod-substrate interface energy and strain energy [48-50]. When the substrate tilted angle becomes greater, the diffusion and collision among the incident species become significant at the surface of the deposited nanorods. Energetic deviation of the minimum value for (100) orientation results to the other crystallographic orientation of the rod growth. The intensity of (100) peak increases to some extent for the sample that incorporated F (3%), but decreases gradually for the samples doped with Ga (5%) and co-doped with Ga and F. This variation of ZnO peak intensity might be due to the incorporation of Ga and F in the interstitial sites of ZnO lattice. Based on the variation of the XRD patterns, it could be deduced that the crytallinity and texture of nanorods are influenced significantly by the substrate tilt angle in the deposition process. Figure 4.35 shows the FE-SEM images of GFZO nanostructures with the ZnO seed layers placed at different tilted-angle and cross sectionals view of all samples. It is clearly observed that all samples are hexagonal in rod-shape and well-grown on the ZnO seed layers. The effects of tilted-angle of substrate placement on the rod size can be clearly seen in Figure 4.35. From top images, the average diameter of the GFZO nanorods ranges from 90 nm, 89 nm, 78 nm, 89 nm, 196 nm and 125 nm with180°, 30° upside-down, 90°, 60° upside-down, 30° upturned and 60° upturned samples, respectively.

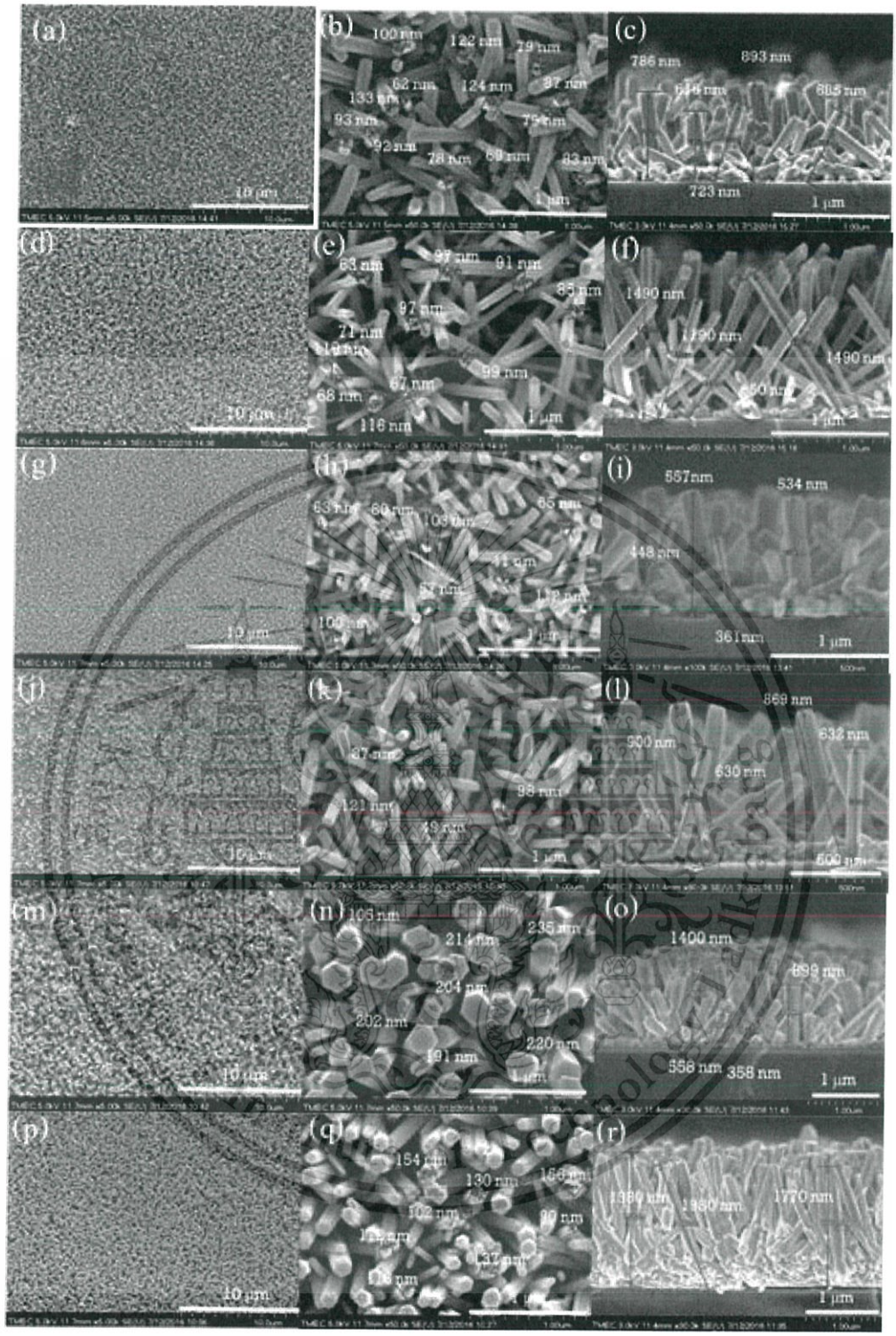

Figure 4.35 FE-SEM micrograph of GFZO nanostructures with the ZnO seeding layer placed at different tilted-angles. [(a, b and c: 180°), (d, e and f: 30° upside down), (g, h and i: 90°), (j, k and l: 60° upside down°), (m, n and o: 30° upturned) and (p, q and r: 60° upturned)].

From cross-sectional FE-SEM images, the average length of the GFZO nanorods were found to be approximately 741 nm, 1185 nm, 475 nm, 758 nm, 802 nm and 1910 nm with 180°, 30° upside-down, 90°, 60° upside-down, 30° upturned and 60°upturned samples, respectively as shown in Figure 4.35. Based on a previous report, it had been reported that the ZnO crystalline size was also strongly dependent on tilted-angle of substrate. The rate of nanorods growth may be influenced by the placement and tilt-angle of substrate during crystal growth. In addition, the Ga and F dopant strongly affects the orientation, size, and length of ZnO nanorods.

The optical transmittance spectra of GFZO nanostructures with the ZnO seeding layer placed at different tilted-angle are exhibited in figure 4.36. All transmission spectra of GFZO nanorods indicate sharp absorption edge in visible range suggesting good quality of GFZO nanorods grown by hydrothermal process. Absorption edge of GFZO nanorods with higher substrate tilt angles of 180°, 30°upside-down, 90° and 60°upside-down shows a significant blue shift to the region of high photon energy. The blue shift of the band-gap energy with considered to be mainly related to the increase of strain in the nanorods induced by defects. Although the increases of the band-gap energy with the increasing tensile strain correlates well with the relation between the nanorod stress and band-gap energy, this empirical relation does not agree with the simulation results of density functional theory based on the bulk ZnO. When the substrate tilt angle becomes relatively high, the increasing strain in ZnO nanocrystal is possibly caused by good crystallinity with a polycrystalline structure. The GFZO nanorods are nearly transparent in the visible region with more than 60 % transparency within 380 nm to 600 nm. The incorporation of Ga and F dopants is confirmed by the EDS results as shown in figure 4.37. The table inserted in the figure (inset of figure 4.37) shows the contents of existing elements in the Ga/F co-doped ZnO nanostructure detected by EDS. The elemental content of the marked area is as follows: Zn = 54.393 wt.%, O = 18.612 wt.%., F = 0.243 wt.% and Ga = 3.407 wt.%. It is deduced that Ga and F were incorporated into the nanostructures via the hydrothermal process. In the EDS spectrum, numerous well-defined peaks for Zn, O, Ga, and F clearly indicate that the GFZO nanorods are made of Zn, O, Ga and F. No other peaks related to impurities were detected in the spectrum further confirms that the synthesized nanorods are Ga/F co-doped ZnO.

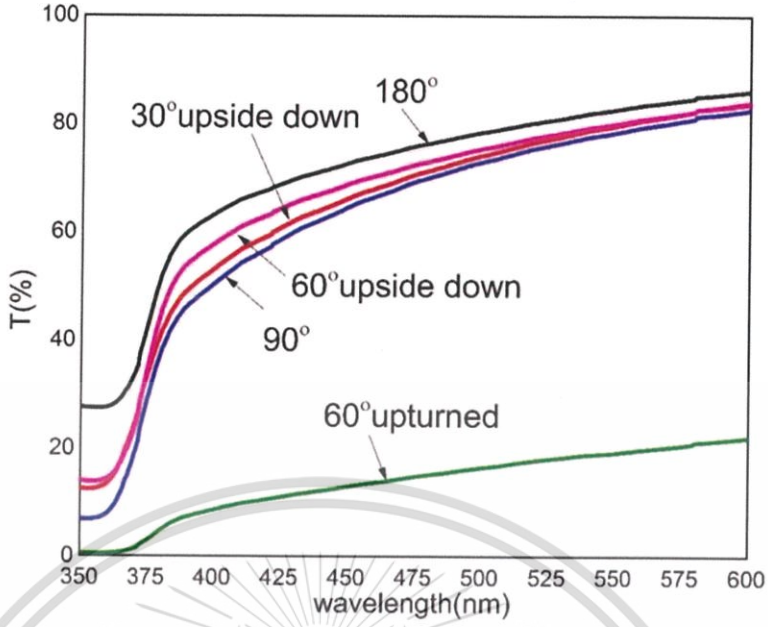

Figure 4.36 Optical transmittance of GFZO nanostructures with the ZnO seeding layer placed at different tilted-angle.

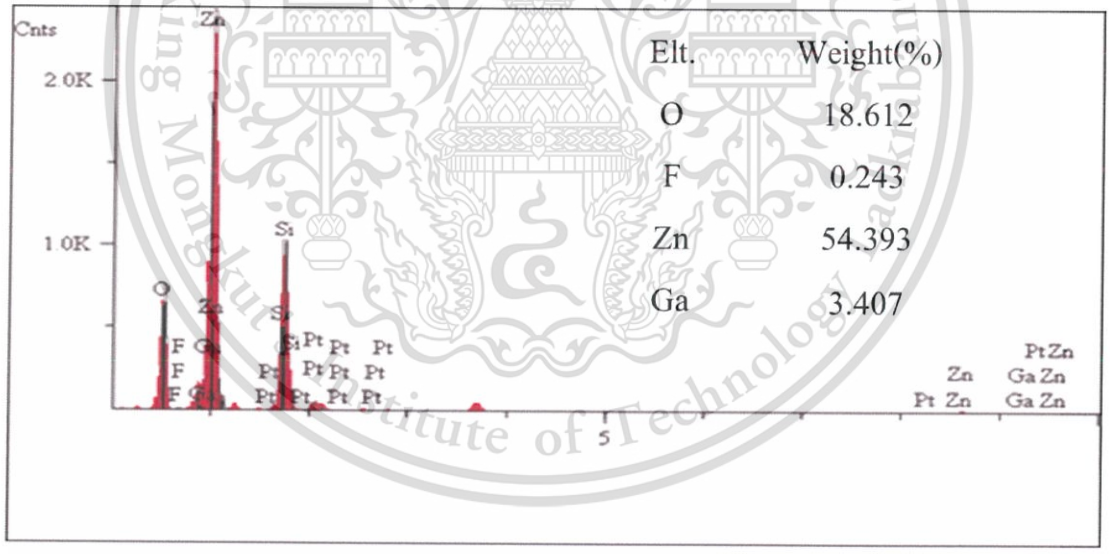

Figure 4.37 EDS spectra of 5G3FZO nanostructure.

4.2 The photoluminescence spectra of GFZO nanostructures

Partial results of the presented work have been published in:
Journal of Nanoscience and Nanotechnology Vol. 18, (2018), 7296–7301.

The results in this topic, based on article published in Journal of Nanoscience and Nanotechnology Vol. 18, 7296–7301, 2018. All samples were measured using a He-Cd laser with a wavelength of 325 nm as an excitation source for photoluminescence spectra as shown in figure 4.38. Figure 4.39 shows PL spectra of ZnO nanostructures and GFZO nanostructures with different Ga and F concentrations grown on ZnO seed layer prepared by hydrothermal process. It can be observed that all PL spectra obtained at low temperature (25 K) have similar features including three sharp UV emission bands (360-400 nm) and a broad yellow-orange emission band (500-700 nm) respectively. The three sharp UV emission bands are naturally related to the near band edge emission from the direct band gap of ZnO. The first peak with shortest wavelength of ~368 nm is correlated to free exciton emission (FX). Second dominated peak located at ~375 nm is typically ascribed to the emission of exciton of bound shallow neutral donor ($D^{\circ}X$). Third peak situated at ~382 nm with broad shoulder can be attributed to the donor to bound exciton emission [51-55]. The broad yellow-orange emission band may be spectrally decomposed to two Gaussian peaks at 590 nm and 653 nm. The yellow-orange emission is suggested to emanate from radiative de-excitation from the conduction band to deep level states attributed to doubly ionized oxygen vacancies (V_o) states (V_o^{++}) [55-60]. The origination of the yellow-orange emission band could be associated to the position of Ga and F elements within the lattice arrangement. Incorporated Ga and F elements can occupy the impurity sites to form interstitials or inhabit the main lattice sites to generate a ternary compound. Probably, Ga and F elements in the as-grown GFZO would substitute Zn atoms and O atoms, respectively. According to PL spectra of 5% Ga doped ZnO nanostructures, it can be observed that the intensity of $D^{\circ}X$ gradually decreases when the Ga doping concentration increases. This indicates that the crystalline quality of GZO nanostructures decreases with increasing Ga doping concentration due to the enhanced distortion of crystal lattice by extensive Ga concentration. Moreover, the over

dopant of Ga atoms may reduce the $D^{o}X$ intensity by introducing either radiative deep levels or nonradiative channels. Moreover, as seen in PL spectra of 5% F doped ZnO, its PL intensity of yellow-orange emission became stronger. This feature implies the greater defect sites in the lattice of doped sample, reflecting to the good incorporation of the dopants that induce emission-related intrinsic defects of oxygen vacancies.

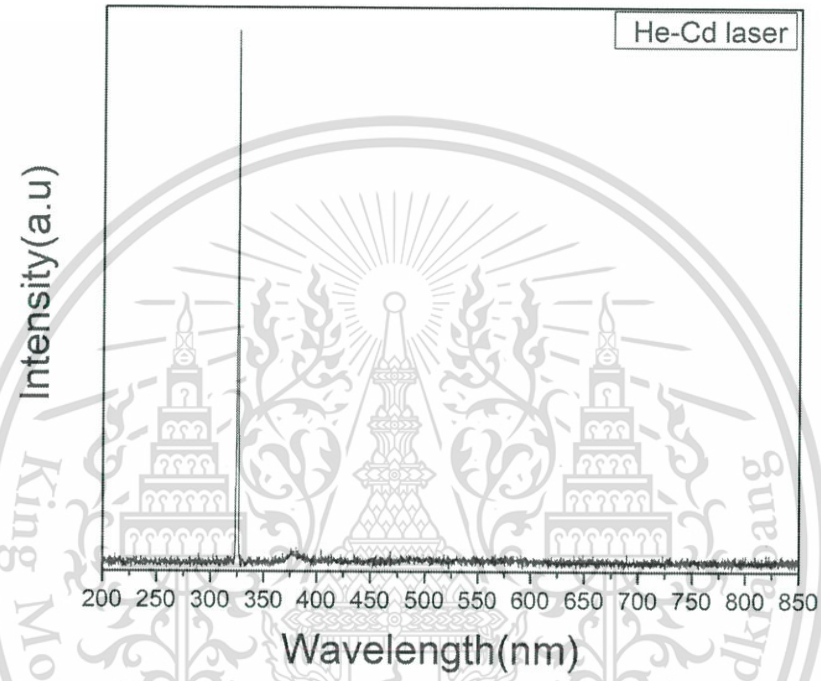

Figure 4.38 Photoluminescence spectra of IK Series He-Cd LASER.

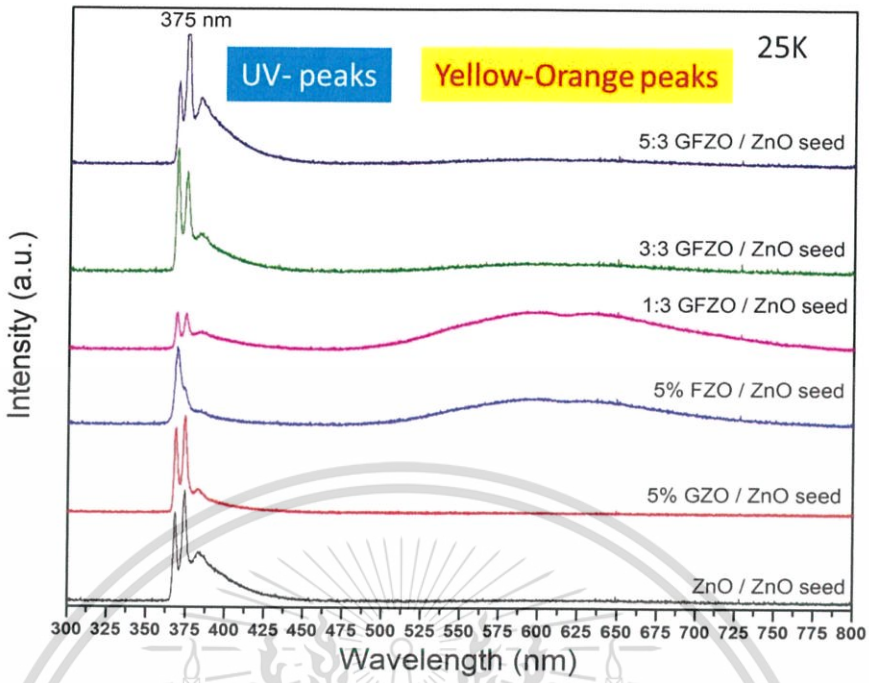

Figure 4.39 Photoluminescence spectra of ZnO nanostructures and GFZO nanostructures with different Ga and F concentrations and growth on ZnO seed layer.

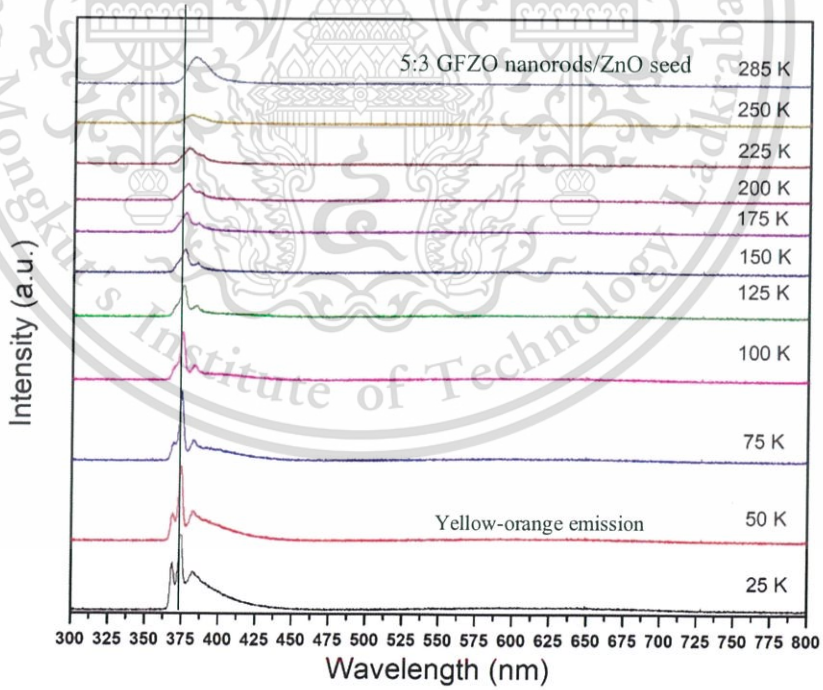

Figure 4.40 Photoluminescence spectra of Ga/F doped GFZO nanorods with 5% Ga and 3% F concentrations.

The fundamental temperature-dependent band gap of semiconductor material is of considerable importance in basic science and technological applications. In typical, two mechanisms are responsible for the temperature dependence of the forbidden gap or excitonic transitions of semiconductor materials such as electron-phonon interaction and thermal expansion of the lattice. Figure 4.40 shows photoluminescence spectra of 5G3FZO nanorods measured as a function of temperature ranging from 25 K to 285K. The intensity of yellow-orange emission component decreases when the Ga/F were co-doped into ZnO, indicating that the yellow-orange emission is closely associated with the surface defect complex V_{Zn}-OH, which inhibits the yellow-orange emission. The PL spectra also possesses observable peak at 360-380 nm. In PL measurement of 5G3FZO nanorods, the important parameters that lead to determination of its properties are the maximum peak, PL peak intensity, and the full width at half maximum. The values were obtained by the fitting as shown in Table 4.2. The temperature dependent energy gap of semiconductor material is typically expressed in term of empirical relations proposed by many analytical models. It is clearly seen in figure 4.40 that there is significant red-shift of major peak of UV-emission with increasing temperature. The relationship of major PL peak position with respect to temperature can be explained by the Vashni empirical model explained by the following equation.

$$E_g(T) = E_g(0K) - \alpha \frac{T^2}{\beta + T} \tag{4.16}$$

When E_g(T) is the energy gap at temperature T, α and β are parameters to fit the experimental data (referred to as Vashni thermal coefficients) [61-64].

Figure 4.41 shows temperature dependent PL spectra of 5G3FZO nanorods with curve fitting of three sharp UV emission bands (A) ~368 nm, (B) ~375 nm and (C) ~382 nm based on Vashni model. It is found that the best fitting process is exhibited in figure 4.41 (B). It can be seen that the fitting curve is in good agreement with the exciton of bound shallow neutral donor (D^0X) at ~375 nm. Furthermore, the broadening of this near band edge emission with increasing operating temperature is also noticed that may due to the natural temperature-induced broadening mechanism in semiconductor.

Figure 4.42 shows schematic electronic level diagram of (A) ZnO nanorods, (B) Ga doped ZnO nanorods, (C) F doped ZnO nanorods and (D) 5G3FZO nanorods. The intensity of UV emission bands and broad yellow-orange emission band changed when the samples were doped by Ga and F. This manner could be due to the presence of amount zinc interstitial (Zn_i) and oxygen vacancies (V_O) defects induced by Ga and F dopants. Ga substitution in the ZnO lattice may be responsible for the UV emission. The UV emission peak may probably come from donor zinc interstitial (Zn_i^O) to zinc interstitial with positive charges (Zn_i^+). On the other hand, F substitution in the ZnO lattice may be responsible for the yellow-orange emission. As the amount of oxygen vacancies is high, the yellow-orange emission peak may probably come from oxygen vacancy with a positive charge (V_o^+) to oxygen vacancy with a two positive charges (V_o^{++}). Based on the PL results, it can highly confirm the existence and the crucial roles of Ga and F dopant and substitution in the ZnO lattice structure.

Table 4.2 FWHM of PL spectra, Energy gap of PL peak of 5G3FZO nanorods.

Temperature(K)	FWHM (meV) at peak			Energy gap (eV) at peak		
	1st	2nd	3rd	1st	2nd	3rd
25	58.91	31.06	19.41	3.23	3.31	3.36
50	25.13	25.88	30.19	3.23	3.31	3.35
75	22.55	25.43	36.84	3.23	3.31	3.35
100	29.12	26.76	78.34	3.23	3.30	3.34
125	29.65	30.57	-	3.23	3.30	-
150	47.01	36.77	-	3.23	3.30	-
175	24.84	41.59	-	3.22	3.29	-
200	-	38.81	-	3.22	3.28	-
225	-	58.04	-	-	3.27	-
285	-	125.15	-	-	3.23	-

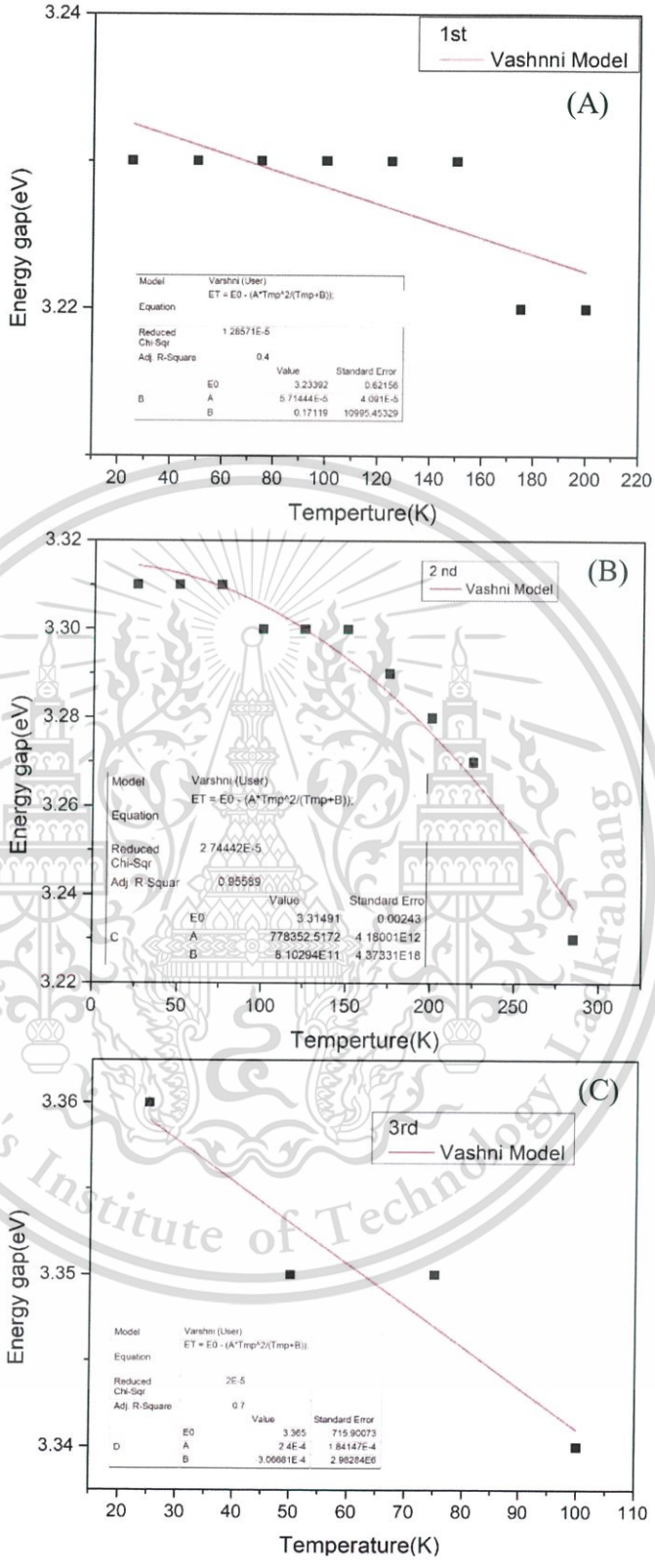

Figure 4.41 Temperature dependent PL spectra of 5G3FZO nanorods with curve fitting of three sharp UV emission bands (A) ~368 nm, (B) ~375 nm and (C) ~382 nm.

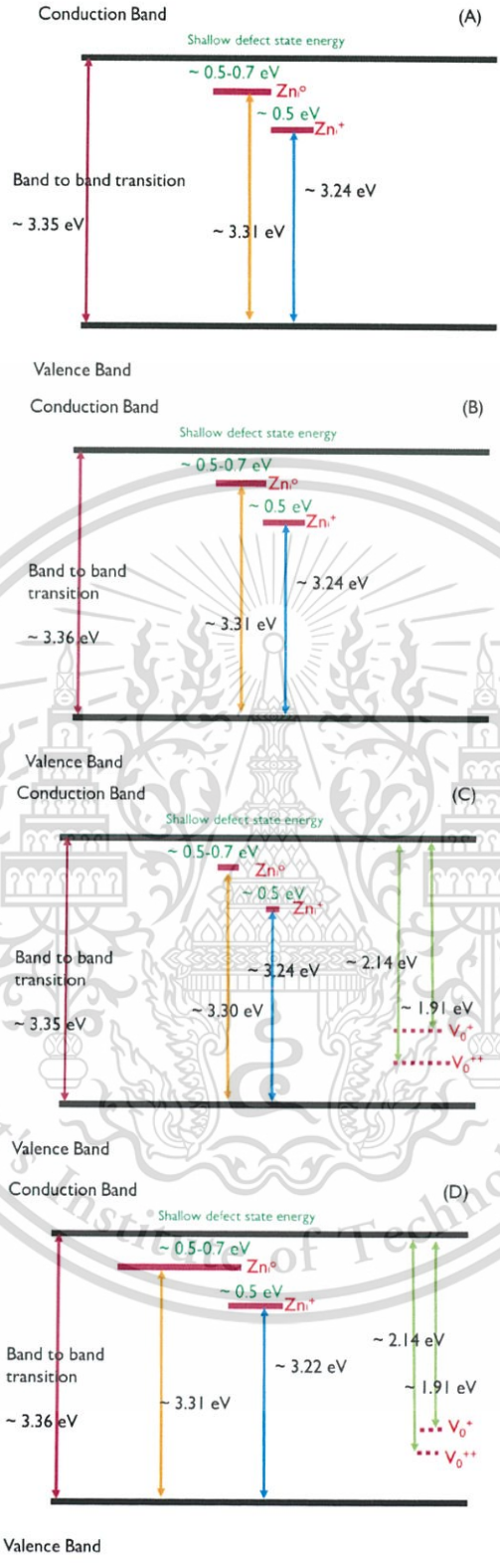

Figure 4.42 Schematic electronic level diagram of (A) ZnO nanorods, (B) GZO nanorods, (C) FZO nanorods and (D) 5G3FZO nanorods.

CHAPTER 5

CONCLUSION

In summary, the effect of annealing temperature of ZnO seed layer was investigated. The Ga/F co-doped ZnO nanostructures were fabricated by hydrothermal process onto dip-coated ZnO seeding layer that was annealed at different temperatures ranging from 200-500°C. The corresponding XRD and FE-SEM results suggested that different shapes of nanostructures of GFZO could be grown on the seed layer annealed at different temperatures. Possible reactions and mechanisms for the formation of GFZO nanostructures during hydrothermal process and the influence of seeding layer annealing temperature on the growth mechanism are suggested. The matching of preferential orientation direction between seeding layer that depends on annealing temperature and hydrothermally grown structures is found to be a key factor on the alternation in morphology of the synthesized products.

Secondly, the effect of the seeding films deposited at different coating times on the growth of GFZO nanorods during hydrothermal synthesis was scrutinized. The changes in diameter and density of hydrothermally grown ZnO nanorods were observed and analyzed. The growth rate of GFZO nanorods has a strong relationship with the intensity of the (002) orientation. The morphology of GFZO nanorods is strongly influenced by the thickness of the seed layer and corresponding crystal size. ZnO seeding layer thickness with ten times of coating exhibited the highest growth rate GFZO nanorods because it possessed the appropriate crystal size of the seed layer. In addition, the crystallinity of GFZO nanorods was also highly related to the thickness and crystal size of ZnO seed layer.

Thirdly, the effect of UV-Ozone treatment on ZnO seeding layer for Ga/F co-doped ZnO nanostructures was examined. The good surface wettability of ZnO seeding layer can be achieved by using UV-Ozone treatment times for 20 min. Overall results indicated high hydrophilicity feature on modified ZnO seeding layer especially improvement in strong Zn-OH bonding on the surface and cleaning surface morphologies which produces a uniform, highest density and high crystallinity growth of GFZO nanostructures confirmed by contact angle, XRD and FE-SEM results.

Finally, the effect of different tilted-angle for growth Ga/F co-doped ZnO nanostructures was studied. The corresponding XRD and SEM results suggested that well-defined GFZO nanostructures could be obtained by this synthesis technique accompanying assistance of dopant atoms incorporated into ZnO materials and the seeding layer placed at different tilted-angle. Possible reactions and mechanisms for the formation of the rods during hydrothermal process are suggested. The absorption edge was found to be blue shifted corresponding to the increase of strain in the nanorods caused by the placement of seeding layer at different tilted-angle. The shape, density, alignment, and orientation of the nanorods can be changed by the tilted-angle of substrate placement. The physical structure and size of GFZO nanorods are steady with diameter rang of 78–196 nm and length rang of 475– 1910 nm, respectively. XRD, SEM and UV–Vis results acknowledged that the seeding layer placed at different tilted-angle had significant effect on the morphological properties, crystallization and optical properties of GFZO nanorods. The corresponding PL spectra of the GFZO nanorods are composed of UV emission bands and yellow-orange emission bands. The UV emission bands are naturally related to the near band edge emission from the direct band gap of ZnO. The yellow-orange emission has been suggested to emanate from radiative de-excitation from the conduction band to deep level states attributed to doubly ionized oxygen vacancies (V_o) states (V_o^{++}). Moreover, the intensity of UV emission bands and broad yellow-orange emission band change when the samples were doped by Ga and F, confirming that the Ga and F substitutions in zinc interstitial (Zn_i) and oxygen vacancies (V_O) the ZnO structures.

REFERENCES

[1] M.S. Bakshi, Cryst. growth des. 16, 104 (2016).

[2] R. Ebrahimifard, M.R. Golobostanfard, H. Abdizadeh, Appl. Surf. Sci. 290, 252(2014).

[3] M.Y. Lu, Y.T. Tseng, C.Y. Chiu, Nanoscale. 9, 1 (2014).

[4] A. Yildiz, H. Cansizlu, M. Turkor, R. Abdulrahman, A.A. Hilo, M.F. Cansizoglu, T.M. Demirkan, T. Karabacak, Thin Solid Films. 589, 764 (2015).

[5] H.S. Yoon, K.S. Lee, T.S. Lee, B. Cheong, D.K. Choi, D.H. Kim, W.M. Kim, Sol. Energ. Mat. Sol. C. 92, 1366 (2008).

[6] K. Thirunavukkarasu, R. Jothiramalingam, Powder Technol. 239, 308 (2013).

[7] D.T. Phan, G.S. Chung, Sens. Actuators B, 187, 191 (2013).

[8] F.S. Pomar, E. Martinez, M.F. Melendrez, E.P. Tijerina, Nanoscale Research Letters, 6, 1 (2011).

[9] Z. Qing, S. Qiong, Y. Fan, Z. Hua, L. Bin, L. Qian, Sens. Actuators B, 195, 71 (2014).

[10] R. Pandey, C.H. Wie, X. Lin, J.W. Lim, K.K. Kim, D.K. Hwang, W.K. Choi, Sol. Energ. Mat. Sol. C, 134, 5 (2015).

[11] J.W. Miao, H.B. Yang, S.Y. Khoo, B. Liu, Nanoscale. 5, 11118 (2013).

[12] S.J. Young, Y.H. Liu, Microelectronic. Eng, 148, 14 (2015).

[13] A.V. Moholkar, S.M. Pawar, K.Y. Rajpure, C.H. Bhosale, J.H. Kim, Applied Surface Science, 255, 9358 (2009).

[14] Z. Pan, Y. Xiao, X. Tian, S. Wu, C. Chen, J. Deng, C. Xiao, G. Hu, Z. Wei, Materials Science in Semiconductor Processing, 17, 162 (2014).

[15] J-H Shin, D-K Shin, H.Y. Lee and J-Y Lee, Journal of the Korean Physical Society, 55, 947 (2009).

[16] A.S. Pugalenthi, R. Balasundaraprabhu, V. Gunasekaran, N. Muthukumarasamy, S. Prasanna, S. Jayakumar, Materials Science in Semiconductor Processing, 29, 176 (2015).

[17] J-S Park, I. Mahmud, H.J. Shin, M-K Park, A. Ranjkesh, D.K. Lee, H-R Kim, Applied Surface Science, 362, 132(2016).

[18] J. Liu, L. Xu, B. Wei, W. Lv, H. Gao, X. Zhang, Cryst. Eng. Comm, 13, 1283 (2011).

[19] P. Yu, J. Wang, H-Y Du, P-J Yao, Y. Hao, X-G Li, Journal of Nanomaterials, 6, 751826 (2013).

[20] S. Sarkar, D, Basak, Royal Society of Chemistry, 4, 39095 (2014).

[21] F.M Li, C. T. Zhu, S. Ma, X. Wang, Materials Science in Semiconductor Processing, 16, 1079 (2013).

[22] S-J Young and Y-H Liu, Microelectronic Engineering, 148, 14 (2015).

[23] H.S. Yoon, K.S. Lee, T.S. Lee, B. Cheong, D.K. Choi, D.H. Kim, W.M. Kim, Solar Energy Materials & Solar Cells, 92, 1366 (2008).

[24] R. Ghosh, M. Dutta, D. Basak, Applied Physics Letters, 91, 073108 (2007).

[25] L. Xu, Y. Guo, Q. Liao, J. Zhang, D. Xu, J. Phys. Chem. B, 109, 13519 (2005).

[26] R.C. Pawar, J. Shaikh, S.S. Suryavanshi, P.S. Patil, Current Applied Physics, 12,778 (2012).

[27] J. Song, S. Li, J. Phys. Chem, 111, 596 (2007).

[28] E. Makarona, B. Athanassiou, Procedia Engineering, 120, 447 (2015).

[29] V. Tvarozek, I. Novotny, P. Sutta, M. Netrvalova, I. Vavra, J. Bruncko, P. Gaspierik, S. Flickyngerova, Physics Procedia, 32, 456 (2012).

[30] A. J. Cheng, Y. Tzeng, Y. Zhou, M. Park, T.-H. Wu, C. Shannon, D. Wang, and W. Lee, Appl. Phys. Lett. 92, 092113 (2008).

[31] M. Ladanov, P. A. Amaris, P. Villalba, Y. Emirov, G. Matthews, S. Thomas, M. K. Ram, A. Kumar, and J. Wang, J. Phys. Chem.Solids 74, 1578 (2013).

[32] G. Ch. Park, S. M. Hwang, S. M. Lee, J. H Choi, K. M. Song, H. Y. Kim, H. S. Kim, S. J. Eum, S. B Jung, J. H. Lim, and J. Joo, Scientific Reports 5, 10410 (2015).

[33] A. R. Kaul, O. Yu. Gorbenko, A. N. Botev, and L. I. Burova, Superlattices Microstruct. 38, 272 (2005).

[34] K. H. Kim, K. Utashiro, Y. Abe, and M. Kawamura, Int. J. Electrochem. Sci. 9, 2080 (2014).

[35] Y. J. Lu, Z. F. Shi C. X. Shan, and D. Z. Shen, Chin. Phys. B 26, 047703 (2017).

[36] G. N. Dar, A. Umar, S. A. Zaidi, S. Baskoutas, S. W. Hwang, M. Abaker, A. Al-Hajry, and S. A. Al-Sayari, Talanta 89, 155 (2012).

[37] C. Z. Yao, B. H. Wei, L. X. Meng, H. Li, Q. J. Gong, H. Sun, H. X. Ma, and X. H. Hu, J. Power Sources 207, 222 (2012).

[38] N. H. Al-Hardan, M. J. Abdullah, N. M. Ahmed, F. K. Yam, and A. A. Aziz, Superlattices Microst. 51, 765 (2012).

[39] R. M. Mohite and R. R. Kothawale, Indian J. Chem. 54A, 872 (2015).

[40] W. Wang, T. Ai, and Q. Yu, Scientific Reports 7, 42615 (2017).

[41] H. C. Wu, Y. C. Peng, and C. C. Chen, Opt. Mater. 35, 509 (2013).

[42] J. H. Lim, S. M. Lee, H. S. Kim, H. Y. Kim, J. Park, S. B. Jung, G. Ch. Park, J. Kim, and J. Joo, Scientific Reports 7, 41992 (2017).

[43] R. Pandey, C. H. Wie, X. Lin, J. W. Lim, K. K. Kim, D. K. Hwang,and W. K. Choi, Sol. Energ. Mat. Sol. Cells 134, 5 (2015).

[44] J. B. Cui, Y. C. Soo, T. P. Chen, and U. J. Gibson, J. Phys. Chem. 112, 4475 (2008).

[45] G. Ch. Park, S. M. Hwang, J. H. Lim, and J. Joo, Nanoscale 6, 1840 (2014).

[46] A. A. Rani and S. Ernest, Superlattices Microstruct. 75, 398 (2014).

[47] A. V. Moholkar, S. M. Pawar, K. Y. Rajpure, C. H. Bhosale, and J. H. Kim, Appl. Surf. Sci. 255, 9358 (2009).

[48] S. K. Kim, S. H. Kim, S. Y. Kim, J. H. Jeon, T. K. Gong, D. H. Choi, D. Son, and D. Kim, Ceram. Int. 40, 6673 (2014).

[49] X. Pan, Z. Ye, J. Li, X. Gu, Y. Zeng, H. He, L. Zhu, and Y. Che, Appl. Surf. Sci. 253, 5067 (2007).

[50] N. Chahmat, T. Souier, A. Mokri, M. Bououdina, M. S. Aida, and M. Ghers, J. Alloys Compd. 593, 148 (2014).

[51] Z. Pan, Y. Xiao, X. Tian, S. Wu, C. Chen, J. Deng, C. Xiao, G. Hu, and Z. Wei, Sci. Semicond. Process. 17, 162 (2014).

[52] Y. Z. Tsai, N. F. Wang, and C. L. Tsai, Thin Solid Films 518, 4955 (2010).

[53] F. H. Alsultany, Z. Hassan, and N. M. Ahmed, Superlattices Microstruct. 92, 68 (2016).

[54] J. Guo, J. Zheng, X. Song, and K. Sun, Mater. Lett. 97, 34 (2013).

[55] K. Chongsri, W. Sinornate, K. Boonyarattanakalin, and W. Pecharapa, J. Nanosci. Nanotechnol. 16, 12962 (2016).

[56] K. Chongsri, K. Boonyarattanakalin, and W. Pecharapa, Ceram. Int. 43, S534 (2017).

[57] K. Chongsri, K. Boonyarattanakalin, and W. Pecharapa, Mater. Today: Proceedings 4, 6133 (2017).

[58] H. T. Kim, S. Y. Lee, and C. Park, Vacuum 143, 312 (2017).

[59] D. G. Ayana, R. Ceccato, C. Collini, L. Lorenzelli, V. Prusakova, and S. Dir, Thin Solid Films 615, 427 (2016).

[60] L. Zhu, J. Li, Z. Ye, H. He, X. Chen, and B. Zhao, Opt. Mater. 31, 237 (2008).

[61] J. S. Park, I. Mahmud, H. J. Shin, M. K. Park, A. Ranjkesh, D. K. Lee, and H. R. Kim, Appl. Surf. Sci. 362, 132 (2016).

[62] Y. Lv, Z. Zhang, J. Yan, W. Zhao, C. Zhai, and J. Liu, J. Alloys Compd. 718, 161 (2017).

[63] F. Xian, G. Zheng, L. Xu, W. Kuang, S. Pei, Z. Cao, J. Li, and M. Lai, J. Alloys Compd. 710, 695 (2017).

[64] V. Sh. Yalishev, Y. S. Kim, X. L. Deng, B. H. Park, and Sh. U.Yuldashev, J. Appl. Phys. 112, 013528 (2012).

APPENDIX A

Ceramics International 43, (2017), S529–S534.

Ceramics International 43 (2017) S529–S534

Contents lists available at ScienceDirect

Ceramics International

journal homepage: www.elsevier.com/locate/ceramint

Substrate placement angle-dependent growth of Ga/F co-doped ZnO nanostructures synthesized by hydrothermal process

Krisana Chongsri[a,b,*], Kanokthip Boonyarattanakalin[a], Wisanu Pecharapa[a]

[a] College of Nanotechnology, King Mongkut's Institute of Technology Ladkrabang, Bangkok 10520, Thailand
[b] Department of Applied Physics, Faculty of Science and Technology, Rajabhat Rajanagarindra University, Chachoengsao 24000, Thailand

ARTICLE INFO

Keywords:
A. Sol–gel processes
A. Grain growth
B. Impurities
D. ZnO

ABSTRACT

In this work, the effect of angle-dependent substrate placement on structural property and morphology of Ga/F co-doped ZnO nanostructures was investigated. The Ga/F co-doped ZnO (GFZO) nanostructures were grown on substrates with ZnO seeding layer placed at different tilted-angle by a hydrothermal process using $Zn(NO_3)_2$, NH_4F, GaN_3O_9 for Zn, F and Ga sources and hexamethylenetetramine as sol stabilizer. The ZnO seeding layer was pre-deposited on glass substrates by dip-coating. The GFZO nanostructures were grown on ZnO substrate at different tilted-angles from 0° to 180° with respect to horizon. The effects of tilted angle of placed substrate on morphologies and structural properties were investigated by X-ray diffraction (XRD), X-ray photoelectron spectroscopy (XPS), scanning electron microscope (SEM), and UV–Vis spectroscopy. The results indicate that this growth parameter has a vital role on preferable growth direction, morphological structure and shape of the as-synthesized nanostructure products.

1. Introduction

It is acknowledged that nanotechnology requires specific synthesis of desired shape and size of nanomaterials for their appropriate applications. Surfactants have been recognized to be one of the effective shape directing agents in nanomaterial synthesis, which has been typically correlated to the surface adsorption of surface active molecules on different crystal planes of nucleating centers, thus controlling their structures and shapes. Different kinds of surfactants have been used for shape-controlled synthesis of nanomaterials, while ionic surfactants have demonstrated clear shape directing effects [1]. Recently, zinc oxide (ZnO)-based nanostructures have received great attention owing to its unique characteristics as transparent conducting oxide (TCO) thin films with potential applications in various optoelectronic devices. ZnO-based thin films possess many advantages such as low material cost, non-toxicity, and high chemical stability, in comparison to tin-doped indium oxide (ITO). ZnO is typically an n-type compound semiconductor with a wide band gap (E_g~3.2–3.4 eV at 300 K) with a large exciton binding energy (60 meV) [2]. Furthermore, electrical and optical properties of ZnO can be further enhanced by suitable doping with either metal or non-metal elements. Much more interest has been focused on ZnO-based TCOs such as undoped ZnO nanowire [3], Al-doped ZnO (AZO) nanostructures [4] F-doped ZnO (FZO) thin films [5], and Ga-doped ZnO (GZO) nanorods [6]. As metallic dopant atoms in group III are incorporated into ZnO, they preferably replace the Zn host atoms that are able to provide extra free electrons leading to conductivity enhancement or better carrier mobility. Among the metal dopants, Ga appears to be a promising element due to its close ionic radius (0.62 Å) and covalent radius (1.26 Å) to those of Zn (0.74 and 1.34 Å, respectively) [7]. Moreover, fluorine with the ionic radius of 0.117 nm which is very close to that of oxygen (0.122 nm) may be a suitable anion doping candidate at oxygen site in ZnO matrix. Although, several methods have been used to growth ZnO nanostructures, hydrothermal growth technique is still one of dominating processes due to its considerable advantages including low temperature processing, low cost, ease of apparatus set-up, and environmental friendliness. With exceptional shapes and structures obtained by specific hydrothermal growth conditions, 1D ZnO nanostructures can be used for wide variety of applications, including ultraviolet light-emitting devices [8], chemical sensors [9], solar cells [10], water splitting [11], and ultraviolet detector devices [12]. During growth, the density distribution of the nanorods at different position of the substrate in the hydrothermal chamber is generally affected by the transfer of physical momentum and kinetic energy from the incident ions to the surface atoms. Therefore, the morphology and orientation of the nanorods can be strongly influenced by the grown atoms impinging onto the substrate with different incident angles. In this work, a systematic way in the influence of angle-dependent substrate place-

* Corresponding author at: College of Nanotechnology, King Mongkut's Institute of Technology Ladkrabang, Bangkok 10520, Thailand.
E-mail address: krisana_81@hotmail.com (K. Chongsri).

http://dx.doi.org/10.1016/j.ceramint.2017.05.279

Available online 26 May 2017

ment during hydrothermal growth on structural properties and morphologies of Ga/F co-doped ZnO nanostructures is investigated. The angle-dependent substrate placement has been found to be one of the key factors that can control the density, length and shape of the hydrothermally grown Ga/F co-doped ZnO nanostructures.

2. Material and methods

Ga/F co-doped ZnO (GFZO) nanostructures were synthesized by hydrothermal process. First, glass substrates were consecutively washed by deionized water, ethanol and acetone in an ultrasonic cleaner, respectively. The precursor solution used for dip coating was prepared by dissolution of zinc acetate dihydrate ($Zn(Ac)_2{\cdot}2H_2O$) and diethanolamine (DEA) in absolute ethanol and stirred until the solution became clear. The seeding solution was dip-coated onto the cleaned glass substrates followed by a 15 min-annealing step on a hot-plate at 100 °C, after each coating. The coating step was repeated for 10 times. After that, the coated films were annealed in a furnace at 500 °C for 2 h to form ZnO seeding film layers. A solution for the growth of Ga/F co-doped ZnO nanostructures was prepared by adding 100 mL of 0.05 M zinc nitrate hexahydrate ($Zn(NO_3)_2{\cdot}6H_2O$), ammonium fluoride (NH_4F) as a F doping source, gallium (III) nitrate hydrate (GaN_3O_9) as a Ga doping source, and hexamethylenetetramine (HMTA) into 50 mL deionized water. The examined concentration of gallium (III) nitrate hydrate and ammonium fluoride was controlled at 5% and 3%, respectively (designated as 5G3FZO). The Ga/F co-doped ZnO (GFZO) nanostructures were grown on substrates with ZnO seeding layer placed at different tilted-angle and dipped into the prepared solution then loaded into a Teflon autoclave for the hydrothermal synthesis operating at 90 °C for 2 h. Finally, the obtained white solid product was separated from the solution by sonication and was washed with distilled water then was finally dried at 100 °C for 24 h. The morphologies of as-prepared samples were observed by FE-SEM (Hitachi S-4700). EDS (Bruker AXS Quanta 4010) was employed for confirming the existences of fluorine and gallium contents in the samples, meanwhile the crystal structures of all samples were characterized by XRD (Bruker D8 discover diffractometer). Optical transmittance (T) measurement was carried out using a spectrophotometer (Thermo electron corporation). XPS measurement was carried out using PHI5000VersaProbII@Ulvac-PHI, Inc. JAPAN at Beamline 5 XPS measurement was carried out at the beamline 5 of the Synchrotron Light Research Institute (SLRI), Nakhon Ratchasima, Thailand.

3. Results and discussion

The formation of ZnO nanostructures are possibly proceeded via following mechanisms accompanying corresponding Eqs. (1)–(6): Firstly, $Zn(NO_3)_2$ precursor is dissolved and provides zinc ions as noticed in Eq. (1). Ammonia molecules (NH_3) and hydroxide ions($OH-$) provided by HMTA following Eqs. (2) and (3) that are abundant in the mixed aqueous solution can react with zinc ions to initially create $Zn(OH)_2$ as expressed in Eq. (4). This intermediate product can be further dissolved by reacting with superfluous OH^- ions and $Zn(OH)_4^{2-}$ solution is consequently achieved following Eq. (5). In the hydrothermal process, the $Zn(OH)_4^{2-}$ would proceed the dehydration process via Eq. (6) to transform into ZnO nuclei simultaneously. Under extreme hydrothermal conditions, these ZnO nuclei could be self-assembled to form the rod-like nanostructures along a preferred axis orientation depending upon growth conditions:

$$Zn(NO_3)_2 \rightarrow Zn^{2+} + 2NO_3^- \quad (1)$$

$$C_6H_{12}N_4 + 6H_2O \leftrightarrow 6HCHO + 4NH_3 \quad (2)$$

$$NH_3 + H_2O \leftrightarrow NH_4 + OH^- \quad (3)$$

$$Zn^{2+} + 2OH^- \rightarrow Zn(OH)_2\downarrow \quad (4)$$

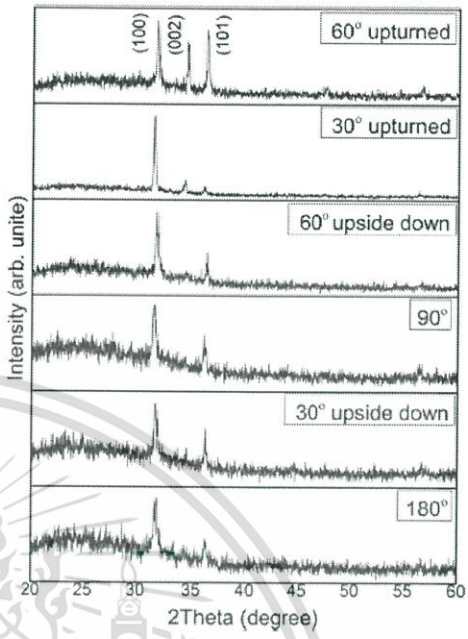

Fig. 1. XRD patterns of GFZO nanostructures with the ZnO seeding layer placed at different tilted-angle.

$$Zn(OH)_2 + 2OH^- \rightarrow Zn(OH)_4^{2-} \quad (5)$$

$$Zn(OH)_4^{2-} \rightarrow ZnO + H_2O + 2OH^- \quad (6)$$

The XRD patterns of Ga/F co-doped ZnO nanostructures with the ZnO seeding layer placed at different tilted-angle are shown in Fig. 1. A broad XRD pattern appeared in all samples in the low 2θ region ranging from 20° to 40° ascribes to a typical diffraction pattern of a glass substrate. Three strong diffraction peaks are observed at 2θ ranging from 30° to 40°, which can be well indexed as wurtzite ZnO crystal structure (JCPDS card No. 36–1451). The diffraction peaks of crystal plane (002) and (101) in 180°, 30° upside-down, 90°, 60° upside-down and 60° upturned samples are nearly negligible but only the diffraction peak of crystal plane (100) can only be observed. For the GFZO nanostructures with a substrate-tilt angle of 60° upturned, non-preferential growing direction is observed accompanying three characteristic peaks of wurtzite ZnO crystal structure. The deterioration of the (100) orientation is considered as the result of the energy minimization, which means the summation of the surface energy in the nanorod, the nanorod-substrate interface energy and strain energy. When the substrate tilted angle becomes greater, the diffusion and collision among the incident species becomes significant at the surface of the deposited nanorods [13]. Energetic deviation of the minimum value for (100) orientation leads to other crystallographic orientation of the rod growth. The intensity of (100) peak increases to some extent for the sample incorporated by F: 3%, but decreases gradually for the samples doped with Ga:5% and co-doped with Ga and F. This variation of ZnO peak intensity might be due to the incorporation of Ga and F in the interstitial sites of ZnO lattice. Based on the variation of the XRD patterns, it could be deduced that the crytallinity and texture of nanorods are influenced significantly by the substrate tilt angle in the deposition process.

Fig. 2 shows the FE-SEM images of GFZO nanostructures with the ZnO seeding layer placed at different tilted-angle and cross sectional view of all samples. It is clearly observed that all samples are hexagonal

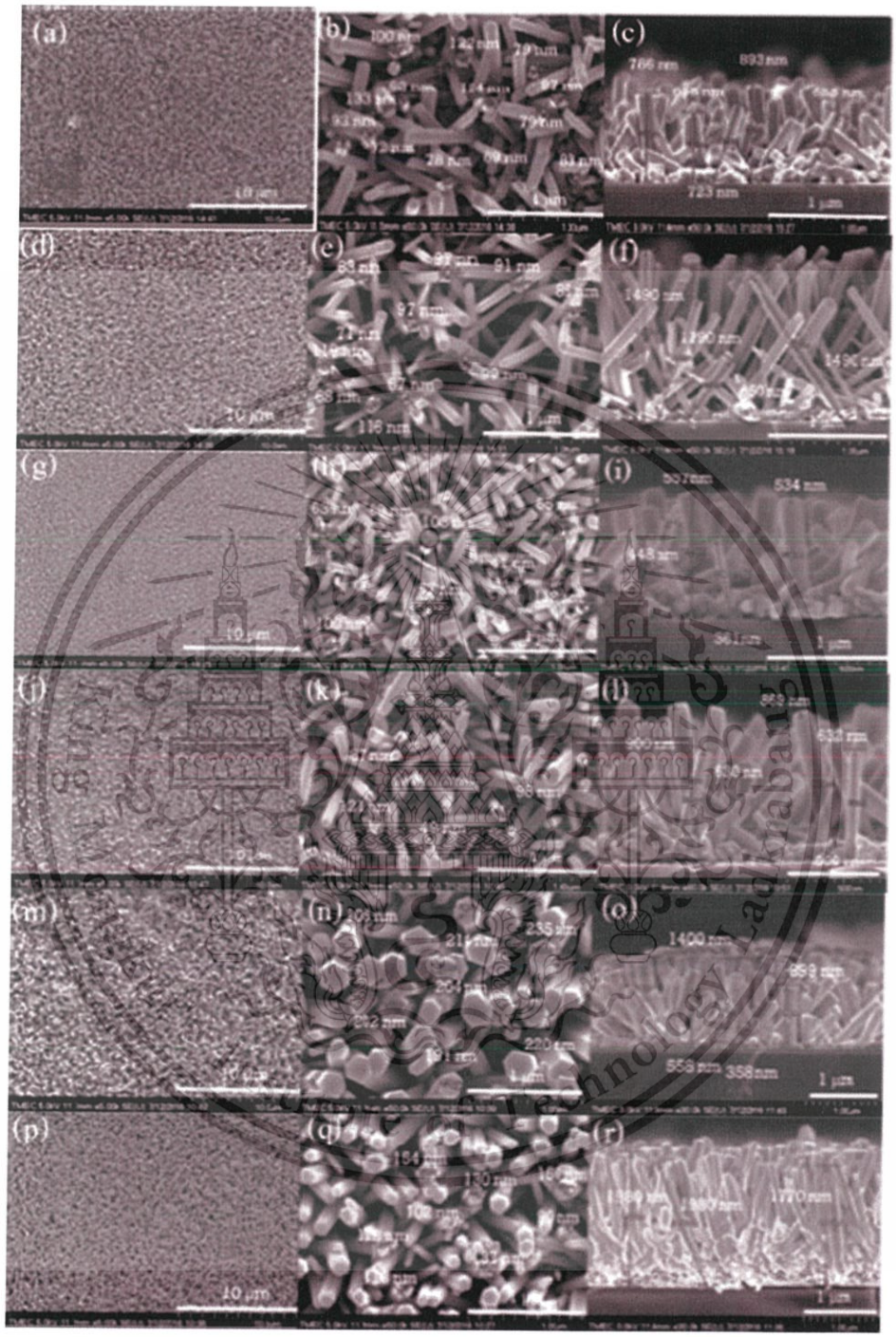

Fig. 2. FE-SEM micrograph of GFZO nanostructures with the ZnO seeding layer placed at different tilted-angles, (180°(a-c), 30°upside-down(d-f), 90°(g-i), 60°upside-down(j-l), 30°upturned(m-o) and60°upturned(p-r)).

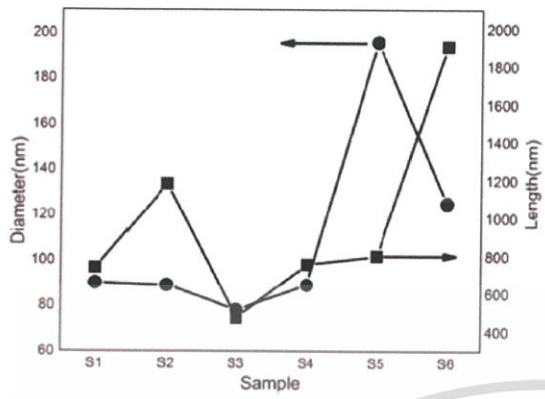

Fig. 3. Average diameter and length of GFZO nanostructures with the ZnO seeding layer placed at different tilted-angles, (180°(S1), 30°upside-down (S2), 90° (S3), 60°upside-down (S4), 30°upturned (S5) and60°upturned (S6)).

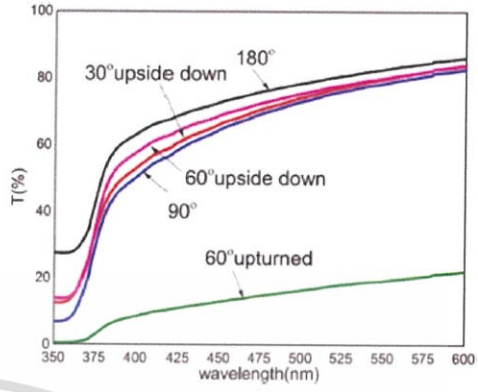

Fig. 4. Optical transmittance of GFZO nanostructures with the ZnO seeding layer placed at different tilted-angle.

in rod-shape and well-grown on the ZnO seed layers. The effects of tilted-angle of substrate placement on the rod size can be clearly seen in Fig. 2. From top images, The average diameter of the GFZO nanorods ranges from 90 nm, 89 nm, 78 nm, 89 nm, 196 nm and 125 nm for 180°, 30°upside-down, 90°, 60°upside-down, 30°upturned and 60°upturned samples, respectively. From cross-sectional FE-SEM images, The average length of the GFZO nanorods is found to be approximately 741 nm, 1185 nm, 475 nm, 758 nm, 802 nm and 1910 nm with 180°, 30°upside-down, 90°, 60°upside-down, 30°upturned and 60°upturned samples, respectively (shown in Fig. 3). Based on previous report, it had been reported that the ZnO crystalline size was also strongly dependent on tilted-angle of substrate. The rate of nanorods growth may be influenced by the placement and tilt-angle of substrate during crystal growth [13]. In fact, the growth rate, crystal features and the preferential in-plane alignment are influenced by the substrate tilt angle. The variation of structural strain due to lattice mismatch between seeding layer of substrate aligned at different tilt angle and the grown rods could arise during hydrothermal growth process. This strain may induce the growth with preferential direction with less strain and inhibit the crystal growth in some directions resulting in the difference in rod shape and size. Moreover, the difference of tilt angle may cause the change in deposited growth flux. The seeding cluster with less structural defect and strain could capture greater deposition flux leading the better nucleation of the grown species on the layer [4]. In addition, the Ga and F dopant also affects the orientation, size, and length of ZnO nanorods [10,11]. The optical transmittance spectra of GFZO nanostructures with the ZnO seeding layer placed at different tilted-angle are exhibited in Fig. 4. All transmission spectra of GFZO nanorods indicate sharp absorption edge in visible range suggesting good quality of GFZO nanorods grown by hydrothermal process. Absorption edge of GFZO nanorods with higher substrate tilt angles of 180°, 30°upside-down, 90° and 60°upside-down shows a significant blue shift to the region of high photon energy. The blue shift of the band-gap energy is considered to be mainly related to the increase of strain in the nanorods induced by defects. Although the increases of the band-gap energy with the increasing tensile strain correlates well with the relation between the nanorod stress and band-gap energy, this empirical relation does not agree with the simulation results of density functional theory based on the bulk ZnO [13]. When the substrate tilt angle becomes relatively high, the increasing strain in ZnO nanocrystal is possibly caused by the good crystallinity with a polycrystalline structure. The GFZO nanorods are nearly transparent in the visible region with more than 60% transparency within 380 nm to 600 nm. The incorporation of Ga and

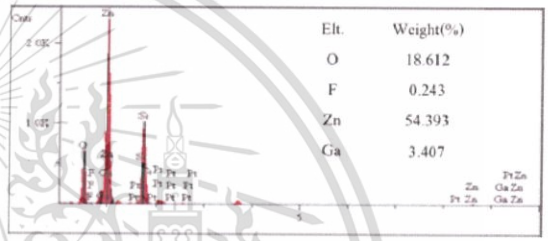

Fig. 5. EDS spectra of 5G3FZO nanostructure.

F dopants is confirmed by the EDS results (Fig. 5). The table inserted in the figure (inset) shows the contents of existing elements in the Ga/F codoped ZnO nanostructure detected by EDS. The elemental content of the marked area is as follows: Zn = 54.393 wt%, O = 18.612 wt%, F = 0.243 wt% and Ga = 3.407 wt%. It is deduced that Ga and F were incorporated into the nanostructures via the hydrothermal process. In the EDS spectrum, numerous well-defined peaks for Zn, O, Ga, and F clearly indicate that the GFZO nanorods are made of Zn, O, Ga and F. No other peaks related to impurities were detected in the spectrum further confirming that the synthesized nanorods are Ga/F co-doped ZnO.

The chemical states of the elements in Ga/F doped ZnO nanostructures were evaluated from XPS measurement. Fig. 6 shows their XPS spectra and Gaussian-resolved components of O, Zn and Ga for the Ga/F doped ZnO nanostructures with the exception of F element. The bonding states of O 1s spectra in bare ZnO sample (assigned as ZnO-O1s) are resolved into two peaks centered at 530.25 eV (O_I) and 531.74 eV (O_{II}). The bonding states of O 1s spectra in Ga-doped ZnO (GZO) sample (designated as GZO-O 1 s) are resolved into two peaks situated at 530.02 eV (O_I) and 531.64 eV (O_{II}) while the bonding states of O 1s spectra in F-doped ZnO (FZO) sample (ascribed as FZO-O1s) are resolved into two peaks positioned at 529.86 eV (O_I) and 531.51 eV (O_{II}). The O_I peak is owing to Zn-O bonds while the O_{II} peak is associated with O_2^- ion in oxygen deficient regions within the ZnO matrix [14]. The electronic states of Zn $2p_{3/2}$ and Zn $2p_{1/2}$ are found at 1021.35 eV and 1044.43 eV for bare ZnO, 1021.27 eV and 1044.34 eV for GZO and 1020.88 eV and 1043.96 eV for FZO sample. Both O 1s and Zn 2p peaks exhibit slight shift in binding energies with Ga and F dopants. This feature implies that the chemical bonding of both Zn and O is altered after Ga and F incorporation into ZnO matrix due to the change of net charge transfer of Zn to O and valence electron density between Zn and O caused by the dopants. [15]. The Ga 2p XPS spectra shows two peaks positioned at 1117.69 eV and 1144.58 eV, which

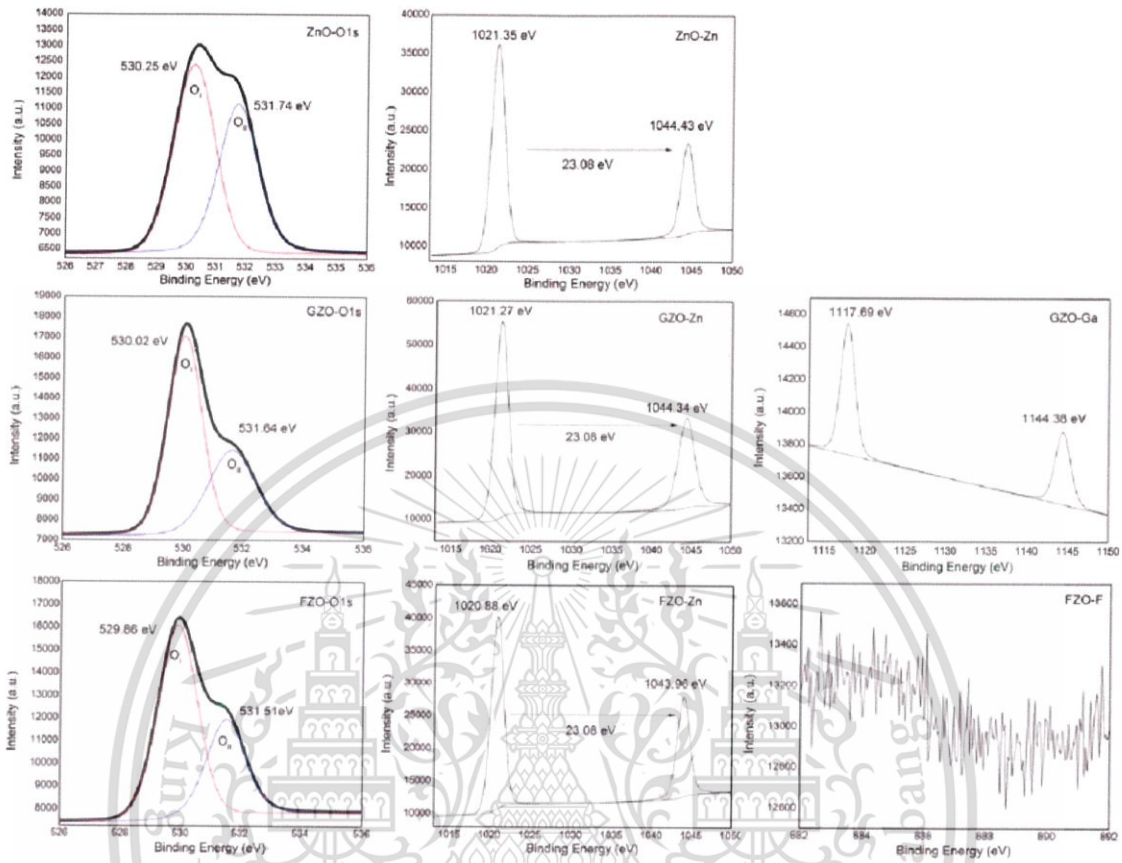

Fig. 6. XPS spectra of the elements in Ga/F doped ZnO nanostructures.

correspond to electronic states of Ga $2p_{3/2}$ and Ga $2p_{1/2}$, respectively. This result confirms the existence of Ga dopant in GZO sample.

4. Conclusions

In summary, Ga/F codoped ZnO nanostructures were successfully prepared by hydrothermal process. The corresponding XRD and SEM results suggested that well-defined GFZO nanostructures could be obtained by this synthesis technique accompanying assistance of dopant atoms incorporated into ZnO materials and the seeding layer placed at different tilted-angle. Possible reactions and mechanisms for the formation of the rods during hydrothermal process are suggested. The absorption edge was found to be blue shifted corresponding to the increase of strain in the nanorods caused by the placement of seeding layer at different tilted-angle. The shape, density, alignment, and orientation of the nanorods can be changed by the tilted-angle of substrate placement. The physical structure and size of GFZO nanorods are steady with diameter rang of 78–196 nm and length rang of 475–1910 nm, respectively. XRD, SEM and UV–Vis results acknowledged that the seeding layer placed at different tilted-angle had significant effect on the morphological properties, crystallization and optical properties of GFZO nanorods.

Conflict of interest

We declare that we do not have any commercial or associative interest that represents a conflict of interest in connection with the work submitted.

Acknowledgements

This work is partially supported by the National Nanotechnology Center (NANOTEC), NSTDA, Ministry of Science and Technology, Thailand, through its program of Center of Excellence and Nation Research Council of Thailand (Grant No. 2559A11802097). Authors would like to thank Department of Applied Physics, Faculty of Science and Technology, Rajabhat Rajanagarindra University Chachoengsao for research fund support.

References

[1] M.S. Bakshi, How surfactants control crystal growth of nanomaterials, Cryst. Growth Des. 16 (2016) 1104–1113.
[2] R. Ebrahimifard, M.R. Golobostanfard, H. Abdizadeh, Sol-gel derived Al and Ga co-doped ZnO thin films: an optoelectronic study, Appl. Surf. Sci. 290 (2014) 252–259.
[3] M.Y. Lu, Y.T. Tseng, C.Y. Chiu, Angle-dependent photodegradation over ZnO nanowire arrays on flexible paper substrates, Nanoscale 9 (2014) 1–8.
[4] A. Yildiz, H. Cansizlu, M. Turkor, R. Abdulrahman, A.A. Hilo, M.F. Cansizoglu, T.M. Demirkan, T. Karabacak, Glancing angle deposite Al-doped ZnO nanostructures with different structural and optical properties, Thin Solid Films 589 (2015) 764–769.
[5] H.S. Yoon, K.S. Lee, T.S. Lee, B. Cheong, D.K. Choi, D.H. Kim, W.M. Kim, Properties of fluorine doped ZnO thin films deposited by magnetron sputtering, Sol. Energy Mater. Sol. Cells 92 (2008) 1366–1372.

[6] K. Thirunavukkarasu, R. Jothiramalingam, Synthesis and structural characterization of Ga-ZnO nanodisk/nanorods formation by polymer assisted hydrothermal process, Powder Technol. 239 (2013) 308–313.
[7] D.T. Phan, G.S. Chung, Effects of defects in Ga-doped ZnO nanorods formed by a hydrothermal method on CO sensing properties, Sens. Actuators B 187 (2013) 191–197.
[8] F.S. Pomar, E. Martinez, M.F. Melendrez, E.P. Tijerina, Growth of vertically aligned ZnO nanorods using textured ZnO films, Nanoscale Res. Lett. 6 (2011) 1–11.
[9] Z. Qing, S. Qiong, Y. Fan, Z. Hua, L. Bin, L. Qian, Direct growth of ZnO nanodisk networks with an exposed (0001) fact on Au comb-shaped interdigitating electrodes and the enhanced gas-sensing property of polar{0001} syrfaces, Sens. Actuators B 195 (2014) 71–79.
[10] R. Pandey, C.H. Wie, X. Lin, J.W. Lim, K.K. Kim, D.K. Hwang, W.K. Choi, Fluorine doped zinc tin oxide multilayer transparent conducting Oxides for organic photovoltaic's Cells, Sol. Energy Mater. Sol. Cells 134 (2015) 5–14.
[11] J.W. Miao, H.B. Yang, S.Y. Khoo, B. Liu, Electrochemcal fabrication of ZnO-CdSe core-shell nanorod arryas for efficient photoelectrochemical water splitting, Nanoscale 5 (2013) 11118–11124.
[12] S.J. Young, Y.H. Liu, Ultraviolet photodetectors with Ga-doped ZnO nanosheets structure, Microelectron. Eng. 148 (2015) 14–16.
[13] H.F. Pang, G.A. Zhang, Y.L. Tang, Y.Q. Fu, L.P. Wang, X.T. Zu, F. Placido, Substrate-tilt angle effect on structural and optical properties of sputtered ZnO film, Appl. Surf. Sci. 259 (2012) 747–753.
[14] B. Paul, B. Singh, S. Ghosh, A. Roy, A comparative study on electrical and optical properties of group III (Al, Ga, In) doped ZnO, Thin Solid Films 603 (2016) 21–28.
[15] H.B. Lee, R.T. Ginting, S.T. Tan, C.H. Tan, A. Alshanableh, H.F. Oleiwi, C.C. Yap, M.H.H. Jumali, M. Yahaya, Controlled defects of fluorine in corporated ZnO nanorods for photovoltaic enhancement, Sci. Rep. 6 (2016) 32645.

APPENDIX B

Journal of Nanoscience and Nanotechnology Vol. 16, (2016), 12962–12966.

Article

Journal of
Nanoscience and Nanotechnology
Vol. 16, 12962–12966, 2016
www.aspbs.com/jnn

Growth and Characterization of Ga/F Co-Doped ZnO Nanorods/Nanodisks via Hydrothermal Process

Krisana Chongsri[1,2], Wuttichai Sinornate[1], Kanokthip Boonyarattanakalin[1], and Wisanu Pecharapa[1,*]

[1]College of Nanotechnology, King Mongkut's Institute of Technology Ladkrabang, Bangkok 10520, Thailand
[2]Department of Applied Physics, Faculty of Science and Technology, Rajabhat Rajanagarindra University, Chachoengsao 24000, Thailand

Ga/F co-doped ZnO nanorods/nanodisks (GFZO) were synthesized using a hydrothermal process by varying the Ga doping levels (1–5 wt.%) and F doping levels (1–5 wt.%). Zinc nitrate, gallium nitrate hydrate and ammonium fluoride were chosen as starting precursors for Zn, Ga and F sources, respectively. The nanorod growth was initiated by zinc oxide seeding film fabricated by spin coating on glass substrate using zinc acetate precursor and annealed at 500 °C for 2 h. Effect of different dopant concentrations on morphologies, structural, and optical properties of the samples were investigated by X-ray diffraction (XRD), scanning electron microscope (SEM) and photoluminescence spectroscopy (PL), respectively. The results of Ga/F codoped ZnO (GFZO) were compared to the single doped specimens including Ga:ZnO (GZO) and F:ZnO (FZO) samples, and bare ZnO sample. The results suggest that content of either Ga or F dopant has high influence on relevant properties of as-synthesized nanorods/nanodisks.

Keywords: GFZO, Nanorods, Nanodisks, Hydrothermal Process.

1. INTRODUCTION

Indium tin oxide (ITO) has been extensively employed for transparent conducting oxide (TCO) material in widerange of optoelectronic devices such as laser diodes, solar cells, transparent thin film transistors and optical detectors because of its high electrical conductivity and high optical transperency.[1] However, ITO is rather expensive and In source is not readily available in nature. Recently, zinc oxide (ZnO) has attracted much attention as a promising alternative TCO material owing to its low cost, non-toxicity, relatively low deposition temperature and comparable optical and electrical properties to ITO. ZnO is typically an *n*-type compound semiconductor with a wide band gap ($E_g \sim 3.2$–3.4 eV at 300 K) with large exciton binding energy (60 meV). The electrical and optical properties of ZnO can be favorably enhanced by appropriate doping with either metal or non-metal elements. It is well recognized that the metal elements from group III including Al, Ga and In have been considered as suitable dopants to adjust both electrical and optical properties of ZnO.[2] When metal dopant atoms are incorporated into ZnO, they preferably replace the Zn host atoms, which can generate extra free electrons resulting in high conductivity or better carrier mobility in ZnO. Among the metal dopants, Ga appears to be a promising element due to its similar ionic radius (0.62 Å) and covalent radius (1.26 Å) to those of Zn (0.74 and 1.34 Å, respectively). In case of non-metal dopant, fluorine is one of the most proper elements widely utilized as a dopant in varieties of host materials including ZnO due to its ionic radius (1.31 Å), which is close to that of oxygen anion (1.38 Å).[3] In contrast to many studies on ZnO doped with cation dopants such as Al or Ga, only few investigations carried out with fluorine as an anion dopant have been found in literatures. Ghosh and colleague[4] reported the self-seeded growth and ultraviolet photo response properties of ZnO nanowire (NW) arrays on glass substrates prepared by solvothermal method using two different sol concentrations. The formation of hexagonal-shaped NWs with diameter of 20–60 nm on the seed layer for 0.1 M sol and mostly of trapezoidal-shaped NWs with base width of 135 nm on the seed layer for 0.03 M sol have been explained considering the longitudinal and transversal growths of ZnO NWs. Hussain and group[5] developed surfactant dependent growth of twinned ZnO nanodisks using a controlled hydrothermal method with the assistance of double surfactants. The morphologies showed wurtzite structure of ZnO with numerous alternating planes which were composed of O^{2-} and Zn^{2+}

*Author to whom correspondence should be addressed.

1533-4880/2016/16/12962/005 doi:10.1166/jnn.2016.13666

ions tetrahedrally coordinated along the *c*-axis. Yousefi and colleague[6] gave the report on the effect of indium concentration on morphologies and optical properties of In-doped ZnO nanostructures with different indium concentrations grown by thermal evaporation method. The In-doped ZnO nanostructures with low concentration of indium exhibited a javelin shape, while the In-doped ZnO nanostructures with a high concentration of indium showed a flake shape. Zhang et al.[7] synthesized high (up to 20 mol%)Ga-doped ZnO (GZO) nanopowders by sol–gel combustion method. The results exhibited that Ga^{3+} ions were successfully doped into ZnO, and all GZO samples were of a single phase and had the same wurtzite structure as pure ZnO. Moreover, the crystal growth rate of ZnO was suppressed by the presence of Ga, and the crystallite size of ZnO could be reduced to be around 5.7 nm at the presence of 20 mol%Ga. Hong et al.[8] represented that the growth of oriented ZnO nanorods can be controlled by hydrothermal method. The concentration of gallium, which was doped into ZnO seed layers prior to ZnO nanorod chemical growth was a key factor for controlling its grain size. Up to now, a number of reports have claimed that ZnO nanostructures could able to synthesize by various growth techniques such as co-precipitation process,[9] sol–gel process[10] and hydrothermal process.[11] Among these techniques, hydrothermal process is considered to be one of the versatile methods for synthesizing various kinds of nanostructures. The advantages of hydrothermal method include lower temperature requirement, lower cost, and ease of method and processes.

In this report, the effort was carried out on the synthesis of Ga and F co-doped ZnO nanorods/nanodisks by hydrothermal process. The effects of Ga and F doped on crucial properties of the nanorod and nanodisks were investigated by X-ray diffraction (XRD), scanning electron microscope (SEM) and photoluminescence spectroscopy (PL).

2. EXPERIMENTAL DETAILS

Ga/F co-doped ZnO (GFZO) nanorods/nanodisks were synthesized by hydrothermal process. First, glass substrates were consecutively washed by deionized water, ethanol and acetone in an ultrasonic cleaner. The precursor solution used for dip-coating was prepared by dissolution of zinc acetate dihydrate ($Zn(Ac)_2 \cdot 2H_2O$) and diethanolamine (DEA) in absolute ethanol under stirring until the solution became clear. The seeding layer was deposited onto the cleaned glass substrates by conventional dip-coating. After that, the coated films were annealed in a furnace at 500 °C for 2 h to form ZnO seeding film layer. The precursor for growth of Ga/F codoped ZnO nanorods/nanodisks was prepared by adding 0.05 M zinc nitrate hexahydrate ($Zn(NO_3)_2 \cdot 6H_2O$), ammonium fluoride (NH_4F) designated as F doping source, gallium(III) nitrate hydrate (GaN_3O_9) determined as Ga doping source and hexamethylenetetramine (HMTA) into 50 mL deionized water. The examined concentrations of gallium(III) nitrate hydrate were: 1%, 3%, and 5% (designated as 1GZO, 3GZO and 5GZO, respectively). The ZnO-seeded substrates were dipped into the prepared solution loaded in a Teflon autoclave for hydrothermal synthesis operating at 90 °C for 2 h. Finally, the obtained white solid product was separated from the solution by centrifugation, washed with distilled water and dried at 100 °C for 24 h. The same procedure was used to prepare the samples with different dopant amounts (1%, 3% and 5%) of F-doped ZnO (designated as 1FZO, 3FZO and 5FZO, respectively) and another Ga/F co-doped ZnO were Ga: 1%, 3%, and 5%, F: 3% (designated as 1G3FZO, 3G3FZO and 5G3FZO, respectively). The morphologies of as-prepared samples were observed by SEM (ZEISS EVO MA10). EDS (Bruker AXS Quantax 4010) was employed for confirming existence of fluorine and gallium contents in the samples, meanwhile the crystal structures of all samples were characterized by XRD (X'Pert PRO). The photoluminescence (Agilent Technologies) emission spectra of the samples deposited at various Ga and F concentrations were collected at room temperature.

3. RESULTS AND DISCUSSION

The XRD patterns of Ga/F co-doped ZnO nanorods/nanodisks on the ZnO seeding film layer are shown in Figure 1. Three strong diffraction peaks are observed at 2θ ranging from 30° to 40°, which can be nicely indexed as wurtzite ZnO crystal structure (JCPDS card No. 36-1451). The diffraction peaks of crystal plane (002) and (101) in 5FZO, 5GZO and 5G3FZO samples are nearly negligible but only the diffraction peak of crystal plane (100) can be observed. The intensity of (100) peak increases to some extent for the sample incorporated by F:

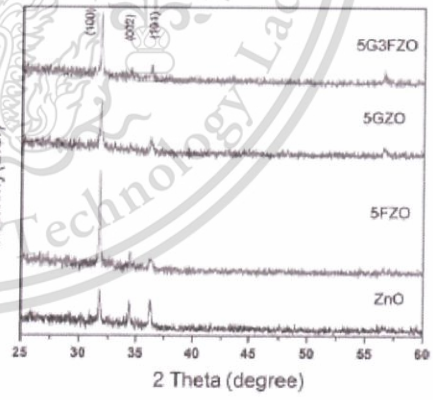

Figure 1. XRD patterns of ZnO, 5GZO, 5FZO and 5G3FZO nanorods/nanodisks with the different Ga and F contents.

5%, but decreases gradually for the samples doped with Ga:5% and co-doped with Ga and F. This variation of ZnO peak intensity might be due to the incorporation of Ga and F in the interstitial sites of ZnO lattice. The growth processes of ZnO crystallites are possibly proceeded via following mechanisms and corresponding Eqs. (1)–(6):[12] Firstly, $Zn(NO_3)_2$ precursor is dissolved and provides zinc ions as noticed in Eq. (1). Ammonia molecules (NH_3) and hydroxide ions (OH^-) provided by HMTA following Eqs. (2)–(3) that is abundant in the mixed aqueous solution can react with zinc ions to from $Zn(OH)_2$ via Eq. (4). This intermediate product can be further dissolved by reacting with superfluous OH^- ions and $Zn(OH)_4^{2-}$ solution is consequently achieved following Eq. (5). In the hydrothermal process, the $Zn(OH)_4^{2-}$ would proceed the dehydration process via Eq. (6) to transform into ZnO nuclei simultaneously. Under extreme hydrothermal conditions, these ZnO nuclei could be self-assembled to form the rod-like nanostructures along a preferred axis orientation:

$$Zn(NO_3)_2 \rightarrow Zn^{2+} + 2NO_3^- \quad (1)$$

$$C_6H_{12}N_4 + 6H_2O \leftrightarrow 6HCHO + 4NH_3 \quad (2)$$

$$NH_3 + H_2O \leftrightarrow NH_4 + OH^- \quad (3)$$

$$Zn^{2+} + 2OH^- \rightarrow Zn(OH)_2 \downarrow \quad (4)$$

$$Zn(OH)_2 + 2OH^- \rightarrow Zn(OH)_4^{2-} \quad (5)$$

$$Zn(OH)_4^{2-} \rightarrow ZnO + H_2O + 2OH^- \quad (6)$$

The full-width at half-maximum (β) of the main diffraction peak (100) was used to calculate the crystallite size of the samples following Scherrer's Eq. (7)

$$D = \frac{0.9\lambda}{\beta \cos\theta} \quad (7)$$

where θ is the diffraction angle, and λ is 1.54 Å of the Cu K_α line. The crystallite size of ZnO, 5GZO, 5FZO and 5G3FZO are in the range of 50–140 nm. From Figure 1, it can be seen that all nanorods/nanodisks have the hexagonal shape, suggesting ZnO nanorods/nanodisks in all the samples grow along the (100) direction. This may originate from the fact that ZnO crystal growth are inhibited in other directions, while the (100) direction is preferable and has the fastest growth rate. However, incorparated dopants may also greatly affect the growth rate of ZnO nanorods/nanodisks along this direction by modifying its surface energies.[13]

Figure 2 shows the SEM images of ZnO, GZO, FZO and GFZO nanorods/nanodisks with different Ga and F contents and cross sectional view of 5G3FZO samples. The effects of Ga and F doping concentration on grain size can be clearly seen in Figure 2. Undoped ZnO, 1FZO, 5GZO, 1G3FZO and 3G3FZO exhibit a granular structure. However, the particle size is significantly dependent on the Ga and F doping concentration. The undoped

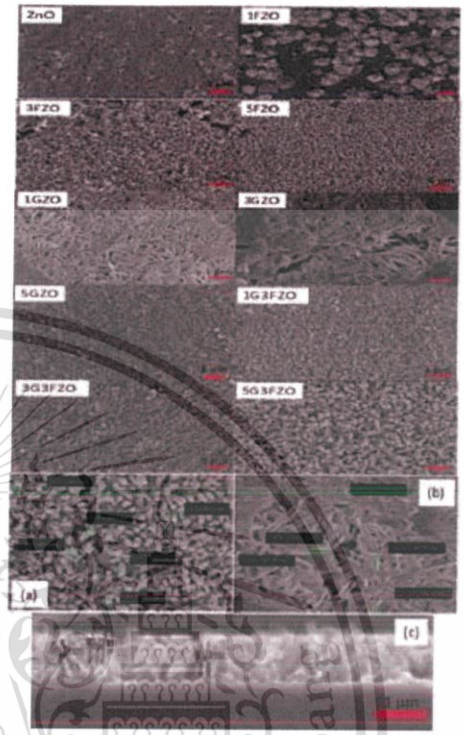

Figure 2. SEM micrograph of ZnO, 5GZO, 5FZO and 5G3FZO nanorods/nanodisks with the different Ga and F contents and cross sectional view of 5G3FZO nanorods.

ZnO has large particle size while increasing Ga doping concentration can induce the reduction in particle size. Based on previous report, the ZnO crystalline size was also strongly dependent on the Ga and F dopant concentration.[14] The 3FZO and 5FZO grown on ZnO seeding layer exhibit slightly poorer vertical alignment. All the nanorods are hexagonal and well-grown on the ZnO seed layers. The F dopant strongly affects the orientation, size, and length of ZnO nanorods. However, the nanorod size shows significant decrease with increasing doping concentration. The smaller size of FZO nanorods grown on ZnO seeding film may results from the decrease in the F concentration. SEM image in Figure 2(a) illustrates that hydrothermally grown ZnO forms uniform rods in large area with an average length of ~250 nm (cross-view not shown) and diameter of ~80 nm. Moreover, nanodisk morphology could be observed in the samples doped with Ga. All nanodisks are hexagonal in shape and well-grown on the ZnO seed layers. The Ga dopant strongly affects the orientation and size of ZnO nanodisk,

especially its size which decreases with increasing doping concentration as observed in Figure 2(b). Meanwhile, the GFZO samples have flat hexagonal crystallographic planes indicating that the ZnO nanorods are hexagonal in crystal structure. In addition, cross-sectional SEM image of the nanorods arrays as noticed in Figure 2(c) reveals that sizes of nanorods are in the range of 190–210 nm and length of about 1 μm. This feature could be attributed to the rapid vertical growth rate of nanorod/nanodisk and its limited growth along the lateral direction. The rate of nanorod/nanodisk growth may greatly depend on the property of seed substrate layer and type of dopants. The grain sites of seed layers typically serve as nucleation sites for nanorod/nanodisk growth, and the roughness of these grain sites has an important function in the initial growth. Smaller nucleation size and smooth seed layer surface are possibly favorable for nanorod/nanodisk formation. In addition, Ga/F codoped into ZnO could induce the growth of smaller grains with an increase in number of grains per unit area. At higher nucleation densities, lateral growth is effectively suppressed, which results in rods with smaller sizes. For rod/disk growth, Zn^{2+} ions may diffuse into the growth site and create bonds with O^{2-} ions. A lower nucleation size requires a smaller number of diffused Zn^{2+} ion and less bonding formation to create rods. These conditions may result in a higher nanorod/nanodisk growth rate and create mixed morphologies of Ga/F codoped ZnO nanorod/nanodisk.[8] The doped concentration and existence of relevant elements in 5G3FZO was measured by EDS and corresponding result is shown in Figure 3. The table inserted in the figure (inset) shows the contents of existing elements in the Ga/F codoped ZnO nanostructure detected by EDS. The elemental content of the marked area is as follows: Zn = 73.595 wt.%, O = 14.938 wt.%, F = 0.068 wt.% and Ga = 10.810 wt.%. It is deduced that Ga and F were incorporated into the nanostructures via the hydrothermal process. Photoluminescence spectroscopy is a powerful technique for investigating the effect of impurity doping on optical properties of host material. Figure 4 shows the room temperature PL spectra of the undoped ZnO and Ga/F codoped ZnO nanorod/nanodisk. The PL spectra of undoped ZnO and Ga/F codoped ZnO exhibit strong peak in the ultraviolet region (378 nm) and a violet emission peak in the visible

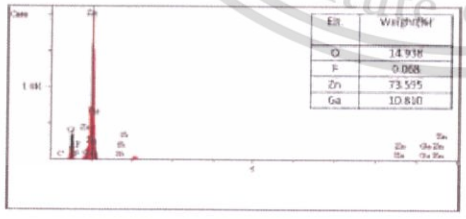

Figure 3. EDS spectra of 5G3FZO nanostructure.

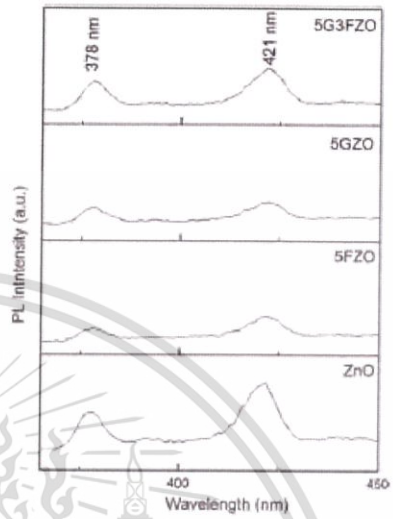

Figure 4. The room temperature photoluminescence spectra of pure ZnO and GFZO nanorods/nanodisks with the different Ga and F contents.

region at around 421 nm. The prominent UV emission, which strongly relates to the crystallite quality of ZnO, is contributed by the conduction–valence band combination (~375 nm), shallow donor (~395 nm) while the violet emission at 421 nm is due to the interstitial zinc (Zn_i).[14] Furthermore, it is observed that the intensity of these peaks gradually decrease with increasing Ga and F doping concentration. In ZnO lattice, Ga and F atoms may substitute Zn atoms or occupy Zn vacancies resulting in the decrease of Zn vacancies and reduction of UV and violet emission intensity. However, doping with suitable amounts of Ga, F (as seen in 5G3FZO sample), the Ga and F atoms may occupy the Zn vacancies at defect positions and increase the donor-related defect (such as shallow donor and zinc interstitial) quantities in ZnO nanorods/nanodisks, leading to strong UV emissions in the PL spectra.[15]

4. CONCLUSION

In summary, Ga/F codoped ZnO nanorods/nanodisks were successfully synthesized by hydrothermal process. The corresponding XRD and SEM results suggest that well-defined GFZO nanorods/nanodisks could be obtained by this synthesis technique. Possible reactions and mechanisms for the formation of these nanostructures during hydrothermal process are suggested. XRD, SEM and PL results illustrated that Ga and F dopant had significant effect on the morphological properties, crystallization and optical properties of G/F codoped ZnO nanorods/nanodisks. The nanodisk morphology was obtained in sample with 1 wt.% Ga doping content while nanorod structure was achieved in 5 wt.%

FZO. Moreover, the co-doped samples have flat hexagonal crystallographic planes indicating that the ZnO are hexagonal in crystal structure.

Acknowledgments: This work has partially been supported by the National Nanotechnology Center (NANOTEC), NSTDA, Ministry of Science and Technology, Thailand, through its program of Center of Excellence Network. Authors gratefully acknowledge the support from College of Nanotechnology, King Mongkut's Institute of Technology Ladkrabang (KMITL), Nation Research Council of Thailand (Grant No. 2559A11802097) and Department of Applied Physics, Nakhon Pathom Rajabhat University (NPRU) for PL measurements. K. Chongsri would like to thank Rajabhat Rajanagarindra University for Doctoral scholarship.

References and Notes

1. S. M. Chung, J. H. Shin, W. S. Cheong, C. S. Hwang, K. I. Cho, and Y. J. Kim, *Ceram. Int.* 38S, S617 (**2012**).
2. Y. S. Zou, H. Yang, H. P. Wang, D. Lou, C. J. Tu, and Y. C. Zhang, *Physica B* 414, 7 (**2013**).
3. H. Mahdhi, Z. B. Ayadi, S. Alaya, J. L. Gauffier, and K. Djessas, *Superlattice. Microst.* 72, 60 (**2014**).
4. R. Ghosh, M. Dutta, and D. Basak, *Appl. Phys. Lett.* 91, 073108 (**2007**).
5. S. Hussain, T. Liu, M. Kashif, B. Miao, J. He, W. Zeng, Y. Zhang, U. Hashim, and F. Pan, *Mater. Lett.* 118, 165 (**2014**).
6. R. Yousefi, F. J. Sheini, A. K. Zak, and M. R. Mahmoudian, *Ceram. Int.* 38, 6295 (**2012**).
7. X. Zhang, X. Pu, Y. Chen, X. Gu, D. Xu, and S. Zhang, *Mater. Lett.* 112, 129 (**2013**).
8. H. S. Hong, and G. S. Chung, *Sensor. Actuat B-Chem.* 195, 446 (**2014**).
9. D. Raoufi, *Renew. Energy* 50, 932 (**2013**).
10. R. Ebrahimifard, M. R. Golobostanfard, and H. Abdizadeh, *Appl. Surf. Sci.* 290, 252 (**2014**).
11. K. Thirunavukkarasu and R. Jothiramalingam, *Powder Technol.* 239, 308 (**2013**).
12. P. Yu, J. Wang, H. Y. Du, P. J. Yao, Y. Hao, and X. G. Li, *J. Nanomater.* 2013, Article ID: 751826 (**2013**).
13. W. J. Li, E. W. Shi, W. Z. Zhong, and Z. W. Yin, *J. Cryst. Growth* 203, 186 (**1999**).
14. M. Willander, O. Nur, J. R. Sadaf, M. I. Qadir, S. Zaman, A. Zainelabdin, N. Bano, and I. Hussain, *Materials* 3, 2643 (**2010**).
15. D. T. Phan and G. S. Chung, *Sensor. Actuat. B-Chem.* 187, 197 (**2013**).

Received: 21 January 2016. Accepted: 29 June 2016.

APPENDIX C

Journal of Nanoscience and Nanotechnology Vol. 18, (2018), 7296–7301.

Article

Journal of
Nanoscience and Nanotechnology
Vol. 18, 7296–7301, 2018
www.aspbs.com/jnn

Effects of Seeding Layer Annealing Temperature on Physical and Morphological Structure of Ga/F Co-Doped ZnO Nanostructures

Krisana Chongsri[1,2], Yoichiro Neo[3], Hidenori Mimura[3], Kanokthip Boonyarattanakalin[1], and Wisanu Pecharapa[1,*]

[1]College of Nanotechnology, King Mongkut's Institute of Technology Ladkrabang, Bangkok 10520, Thailand
[2]Department of Applied Physics, Faculty of Science and Technology, Rajabhat Rajanagarindra University, Chachoengsao 24000, Thailand
[3]Research Institute of Electronics, Shizuoka University, 3-5-1 Johoku Naka-ku Hamamatsu 432-8011, Japan

In this work, effects of annealing temperature of seeding layer on structural properties and morphologies of Ga/F co-doped ZnO nanostructures synthesized by hydrothermal process were investigated by varying the annealing temperature of seed layer as 300–500 °C. The ZnO seeding layers were deposited onto cleaned glass substrates by dip-coating technique using zinc acetate dehydrate $(CH_3COO)_2Zn \cdot 2H_2O$ as starting coating precursor. The Ga/F co-doped ZnO nanostructures were then grown on these seed layers by conventional hydrothermal process using $Zn(NO_3)_2$, NH_4F, GaN_3O_9 and hexamethyltetramine as Zn, F and Ga sources, respectively. Effect of seed layer annealing temperature on morphologies, structural and Photoluminescence properties was investigated by X-ray diffraction (XRD), Field emission scanning electron microscope (FE-SEM), and Photoluminescence spectra, respectively. Variation of annealing temperature of seed layers can significantly result to the difference in morphological, structure and shape of the as-synthesized nanostructure products. It is found that the increase in annealing temperature leads to alternation in their shape from vertically-aligned nanosheets to nanorods with their average size ranging from 50 to 200 nm. Furthermore, the luminescence could be ascribed to the different contributions of the defect emissions, such asthe increase in the oxygen vacancy (V_O) emissionor the decrease of the Zinc vacancy (V_{zn}). However, it can be speculated from the photoluminescence that the incorporated Ga and F substitute into ZnO.

Keywords: ZnO, Ga/F Co-Doped ZnO, Seed Layer Annealing Temperature, Hydrothermal Process.

1. INTRODUCTION

Recently, one-dimensional (1D) nanostructures have been extensively researched because of their high potential in practical applications in nanoelectronic and optoelectronic devices. Various techniques have been employed and developed for synthesizing 1D nanostructures such as thermal chemical vapor deposition,[1] hydrothermal method,[2,3] metal-organic chemical vapor deposition (MOCVD)[4] and electrodeposition.[5] The hydrothermal method has become one of promising routes for the large scale production of nanomaterials because of its simplicity, ease of equipped system, fastness, economical and low growth temperature characteristics.[6] ZnO nanostructures have been extensively studied as a key optoelectronic material. Owing to their uniqueness combined with electrical and optical properties, ZnO-based materials have been widely applied for transparent and flexible device applications such as ultraviolet light-emitting devices,[7] chemical sensors,[8] solar cells,[9] and ultraviolet detector devices.[10] When ZnO is doped with group III (Al,[11] B,[12] Ga[13,14]) or group VII (F,[15] Cl[16]) elements, the dopants preferably replace the Zn host atoms that could offer extra free electrons to the system resulting in enhancement in electrical conductivity and carrier mobility.[17] Among metal dopants, Gallium ion emerges to be a promising element due to its close ionic radius (0.62 Å) and covalent radius (1.26 Å) to those of Zn (0.74

*Author to whom correspondence should be addressed.

1533-4880/2018/18/7296/006 doi:10.1166/jnn.2018.15716

and 1.34 Å, respectively).[18] Furthermore, the ionic radius of fluorine ion (0.117 nm) is similar to that of oxygen (0.122 nm).[19] It is implied that fluorine may be a suitable anion doping candidate at oxygen site in ZnO matrix.

Various chemical and physical deposition techniques have recently been used to deposit ZnO-based thin films. These mentioned techniques include vapor–liquid–solid epitaxial deposition,[20] pulsed laser deposition,[21] spray pyrolysis,[22] sol–gel[23] and radiofrequency magnetron sputtering.[24] Moreover, thin film or seed layer materials are also crucial factors for the high-quality growth of nanostructures. It is evident that nanostructure growth assisted by seeding layer is strongly dependent on the seed layer and dopants, which play important roles in nucleation and dissimilar growth of the nanostructures with varying sizes, density, geometric shapeand direction of ZnO nanostructures. Alsultany et al.[25] reported on the growth of ZnO nanowires on ITO seed layer/glass by thermal evaporation method and effects of ITO seed layer annealing temperature on the properties of the grown nanowires. The seed annealing temperature was considered as crucial factor in the growth of ZnO-NWs and the improvement in the morphological, structural, and optical properties of nanowires strongly depended on the properties of the seed layer, where the nucleation process on the substrate depended on the nucleation sites and the formation of seed particles. Guo et al.[26] reported on the hydrothermal synthesis and conductive properties of Ga-doped ZnO nanostructures. The synthesized samples were in nanosheet-like structure possessing good crystallinity with wurtzite structure and decreasing grain size with the increase of Ga content. It was also mentioned that Ga could effectively act as donor guest to the ZnO host leading to the lessening in electrical resistivity of the matrix when it was incorporated by Ga with specific 2% doping content. In our previous works, effects of crucial process parameters including Ga and F dopant,[27] tilted-angle of seeding layer[28] and seeding layer thickness[29] were experimentally conducted and investigated. The results evidently disclosed that Ga and F dopants have strong influence not only in an alternation of its morphological properties including shape, size and density but also in the structural defect-related optical properties of grown structures. Meanwhile, growth direction and morphology of the hydrothermally grown structures were significantly affected by tilted-angle of seeding layer and seeding layer thickness. It is believed that annealing temperature would be one of key process factors directly affecting on the structural properties of seeding layer for hydrothermal growth of ZnO-based nanostructures.

In this work, we systematically investigate the influence of seed layer annealing temperature on structural properties of Ga/F co-doped ZnO (GFZO) nanostructures. The seed layer annealing temperature has been considered to be one of the crucial factors that control the morphology, structures and shape of the hydrothermally grown Ga/F co-doped ZnO nanostructures.

2. EXPERIMENTAL DETAILS

Ga/F co-doped ZnO (GFZO) nanostructures were synthesized by hydrothermal process. First, glass substrates were consecutively washed by deionized water, ethanol and acetone in an ultrasonic cleaner. The precursor solution used for dip coating was prepared by dissolving zinc acetate dihydrate ($Zn(Ac)_2 \cdot 2H_2O$) and diethanolamine (DEA) in absolute ethanol and stirred until the solution became clear. The seeding solution was dip-coated onto the cleaned glass substrates followed by a 15 min-annealing step on a hot-plate at 100 °C, after each coating. The coating step was repeated for 10 times. After that, the coated films were annealed in a furnace at different temperature range of 200–500 °C for 2 h to form ZnO seeding film layer. A solution for the growth of Ga/F co-doped ZnO nanorods/nanodisks was prepared by adding 100 mL of 0.05 M zinc nitrate hexahydrate ($Zn(NO_3)_2 \cdot 6H_2O$), ammonium fluoride (NH_4F) as a F doping source, gallium (III) nitrate hydrate (GaN_3O_9) as a Ga doping source, and hexamethylenetetramine (HMTA) into 50 mL deionized water. The examined concentrations of gallium (III) nitrate hydrate and ammonium fluoride was designated at 5% and 3%, respectively (referred as 5G3FZO). The ZnO-seeded substrates were dipped into the prepared solution then loaded in a Teflon autoclave for the hydrothermal synthesis operating at 90 °C for 2 h. The samples were washed with distilled water and dried at 100 °C for 24 h. The morphologies of as-prepared samples were observed by FE-SEM (Hitachi S-4700). EDS (Bruker AXS Quanta 4010) was employed for confirming the existence and content of relevant elements in the samples, meanwhile the crystal structures of all samples were characterized by XRD (Bruker D8 discover diffractometer). The photoluminescence spectroscopy was conducted to investigate the defect induced by dopant in the sample. In PL experiment, helium–cadmium laser with wavelength of 325 nm was used as optical excitation source. The sample was cooled down from room temperature (RT) to 25 K in a typical cryostat. The luminescence signal from the sample was collected by fiber optic spectrophotometer (Ocean Optics Inc. USB 4000).

3. RESULTS AND DISCUSSION

Figure 1 shows XRD patterns of ZnO seed layers deposited by the dip coating process and annealed at 200 °C, 300 °C, 400 °C and 500 °C. For the sample annealed at 200 °C, no noticeable diffracted peak is observed, indicating the amorphous phase of the seeding layer or incompleteness in ZnO compound at this specific temperature. Diffraction patterns of ZnO began to appear as the coated layer was annealed at 300 °C. This feature indicates the change of the seed structure from amorphous to polycrystalline phase ZnO. Based on previous work reported by Kim,[30] the corresponding thermogravimetric (TG) result of zinc acetate dehydrate revealed

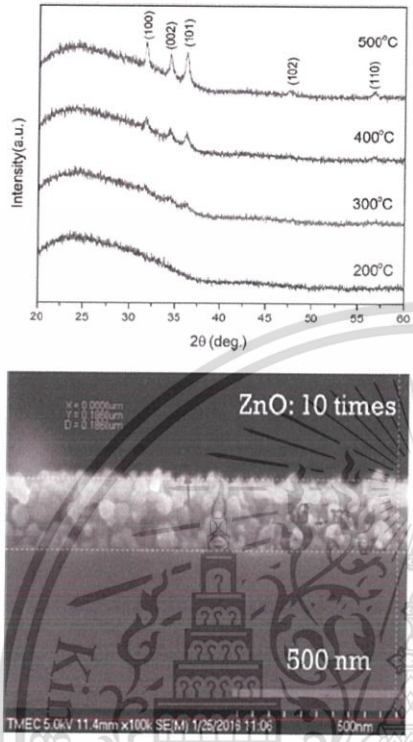

Figure 1. XRD patterns of ZnO seed layers and FE-SEM images of cross section for ZnO seed layer annealed at different temperatures.

that the decomposition of acetate groups started when the annealing temperature elevated to 220 °C and the formation of ZnO would initiate beyond this point. The diffraction peaks became pronounced and distinct as annealing temperature was further increased to 400 °C due to the ZnO crystallization that normally started beyond 375 °C.[31] The presence of significant peaks along (100), (002) and (101) are positioned at $2\theta = 31.8°$, 34.5° and 36.2°, respectively. The orientation informed by XRD data of samples annealed at this temperature range indicates the polycrystalline nature of these seed layers that are well agreeable to JCPDS Card No. 36-1451. The crystal sizes were derived from the X-ray diffraction spectra following the Scherrer's relation expressed in Eq. (1):

$$D = \frac{0.9\lambda}{\beta \cos\theta} \tag{1}$$

Where D is the crystallite size of the sample, constant K (0.9) is the shape factor, λ is the X-ray wavelength of Cu K_α (0.154 nm), β is the full-width at half maximum (FWHM), and θ is the Bragg angle. It is obviously noticed that the crystal size of the seed layer significantly increases from 12.36 nm to 26.23 nm as the annealing temperature increases from 400 °C to 500 °C, respectively. This manner indicates that the crystallinity of the ZnO seed layer is enhanced with increasing annealing temperature, which is also confirmed by the FE-SEM images (cross section). The FE-SEM image exhibits uniformity in grain size distribution and thickness whose average thickness is approximately 186 nm.

The X-ray diffraction patterns of 5G3FZO nanostructures grown on ZnO seed layers with different seed annealing temperatures are shown in Figure 2. The characteristic peaks indicate that 5G3FZO nanostructures with wurtzite structure were successfully fabricated on ZnO seed layer with different annealing temperatures. Regarding to the difference in XRD patterns, It is suggested that seed layer with different annealing temperature has strong influence on crystallinity and preferred orientation direction of the grown structure. At annealing temperature of 200–300 °C, no any characteristic peak of ZnO was observed, reflecting to imperfection of crystal growth or amorphous phase of the product. As the annealing temperature was raised to 400 °C, corresponding XRD pattern indicated the crystal growth of hexagonal wurtzite ZnO structure without preferable growth direction onto the seeding layer. After the annealing temperature of seeding layer elevated to 500 °C, the hydrothermally grown structure had wurtzite structure with (002) preferable growth direction, implying the vertically-aligned rod structures of the product. Moreover, no second phase of impurity was detected in XRD pattern, suggesting good incorporation of the dopants in ZnO structure.

In addition, the lattice constant, c, of the (002) plane was evaluated by following equation:

$$c = \frac{\lambda}{\sin\theta} \tag{2}$$

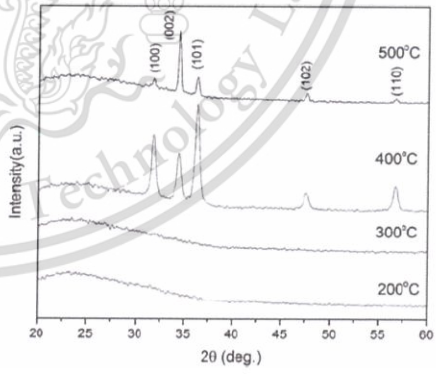

Figure 2. XRD patterns of 5G3FZO nanostructures grown on ZnO seed layer annealed at different temperatures of 200–500 °C.

Table I. Structural properties of 5G3FZO nanostructures on ZnO seed layer as grown and with different seeds annealing temperature.

Seed layers annealing temp. (°C)	$2\theta_{(002)}$ (°)	FWHM (°)	C (Å)	D (nm)	Strain ε_{zz} (%)
400	34.40	0.488	5.210	15.54	0.0901
500	34.46	0.281	5.443	26.98	0.0945

Another important parameter is the strain ε_{zz} along the c-axis that can be calculated using the following formula.

$$\varepsilon_{zz} = \frac{C - C_o}{C_o} \times 100 \tag{3}$$

where C_o is 0.5206 nm which represents standard lattice constant.[32]

The c-axis lengths for 5G3FZO nanostructures grown on ZnO seed layer annealed at 400–500 °C were calculated using the standard equation for the wurtzite crystal structure and are given in Table I. These results indicate that, depending on the different seed annealing temperatures, the nanostructures could grow with different values of c-axis lattice parameter. Since the growth is highly preferred along c-axis and the c-axis parameter changes, the strain values along the c-axis (ε_{zz}) of the seed layer has been calculated. In typical, strain ε_{zz} of the seed layer is considered to be one crucial factor that has significant influence on structural properties of the grown structures on the layer as a result of the lattice mismatch between two materials. However, it has been also demonstrated that when the crystallite sizes are small enough, such as at early stages of the deposition, film can develop a tensile stress due to the atom-to-atom attraction forces at the grain boundaries.

The morphologies of 5G3FZO nanostructures grown on ZnO seed layer annealed at 200 °C, 300 °C, 400 °C and 500 °C, measured by FE-SEM are shown in Figure 3. With increasing seed layer annealing temperature, the structure of 5G3FZO nanodisks has been changed to nanorods hexagonal-like structure. The diameters and length of 5G3FZO nanorods evaluated from SEM image are found to be in the range of 50–200 nm and approximately 1 μm, respectively. The increase in annealing temperature gives the positive effect of enhancing strain of the ZnO seed layer which will act as the active nucleation sites during GFZO nanostructures growth.

The formation of ZnO nanostructures during hydrothermal process can possibly proceed via following mechanisms accompanying corresponding Eqs. (4)–(9):

$$Zn(NO_3)_2 \rightarrow Zn^{2+} + 2NO_3^- \tag{4}$$

$$C_6H_{12}N_4 + 6H_2O \leftrightarrow 6HCHO + 4NH_3 \tag{5}$$

$$NH_3 + H_2O \leftrightarrow NH_4 + OH^- \tag{6}$$

$$Zn^{2+} + 2OH^- \rightarrow Zn(OH)_2 \downarrow \tag{7}$$

$$Zn(OH)_2 + 2OH^- \rightarrow Zn(OH)_4^{2-} \tag{8}$$

$$Zn(OH)_4^{2-} \rightarrow ZnO + H_2O + 2OH^- \tag{9}$$

At low annealing temperature range of 200 °C–300 °C, the seed layer is still in amorphous phase that would prevent the complete growth of good crystalline structure during hydrothermal process. Hydrothermally grown structure

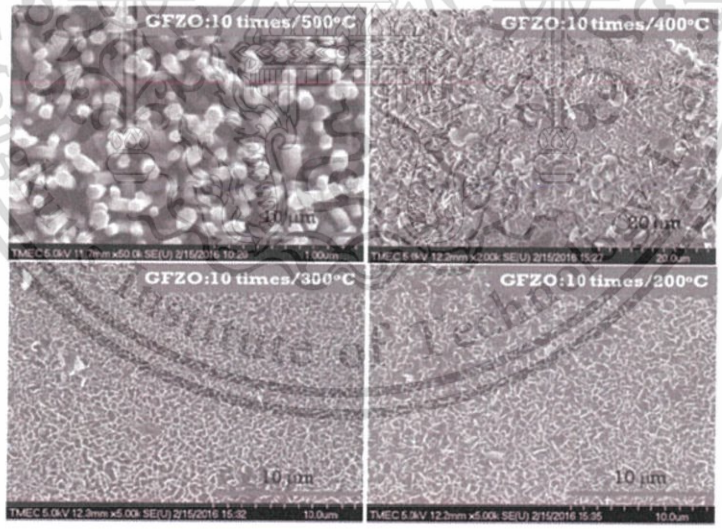

Figure 3. FE-SEM images of 5G3FZO nanostructures with the different annealing temperature of seed layer as 200–500 °C.

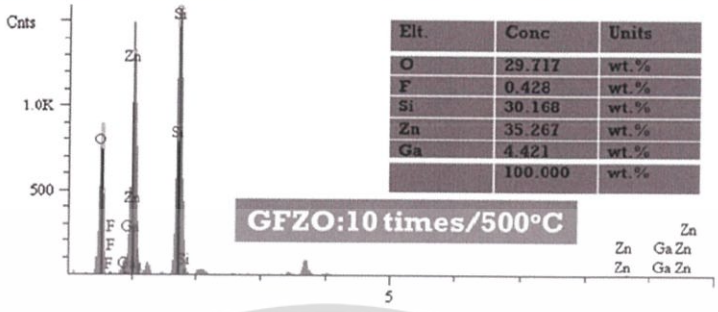

Elt.	Conc	Units
O	29.717	wt.%
F	0.428	wt.%
Si	30.168	wt.%
Zn	35.267	wt.%
Ga	4.421	wt.%
	100.000	wt.%

Figure 4. EDX spectra of 5G3FZO nanostructure.

drastically changed from irregular structure to vertically-aligned and side-aligned nanodisks when annealing temperature of seed layer elevated to 400 °C. According to XRD result of seed layer with annealed temperature of 400 °C, the dominated diffracted peak is along (101) plane. Due to lattice matching between seed layer and grown structure, this preferential plane of seed layer should a crucial factor that affect to the growth direction and shape of the grown structure. This presumption is supported by the nanorod structures on the seed layer annealed at 500 °C whose preferred orientation is along (002) plane. The concentration of OH^- strongly influences the nucleation rate of ZnO. The system with high concentration of OH^- and high chemical potential can induce ZnO nanorod crystal growth.[33] On the contrary, because of lower driving force and chemical potential, it would produce nanodisks. The crystal growth was affected by doping concentration (Ga and F). Figure 4 shows the energy dispersive X-ray (EDX) spectrum of the GFZO nanostructures, indicating that these nanostructures consist of Zn, O, F and Ga. The Ga and F content of the sample is 4.421% and 0.428%, respectively.

Figure 5(A) shows temperature dependent PL spectra of 5G3FZO nanorods grown on ZnO seed layer annealed at 500 °C. It can be observed that all PL spectra of 5G3FZO nanorod structure held at low temperatures have similar features including three sharp UV emission band and a broad yellow-orange emission band, respectively. The three sharp UV emission bands are naturally related to the near band edge emission from the direct band gap of ZnO.[34] The first peak with shortest wavelength of ~368 nm (measured at 25 K) is correlated to free exciton emission.[35] The second dominated peak located at ~375 nm is typically ascribed to the emission of exciton of bound shallow neutral donor.[36] The third peak situated at ~382 nm with broad shoulder can be attributed to the donor to bound exciton emission.[34] It is clearly seen in Figure 5(A) that there is significant red-shift of major peak of UV-emission with increasing temperature. The relationship of major PL peak position with respect to temperature can be explained by the Varshni relation.[31] Furthermore, the broadening of these near band edge emission with increasing operating temperature is also noticed, that is due to the natural temperature-induced broadening mechanism in semiconductor. The origination of the yellow-orange emission band could be associated to the position

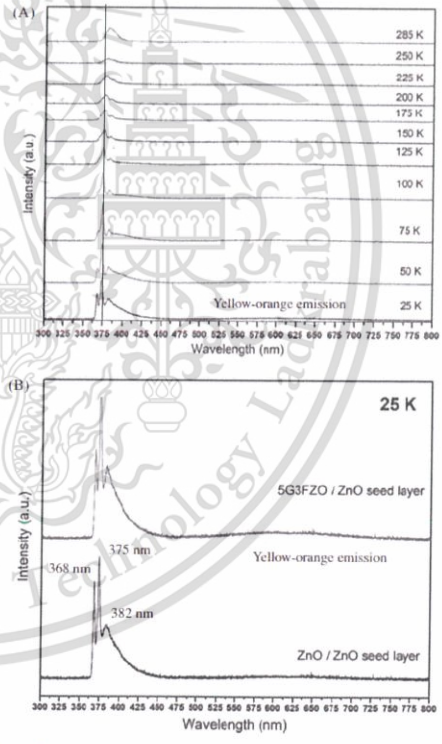

Figure 5. (A) Temperature dependent PL spectra of 5G3FZO nanorods and (B) PL spectra of ZnO nanorods and 5G3FZO nanorods operated at 25 K.

of Ga and F elements within the lattice arrangement.[33] Incorporated Ga and F elements can occupy the impurity sites to form interstitials or inhabit the main lattice sites to generate a ternary compound. Probably, Ga and F elements in the as-grown GFZO would substitute Zn atoms and O atoms, respectively. For comparison, PL spectra of bare ZnO and Ga/F co-doped ZnO were carried out at 25 K and depicted in Figure 5(B). It is obvious that stronger PL intensity of yellow-orange emission from codoped sample is observed. This feature implies the greater defect sites in the lattice of doped sample, reflecting to the good incorporation of the dopants that induce emission-related intrinsic defects, such as zinc and oxygen vacancies.

4. CONCLUSION

In summary, Ga/F codoped ZnO nanostructures were fabricated by hydrothermal process onto dip-coated ZnO seeding layer that was annealed at different temperatures ranging from 200–500 °C. The corresponding XRD and FE-SEM results suggested that different shapes of nanostructures of GFZO could be grown on the seed layer annealed at different temperatures. Possible reactions and mechanisms for the formation of GFZO nanostructures during hydrothermal process and the influence of seeding layer annealing temperature on the growth mechanism are suggested. The matching of preferential orientation direction between seeding layer that depends on annealing temperature and hydrothermally grown structures was suggested to be a key factor on the alternation in morphology of the synthesized products. The corresponding PL spectra of the GFZO are composed of narrow near band edge (NBE) emission and yellow-orange defect-related emission. The yellow-orange PL emission spectra qualitatively suggest the existence and good incorporation of the dopants into the ZnO matrix.

Acknowledgments: This work has partially been supported by the National Nanotechnology Center (NANOTEC), NSTDA, Ministry of Science and Technology, Thailand, through its program of Center of Excellence Network. Authors gratefully acknowledge the support from College of Nanotechnology, King Mongkut's Institute of Technology Ladkrabang (KMITL) and Research Institute of Electronics (RIE), Shizuoka University for PL measurement. Krisana Chongsri would like to thank Rajabhat Rajanagarindra University for Doctoral scholarship.

References and Notes

1. A. J. Cheng, Y. Tzeng, Y. Zhou, M. Park, T.-H. Wu, C. Shannon, D. Wang, and W. Lee, *Appl. Phys. Lett.* 92, 092113 (2008).
2. M. Ladanov, P. A. Amaris, P. Villalba, Y. Emirov, G. Matthews, S. Thomas, M. K. Ram, A. Kumar, and J. Wang, *J. Phys. Chem. Solids* 74, 1578 (2013).
3. G. Ch. Park, S. M. Hwang, S. M. Lee, J. H Choi, K. M. Song, H. Y. Kim, H. S. Kim, S. J. Eum, S. B Jung, J. H. Lim, and J. Joo, *Scientific Reports* 5, 10410 (2015).
4. A. R. Kaul, O. Yu. Gorbenko, A. N. Botev, and L. I. Burova, *Superlattices Microstruct.* 38, 272 (2005).
5. L. Xu, Y. Guo, Q. Liao, J. Zhang, and D. Xu, *J. Phys. Chem. B* 109, 13519 (2005).
6. K. H. Kim, K. Utashiro, Y. Abe, and M. Kawamura, *Int. J. Electrochem. Sci.* 9, 2080 (2014).
7. Y. J. Lu, Z. F. Shi C. X. Shan, and D. Z. Shen, *Chin. Phys. B* 26, 047703 (2017).
8. G. N. Dar, A. Umar, S. A. Zaidi, S. Baskoutas, S. W. Hwang, M. Abaker, A. Al-Hajry, and S. A. Al-Sayari, *Talanta* 89, 155 (2012).
9. C. Z. Yao, B. H. Wei, L. X. Meng, H. Li, Q. J. Gong, H. Sun, H. X. Ma, and X. H. Hu, *J. Power Sources* 207, 222 (2012).
10. N. H. Al-Hardan, M. J. Abdullah, N. M. Ahmed, F. K. Yam, and A. A. Aziz, *Superlattices Microst.* 51, 765 (2012).
11. R. M. Mohite and R. R. Kothawale, *Indian J. Chem.* 54A, 872 (2015).
12. W. Wang, T. Ai, and Q. Yu, *Scientific Reports* 7, 42615 (2017).
13. H. C. Wu, Y. C. Peng, and C. C. Chen, *Opt. Mater.* 35, 509 (2013).
14. J. H. Lim, S. M. Lee, H. S. Kim, H. Y. Kim, J. Park, S. B. Jung, G. Ch. Park, J. Kim, and J. Joo, *Scientific Reports* 7, 41992 (2017).
15. R. Pandey, C. H. Wie, X. Lin, J. W. Lim, K. K. Kim, D. K. Hwang, and W. K. Choi, *Sol. Energ. Mat. Sol. Cells* 134, 5 (2015).
16. J. B. Cui, Y. C. Soo, T. P. Chen, and U. J. Gibson, *J. Phys. Chem.* 112, 4475 (2008).
17. G. Ch. Park, S. M. Hwang, J. H. Lim, and J. Joo, *Nanoscale* 6, 1840 (2014).
18. A. A. Rani and S. Ernest, *Superlattices Microstruct.* 75, 398 (2014).
19. A. V. Moholkar, S. M. Pawar, K. Y. Rajpure, C. H. Bhosale, and J. H. Kim, *Appl. Surf. Sci.* 255, 9358 (2009).
20. S. K. Kim, S. H. Kim, S. Y. Kim, J. H. Jeon, T. K. Gong, D. H. Choi, D. Son, and D. Kim, *Ceram. Int.* 40, 6673 (2014).
21. X. Pan, Z. Ye, J. Li, X. Gu, Y. Zeng, H. He, L. Zhu, and Y. Che, *Appl. Surf. Sci.* 253, 5067 (2007).
22. N. Chahmat, T. Souier, A. Mokri, M. Bououdina, M. S. Aida, and M. Ghers, *J. Alloys Compd.* 593, 148 (2014).
23. Z. Pan, Y. Xiao, X. Tian, S. Wu, C. Chen, J. Deng, C. Xiao, G. Hu, and Z. Wei, *Sci. Semicond. Process.* 17, 162 (2014).
24. Y. Z. Tsai, N. F. Wang, and C. L. Tsai, *Thin Solid Films* 518, 4955 (2010).
25. F. H. Alsultany, Z. Hassan, and N. M. Ahmed, *Superlattices Microstruct.* 92, 68 (2016).
26. J. Guo, J. Zheng, X. Song, and K. Sun, *Mater. Lett.* 97, 34 (2013).
27. K. Chongsri, W. Sinornate, K. Boonyarattanakalin, and W. Pecharapa, *J. Nanosci. Nanotechnol.* 16, 12962 (2016).
28. K. Chongsri, K. Boonyarattanakalin, and W. Pecharapa, *Ceram. Int.* 43, S534 (2017).
29. K. Chongsri, K. Boonyarattanakalin, and W. Pecharapa, *Mater. Today: Proceedings* 4, 6133 (2017).
30. H. T. Kim, S. Y. Lee, and C. Park, *Vacuum* 143, 312 (2017).
31. D. G. Ayana, R. Ceccato, C. Collini, L. Lorenzelli, V. Prusakova, and S. Dir, *Thin Solid Films* 615, 427 (2016).
32. L. Zhu, J. Li, Z. Ye, H. He, X. Chen, and B. Zhao, *Opt. Mater.* 31, 237 (2008).
33. J. S. Park, I. Mahmud, H. J. Shin, M. K. Park, A. Ranjkesh, D. K. Lee, and H. R. Kim, *Appl. Surf. Sci.* 362, 132 (2016).
34. Y. Lv, Z. Zhang, J. Yan, W. Zhao, C. Zhai, and J. Liu, *J. Alloys Compd.* 718, 161 (2017).
35. F. Xian, G. Zheng, L. Xu, W. Kuang, S. Pei, Z. Cao, J. Li, and M. Lai, *J. Alloys Compd.* 710, 695 (2017).
36. V. Sh. Yalishev, Y. S. Kim, X. L. Deng, B. H. Park, and Sh. U. Yuldashev, *J. Appl. Phys.* 112, 013528 (2012).

Received: 13 August 2017. Accepted: 13 October 2017.

APPENDIX D

Materials Today: Proceedings 4, (2017), 6129–6133.

Available online at www.sciencedirect.com

ScienceDirect

Materials Today: Proceedings 4 (2017) 6129–6133

materialstoday: PROCEEDINGS

www.materialstoday.com/proceedings

STEMa2016

Effects of seeding layer thickness on physical and morphological structure of Ga/F co-doped ZnO nanostructures

Krisana Chongsri[a,b,*], Kanokthip Boonyarattanakalin[a], Wisanu Pecharapa[a]

[a]College of Nanotechnology, King Mongkut's Institute of Technology Ladkrabang, Bangkok 10520, Thailand
[b]Department of Applied Physics, Faculty of Science and Technology, Rajabhat Rajanagarindra University, Chachoengsao 24000, Thailand

Abstract

The effects of seed layer thickness on structural properties and morphology of Ga/F co-doped ZnO nanostructures were investigated in this work. The seed layers with various thicknesses were deposited on glass substrates by dip-coating. It is hypothesized that a certain range of seed layer thickness can significantly alter the outcomes of the morphological structure, density, and shape of the as-synthesized nanostructure products. The Ga/F co-doped ZnO nanostructures were grown on these seed layers by a hydrothermal process using $Zn(NO_3)_2$, NH_4F, GaN_3O_9 and hexamethyltetramine. The effects of seeding layer thickness on morphologies and structural properties were investigated by X-ray diffraction (XRD), scanning electron microscope (SEM), and UV-Vis spectroscopy. More detailed studies to clarify the seed layer effect on the growth of Ga/F co-doped ZnO nanostructures are further discussed.

Selection and Peer-review under responsibility of International Conference on Science and Technology of the Emerging Materials.

Keywords: Co-doped; nanostructure; hydrothermal process; seeding layer

1. Introduction

Zinc oxide (ZnO) has drawn much attention due to its unique characteristics as transparent conducting oxide (TCO) thin films with potential applications in various optoelectronic devices. ZnO thin films present many advantages such as low material cost, non-toxicity, and high chemical stability, in comparison to tin-doped indium oxide (ITO). ZnO is typically an n-type compound semiconductor with a wide band gap (E_g– 3.2-3.4 eV at 300 K) with a large exciton binding energy (60 meV)[1]. The electrical and optical properties of ZnO can be considerably enhanced by appropriate doping with either metal or non-metal elements. Much more interest has been given to ZnO-based TCOs such as undoped ZnO thin films, Al-doped ZnO (AZO) thin films[2], and Ga-doped ZnO(GZO) thin films[3]. When metal dopant atoms are incorporated into ZnO, they preferably replace

*Corresponding author. Tel.:+66-909603781; fax+66-23298265
E-mail address: Krisana_81@hotmail.com

Selection and Peer-review under responsibility of International Conference on Science and Technology of the Emerging Materials.

the Zn host atoms that could provide extra free electrons resulting in a high conductivity or better carrier mobility. Among the metal dopants, Ga appears to be a promising element due to its similar ionic radius (0.62Å) and covalent radius (1.26 Å) to those of Zn (0.74 and 1.34 Å, respectively)[4]. The similar ionic radius would lead to lower lattice distortion, when doping, compared with Al[5], and In[6]. Furthermore, the ionic radius of fluorine (0.117 nm) is similar to that of oxygen (0.122 nm)[7], fluorine may be a suitable anion doping candidate at oxygen site in ZnO matrix. It is well-known that the one-dimensional (1D) nanostructures have been extensively studied because of their potential applications in nanoelectronic devices. Although several technologies have been established for the growth of a variety of ZnO nanostructures, hydrothermal growth technique is one of dominating processes due to their low temperature processing, low cost, ease of apparatus set-up, and environmental friendliness. Therefore, 1D ZnO nanorods can be used for many applications, including ultraviolet light-emitting devices[8], chemical sensors[9], solar cells[10], and ultraviolet detector devices[11]. In this work, we investigate in a systematic way the influence of seeding layer thickness on the structural properties of Ga/F co-doped ZnO (GFZO) nanostructures. The seed layer thickness has been found to be one of the key factors that can control the morphology, density, and shape of the hydrothermally grown Ga/F co-doped ZnO nanostructures.

2. Experimental procedure

Ga/F co-doped ZnO (GFZO) nanostructures were synthesized by hydrothermal process. First, glass substrates were consecutively washed by deionized water, ethanol and acetone in an ultrasonic cleaner. The precursor solution used for dip coating was prepared by dissolution of zinc acetate dihydrate ($Zn(Ac)_2{\cdot}2H_2O$) and diethanolamine (DEA) in absolute ethanol and stirred until the solution became clear. The seeding solution was dip-coated onto the cleaned glass substrates followed by a 15 min-annealing step on a hot-plate at 100°C, after each coating. The coating step was repeated for 5 to 15 times. After that, the coated films were annealed in a furnace at 500°C for 2 h to form ZnO seeding film layer. A solution for the growth of Ga/F co-doped ZnO nanorods/nanodisks was prepared by adding 100 mL of 0.05 M zinc nitrate hexahydrate ($Zn(NO_3)_2{\cdot}6H_2O$), ammonium fluoride (NH_4F) as a F doping source, gallium (III) nitrate hydrate (GaN_3O_9) as a Ga doping source, and hexamethylenetetramine (HMTA) into 50 mL deionized water. The examined concentrations of ammonium fluoride and gallium (III) nitrate hydrate was 3% and 5%, respectively (designated as 5G3FZO). The ZnO-seeded substrates were dipped into the prepared solution and loaded in a Teflon autoclave for the hydrothermal synthesis operating at 90°C for 2 h. Finally, the obtained white solid product was separated from the solution by centrifugation, washed with distilled water and dried at 100°C for 24 h. The morphologies of as-prepared samples were observed by Fe-SEM (Hitachi S-4700). EDS (Bruker AXS Quanta 4010) was employed for confirming the existences of fluorine and gallium contents in the samples, meanwhile the crystal structures of all samples were characterized by XRD (Bruker D8 discover diffractometer).

3. Results and discussion

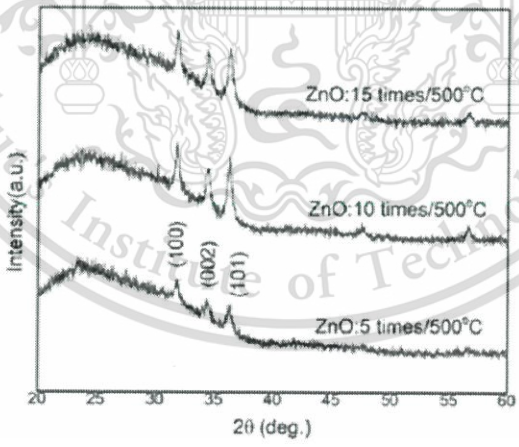

Fig. 1. X-ray diffraction patterns of ZnO seed layers grown on glass substrates when the seeding layer solution was dip-coated: 5, 10, and 15 times and annealed at 500°C

and bigger crystal sizes compared to the ZnO thin film deposited at ten times of coating, which is the main reason for the higher density of nanorods. Top view and cross-sectional FE-SEM images of GFZO nanorods grown on glass substrates when the seeding layer solution was dip-coated for 5, 10, and 15 times, and annealed at 500°C are shown in Figure 5. GFZO nanorods were grown in vertical direction with respect to the surface as hexagonal pillars with a flat facet surface. It is also clear that the size and orientation of the nanorods are strongly affected by the properties of ZnO seed layers with various thicknesses. The GFZO nanorods active nucleation sites possess higher density with an increase in the ZnO seed layer thickness with ten times of coating. The cross-sectional analyses illustrate that the hydrothermally grown GFZO forms uniform rods in large area with an average length of ~613 nm (for five times of coating) and ~343 nm (for ten times of coating).

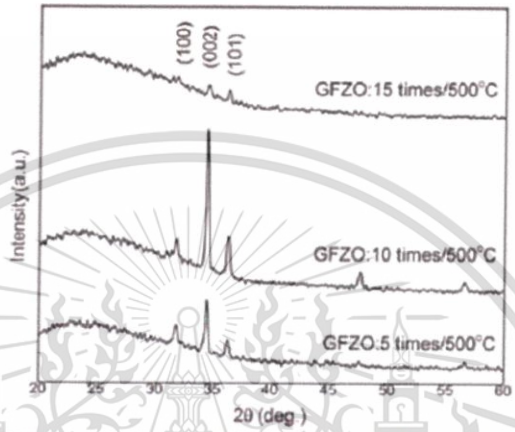

Fig. 4. X-ray diffraction patterns of GFZO nanostructures grown on ZnO seed layers when the seeding layer solution was dip-coated: 5, 10, and 15 times and annealed at 500°C.

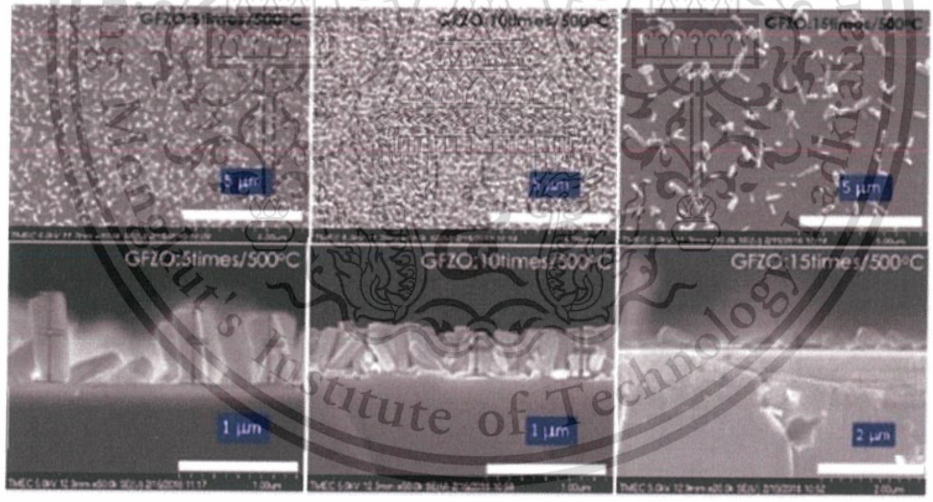

Fig. 5. FE-SEM micrographs of GFZO nanostructures grown on ZnO seed layers when the seeding layer solution was dip-coated: 5, 10, and 15 times and annealed at 500°C.

The Ga and F concentration in ZnO is attributed to the interstitial substitution of Ga and F ions in Zn and O sites into ZnO lattice, respectively, as confirmed by the EDS results. To assess the elemental composition of the synthesized GFZO (contains

Ga: 5 wt% and F: 3 wt%) nanorods, the EDS analysis was done and the corresponding result is shown in Fig. 6. In the EDS spectrum, numerous well-defined peaks for Zn, O, Ga, and F clearly indicate that the GFZO nanorods are made of Zn, O, Ga and F. No other peaks related to impurities were detected in the spectrum further confirming that the synthesized nanorods are Ga/F co-doped ZnO.

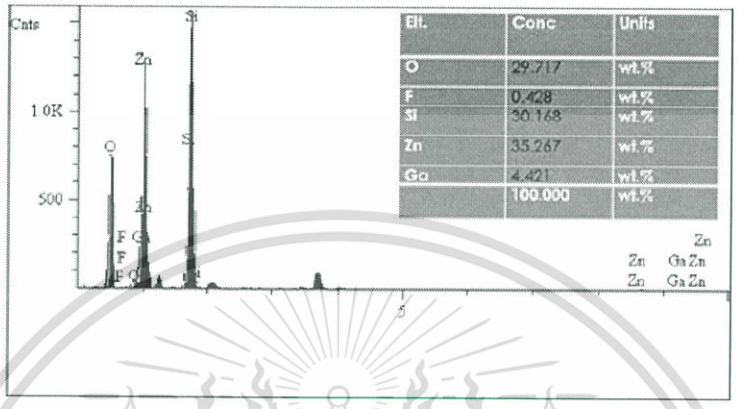

Fig. 6. EDS spectrum of GFZO nanostructures grown on ZnO seed layers.

Conclusion

The effects of the seeding films deposited at different coating times on the growth of GFZO nanorods during hydrothermal synthesis was investigated. The changes in diameter and density of hydrothermally grown ZnO nanorods were observed and analyzed. The growth rate of GFZO nanorods has a strong relationship with the intensity of the (002) orientation. The morphology of GFZO nanorods is strongly influenced by the thickness of the seed layer and corresponding crystal size. ZnO seeding layer thickness with ten times of coating exhibited the highest growth rate GFZO nanorods because it possessed the appropriate crystal size of the seed layer. In addition, the crystallinity of GFZO nanorods was also strongly related to the thickness and crystal size of ZnO seed layer.

Acknowledgements

This work is partially supported by the National Nanotechnology Center (NANOTEC), NSTDA, Ministry of Science and Technology, Thailand, through its program of Center of Excellence and Nation Research Council of Thailand (Grant No. 2559A11802097). Authors would like to thank Department of Applied Physics, Faculty of Science and Technology, Rajabhat Rajanagarindra University Chachoengsao for research fund support.

References

[1] K.H. Kim, K. Utashiro, Y. Abe, M. Kawamura, Int. J. Electrochem. Sci. 9 (2014) 2080-2089.
[2] R. Ebrahimfard, M.R. Golobostanfard, H. Abdizadeh, Appl. Surf. Sci. 290 (2014) 252-259.
[3] K. Thirumavkkarasu, R. Jothiramaligam, Powder Techno. 239 (2013) 308-313.
[4] D.T. Phan, G.S. Chung. Sensor and Actuat. B.187 (2013) 191-197.
[5] Z. Pan, Y. Xiao, S. Wu, C. Chen, J. Deng, C. Xiao, G. Hu, Z. Wei, Mater. Sci. Semicond. Process. 17 (2014) 162-167.
[6] R. Yousefi, F.J. Sheini, A.K. Zak, M.R. Mahmoudian, Ceram. Int. 38 (2012) 6295-6301.
[7] A.V. Moholkar, S.M. Pawar, K.Y. Rajpure, C.H. Bhosale, J.H. Kim, Appl. Surf. Sci. 255 (2009) 9358-9364.
[8] X.H. Wang, F.B. Zhang, K. Saito, T. Tanaka, M. Nishio, Q.X. Guo, J. Phys. Chem. Solids 75 (2014) 1201-1204.
[9] P. Yu, J. Wang, H.Y. Du, P.J. Yao, Y. Hao, X.G. Li, J. Nanomater. 751826 (2013)
[10] A. Verma, F. Khan, D. Kumar, M. Kar, B.C. Chakravarty, S.N. Singh, M. Husain, Thin Solid Films 518 (2010) 2649-2653.
[11] K. Khun, S. Elhag, Z.H. Ibupoto, V. Khranovskyy, O. Nur, M. Willander, Solid State Sci. 41 (2015) 14-18.
[12] R. Noonuruk, W. Techitdheera, W. Pecharapa, Thin Solid Films 520 (2012) 2769-2775.
[13] J. Song, S. Lim, J. Phys. Chem. C. 111 (2007) 596-600.

APPENDIX E

Other Publication

Key Engineering Materials
ISSN: 1662-9795, Vols. 675-676, pp 69-72
doi:10.4028/www.scientific.net/KEM.675-676.69

Submitted: 2015-06-15
Revised: 2015-08-14
Accepted: 2015-08-18
Online: 2016-01-25

Structural and optical Properties of F-doped ZnO nanoparticles synthesized by co-precipitation process

Krisana Chongsri [1,a], Wanichaya Mekprasart [1,b] and Wisanu Pecharapa [1,c]

[1]College of Nanotechnology, King Mongkut's Institute of Technology Ladkrabang, Bangkok 10520, Thailand

[a]krisana_81@hotmail.com, [b]wanichaya_am@hotmail.com and [c]kpewisan@gmail.com

Keywords: F-doped ZnO; Co-precipitation; Physical properties

Abstract. In this work, we reported the preparation of F-doped ZnO nanoparticles by facile precipitation process using zinc nitrate and ammonium fluoride as starting precursors for Zn and F, respectively dissolved in deionized water. The precursor solution was prepared at various fluoride composition ranging from 1-5 wt%. The as-precipitated powders were calcined at different temperature from 500 °C to 700 °C for 2 h. Effect of calcination temperature and fluoride concentration on structural, morphologies, optical and electrical properties were investigated by X-ray diffraction (XRD), scanning electron microscope (SEM), UV-Vis spectroscopy, respectively. XRD results indicated the complete formation of hexagonal wurtzite structure of ZnO. SEM micrographs showed the agglomeration for each sample that noticeably influenced by fluoride content.

Introduction

Zinc oxide (ZnO) is one of potential substituted materials for many applications in optoelectronic devices according to its considerable advantages such as non-toxicity, easy fabrication and low cost. ZnO has a hexagonal wurtzite structure with the lattice parameters of 5.205 Å (*c*) and 3.249 Å (*a*), wide direct band gap (E_g≈ 3.2-3.4 eV at 300 K), high exciton binding energy of 60 meV and n-type semiconductor [1]. Recently, elements from group V including Al, Ga and In have been considered proper dopants to adjust its performance both electrical and optical properties [2,3]. These doped substances have been synthesized by various techniques such as radio frequency magnetron sputtering [4], sol–gel process [5] and combustion process [6]. Among these techniques, co-precipitation process [7] is one of versatile methods for synthesizing various kinds of nanoparticles regarding to significant advantages over other methods including cost effectiveness, high purity, homogeneity and small crystalline size of obtained product. Recently, there have been correlated works employed the potential of co-precipitation process to synthesize nanostructures of ZnO. In case of non-metal dopant, Fluorine is one of the most proper elements widely utilized as a dopant in varieties of host materials including ZnO due to its ionic radius (0.131 nm), which is close to that of oxygen anion (0.138 nm) [5].

The purpose of this work is to study the effects of calcination temperature and fluorine content on physical structures and optical properties of ZnO nanoparticles by XRD, SEM and UV-Vis spectroscopy, respectively.

Experimental Details

F-doped ZnO (FZO) nanoparticles were synthesized by co-precipitation method. Firtly, zinc dichloride ($ZnCl_2$), ammonium fluoride (NH_4F) were used as starting material and ammonia (NH_3) was use as precipitating agent. The 0.5 M zinc dichloride ($ZnCl_2$) and ammonium fluoride (NH_4F) with differently designated F doping contents (1, 3, and 5 wt.%) were dissolved in 100 ml of deionized water and vigorously mixed by magnetic stirrer at 65°C for 1 h. Ammonia (NH_3) was dropped into the mixed solution while continuous stirring for 1 h, then aged at room temperature for 24 hr. The precipitate was repeatly washed with deionized water in order to eliminate chlorine ions. After chloride removal, it was slowly dried at 100 °C for 24 h to remove moisture and calcined at 500°C and 700°C for 2 h. The crystallinity of the powders was characterized by XRD (Panalytical

x' Pert pro MPD) using Cu-K_α radiation in the 2θ range of 20° to 60° with a scanning rate of 0.02° s^{-1}. Thermal analyses were carried out by NETZSCH TG 209F3 instrument using Al_2O_3 crucible and taking equal amount of Al_2O_3 as reference with a heating rate 10 °C/min. The size, shape and microstructure of particles were observed by SEM (ZEISS EVO MA10). Chemical composition was investigated by energy-dispersive X-ray Spectrophotometer (EDS, Oxford instruments X-Max^N). The optical properties of all samples were executed from their reflectance spectra carried out by UV-VIS spetrophotometer (UV-3600 Shimadzu).

Results and Discussion

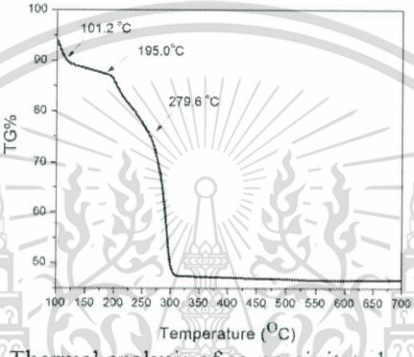

Fig. 1 Thermal analysis of as-precipitated product.

Figure 1 shows the thermal analysis curve (TGA) of as-precipitated product with 5 wt.% Fluoride content ()performed under ambient atmospheric in the temperature range of 100 °C to 700 °C with a heating rate of 10 °C/min. The first weigh loss at about 100 °C to 150 °C is attributed to the evaporation of physically absorbed water on the surface. The next weight loss at 150 °C to 250 °C indicated that the intermediate product of ZnF_2 may proceed the decomposition. Finally, after 300 °C, fluorine-doped ZnO is completely formed [3]. The overall reactions could be possibly written in the following equation:

$$NH_3 + H_2O \leftrightarrow NH_4^+ + OH^- \quad (1)$$

$$Zn^{2+} + 2OH^- \rightarrow Zn(OH)_2 \quad (2)$$

$$Zn(OH)_2 + 2NH_4F \rightarrow ZnF_2 + 2NH_3 + 2H_2O \quad (3)$$

Figure 2 shows X-ray diffraction patterns of F-doped ZnO (FZO) nanoparticles with various F doping contents from 1 wt.% to 5 wt.% calcined at 500 °C (Fig. 2a) and 700 °C (Fig. 2b). All diffraction patterns confirmed the existence of only ZnO phase without any impurities [7]. These occurrences implied that F atom could properly substituted at Zn site in ZnO structure. The average crystallite size of all samples were calculated from the full width at half-maximum (FWHM) of the (002) diffraction peak by Scherrer's equation (4), where D is crystallite size, λ is wavelength of

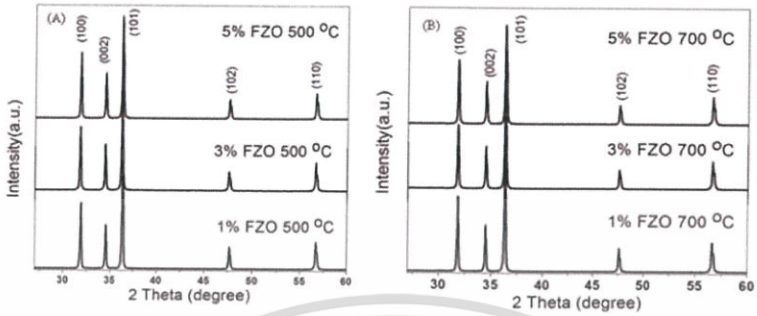

Fig. 2 XRD patterns of FZO nanoparticles with the different F contents calcined at (a) 500 °C and (b) 700 °C.

X-ray source (Cu K_α = 1.54 Å). β is FWHM of the (002) diffraction peak and Θ is the position of diffraction angle. The calculated crystallite size of the samples is approximately 56-70 nm.

$$D = \frac{0.9\lambda}{\beta \cos\theta} \tag{4}$$

Figure 3 shows SEM photograph of F-doped ZnO nanoparticles calcined at 500 °C and 700 °C. It is obviously noticed that the increase of F doping content significantly causes the increase of their particle sizes . It can be clearly seen that when doping level is 1 wt.%, its shape is nanorod. However, its shape changes to be hexagonal sheet with increasing F content to 3 wt.% and 5 wt.%. The corresponding EDS measurement was carried out to estimate at the doping concentration quantitatively. The EDS analysis of 5 wt.% F-doped ZnO sample as shown in Fig. 4 affirmed the existence of 2.85 wt.% F doping concentration in ZnO matrix.

Figure 5 (A) shows the diffuse reflectance spectra of undoped ZnO and F-doped ZnO nanoparticles in the wavelength ranging from 250 nm to 1200 nm. It is noticed that the increasing content of F ion in crystal structures leading to the decrease of band gap from 3.34 eV to 2.9 eV (Fig. 5(B)). This can be explained by increasing of the defects or impurities [6]. In addition, the decrease of optical band gap is attributed to not only lattice parameter and nano-crystal effect but also the influence of various factors such as grain size, carrier concentration, deviation from the stoichiometry and lattice strain

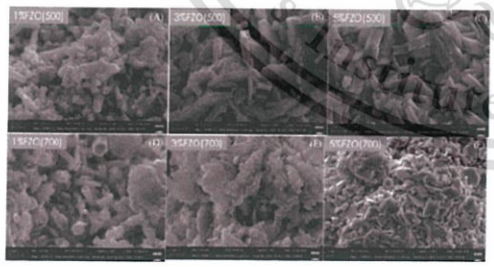

Fig. 3 FE-SEM micrograph of FZO nanoparticles with various F doping content from 1 wt.% , 3 wt.% and 5 wt.% calcined at 500 °C (A, B and C) and 700 °C (D, E and F).

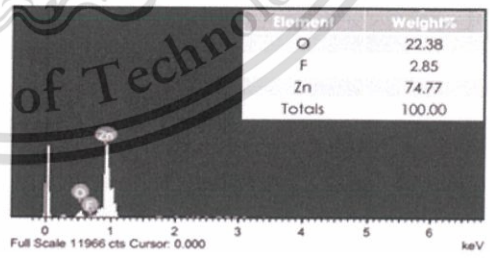

Fig. 4 EDS spectra of FZO nanoparticles at 5 wt.% of F content.

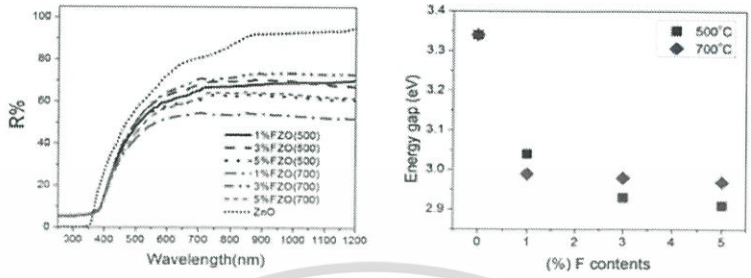

Fig. 5 (A) Diffuse reflectance spectra of FZO nanoparticles with the different F contents calcined at 500 °C and 700 °C and (B) The band gap values of all samples.

Conclusion

In this work, F-doped ZnO nanoparticles were successfully synthesized by co-precipitation method. XRD results showed the only hexagonal structure of ZnO suggesting the complete substitution of F ion in ZnO crystal structure meanwhile SEM photographs revealed the different aspect of these powders when using different calcination temperature and F doping contents. Moreover, the different F concentration and calcination temperature prove themselves to be crucial factors on significant change to structure and optical properties of ZnO.

Acknowledgements

This work has partially been supported by the National Nanotechnology Center (NANOTEC), NSTDA, Ministry of Science and Technology, Thailand, through its program of Center of Excellence Network. Authors gratefully acknowledge the support from College of Nanotechnology, King Mongkut's Institute of Technology Ladkrabang (KMITL) and Department of Applied Physics, Nakhon Pathom Rajabhat University (NPRU) for XRD measurement. This work was financially supported by KMITL research fund [KREF045711]. K. Chongsri would like to thank Rajabhat Rajanagarindra University for Doctoral scholarship.

References

[1] Z. Banu Bahsi, A. Yavuz Oral, Effects of Mn and Cu doping on the microstructures and optical properties of sol-gel derived ZnO thin films, Opt. Mater. 29 (2007) 672-678.

[2] R. Ebrahimifard, M.R. Golobostanfand, H. Abdizadeh, Sol-gel derived Al and Ga co-doped ZnO thin films: An optoelectronic study, Appl. Surf. Sci. 290 (2014) 252-259.

[3] J.S. Seo, J.H. Jeon, Y.H. Hwang, H. Park, M. Park, S.H. Ko Park, B.S. Bae, Solution-processed flexible fluorine-doped Indium zinc oxide thin-film transistors fabricated on plastic film at low temperature, Sci. Rep 3. Article number 2085 (2013)..

[4] H.S. Yoon, K.S. Lee, T.S. Lee, B. Cheong, D.K. Choi, D.H. Kim, W.M. Kim, Properties of fluorine doped ZnO thin fims deposited by magnetron sputtering, Sol. Energy Mater.Sol.Cells. 92 (2008) 1366-1372

[5] Z. Pan, J. Luo, X. Tian, S. Wu, C. Chen, J. Deng, C. Xiao, G. Hu, Z. Wei, Highly transparent and conductive Sn/F and Al co-doped ZnO thiin films prepared by sol-gel method, J. Alloys Compd. 583 (2014) 32-38.

[6] K. Ravichandran, P. Sathish, S. Snega, K. Karthika, P.V. Rajkumar, K. Subha, B. Sakthivel, Improving the antbacterial efficiency of ZnO nanopowders through simultaneous anionic (F) And cationic (Ag) doping, Powder Technol. 274 (2015) 250-257.

[7] D. Raoufi, Synthesis and microstructural properties of ZnO nanoparticles prepared by precipitation method, Renew Energ. 50 (2013) 932-937.

Applied Physics and Material Applications II
10.4028/www.scientific.net/KEM.675-676

Structural and Optical Properties of F-Doped ZnO Nanoparticles Synthesized by Co-Precipitation Process

10.4028/www.scientific.net/KEM.675-676.69

DOI References

[1] Z. Banu Bahsi, A. Yavuz Oral, Effects of Mn and Cu doping on the microstructures and optical properties of sol-gel derived ZnO thin films, Opt. Mater. 29 (2007) 672-678.
10.1016/j.optmat.2005.11.016
[2] R. Ebrahimifard, M.R. Golobostanfand, H. Abdizadeh, Sol-gel derived Al and Ga co-doped ZnO thin films: An optoelectronic study, Appl. Surf. Sci. 290 (2014) 252-259.
10.1016/j.apsusc.2013.11.062
[3] J.S. Seo, J.H. Jeon, Y.H. Hwang, H. Park, M. Park, S.H. Ko Park, B.S. Bae, Solution-processed flexible fluorine-doped Indium zinc oxide thin-film transistors fabricated on plastic film at low temperature, Sci. Rep 3, Article number 2085 (2013).
10.1038/srep02085
[4] H.S. Yoon, K.S. Lee, T.S. Lee, B. Cheong, D.K. Choi, D.H. Kim, W.M. Kim, Properties of fluorine doped ZnO thin films deposited by magnetron sputtering, Sol. Energy Mater. Sol. Cells. 92 (2008) 1366-1372.
10.1016/j.solmat.2008.05.010
[5] Z. Pan, J. Luo, X. Tian, S. Wu, C. Chen, J. Deng, C. Xiao, G. Hu, Z. Wei, Highly transparent and conductive Sn/F and Al co-doped ZnO thin films prepared by sol-gel method, J. Alloys Compd. 583 (2014) 32-38.
10.1016/j.jallcom.2013.06.192
[6] K. Ravichandran, P. Sathish, S. Snega, K. Karthika, P.V. Rajkumar, K. Subha, B. Sakthivel, Improving the antbacterial efficiency of ZnO nanopowders through simultaneous anionic (F) And cationic (Ag) doping, Powder Technol. 274 (2015) 250-257.
10.1016/j.powtec.2014.12.053
[7] D. Raoufi, Synthesis and microstructural properties of ZnO nanoparticles prepared by precipitation method, Renew Energ. 50 (2013) 932-937.
10.1016/j.renene.2012.08.076

AUTHOR BIOGRAPHY

Name	Mr.Krisana Chongsri
Date of Birth	06 December 1986
Address	413/4 Onnut 54, Sunanluang, Bangkok 10250
Education	(2008) Bachelor of Science in Applied Physics, Department of Applied, King Mongkut's Institute of Technology Ladkrabang (2011) Master of Science in Nanotechnology, College of Nanotechnology, King Mongkut's Institute of Technology Ladkrabang
Scholarship	(2014) Rajabhat Rajanagarindra University for Doctoral scholarship

Academic Publications:

1. Krisana Chongsri, Wanichaya Mekprasart and Wisanu Pecharapa, "Structural and optical Properties of F-doped ZnO nanoparticles synthesized by co-precipitation process" Key Engineering Materials Submitted: 2015-06-15 ISSN: 1662-9795, Vols. 675-676, pp 69-72.
2. Krisana Chongsri, Wuttichai Sinornate, Kanokthip Boonyarattanakalin and Wisanu Pecharapa, "Growth and Characterization of Ga/F Co-Doped ZnO Nanorods/Nanodisks via Hydrothermal Process" Journal of Nanoscience and Nanotechnology Vol. 16, (2016), 12962–12966.
3. Krisana Chongsri, Kanokthip Boonyarattanakalin and Wisanu Pecharapa, "Effects of seeding layer thickness on physical and morphological structure of Ga/F co-doped ZnO nanostructures" Materials Today: Proceedings 4 (2017) 6129–6133.
4. Krisana Chongsri, Kanokthip Boonyarattanakalin and Wisanu Pecharapa, "Substrate placement angle-dependent growth of Ga/F co-doped ZnO nanostructures synthesized by hydrothermal process" Ceramics International 43 (2017) S529–S534.

5. Krisana Chongsri, Yoichiro Neo, Hidenori Mimura, Kanokthip Boonyarattanakalin, and Wisanu Pecharapa, "Effects of Seeding Layer Annealing Temperature on Physical and Morphological Structure of Ga/F Co-Doped ZnO Nanostructures" Journal of Nanoscience and Nanotechnology Vol. 18, (2018), 7296–7301.